ACCREU
Assessing
Climate Change
Risk in EUrope

ACCREU
Assessing Climate Change Risk in EUrope

GA number: 101081358, Funding type: HORIZON-CL5-2022-D1-07-two-stage

Deliverable number (relative in WP)	**D2.2** Deliverable 2.2
Deliverable name:	Impacts on food, energy, and water
WP / WP number:	
Delivery due date:	Project month 17 (31/10/2024)
Actual date of submission:	xx/yy/201z
Dissemination level:	PUBLIC
Lead beneficiary:	IIASA
Responsible scientist/administrator:	Palazzo, Amanda
Contributor(s):	Amanda Palazzo (IIASA), Juliana Arbelaez-Gaviria (IIASA/CzechGlobe), Peter Burek (IIASA), Stefan Frank (IIASA), Dor Fridman (IIASA), Petr Havlik (IIASA), Andrey Lessa Derci Augustynczik (IIASA), Michael Wogerer (IIASA), Enrica De Cian (CMCC), Francesco Colelli (CMCC), Giacomo Falchetta (CMCC, IIASA)
Internal reviewer:	e.g. WP leaders, coordinator

Funded by the European Union. Views and opinions expressed are however those of the author(s) only and do not necessarily reflect those of the European Union. Neither the European Union nor the granting authority can be held responsible for them.

Funded by
the European Union

Changes with respect to the DoA

There are no changes with respect to the description of work

1. Dissemination and uptake

A dataset of gridded water demand projections for households and industries for Europe by Fridman et al (2024) has been made publicly available on Zenodo, allowing researchers, policymakers, and developers to access and utilize the data freely. This open-access approach supports the principles of FAIR (Findable, Accessible, Interoperable, and Reusable) data management, promoting reuse across a wide range of applications. Since August 2024, this dataset has been downloaded 2,623 times.

The CWatM hydrological modeling results for RCP4.5 that are needed within the ACCREU project and run have been shared with project partners already and will be shared in an open-access platform following the project timelines.

The climate impacts and adaptation scenarios from the impact assessment modeling chain will be shared with the WP4 modeling teams (GLOBIOM modeling results as well as the CWatM results). Draft version of the modeling results have already been shared with WP4 teams to ensure that the scope and geographic scale of the modeling results is appropriate for the WP4 models. The GLOBIOM modeling results have been appropriately downscaled and made available to be used within the WP2 tasks: to the biodiversity Task 2.4 and energy modeling teams Task 2.6.

The output gridded data on air-conditioning ownership and the underlying machine learning (ML) model trained on household survey data are made publicly available on Zenodo (https://zenodo.org/records/12697821) for future use by the scientific community, policy makers and industry stakeholders. In particular, we release global netCDF files with a 0.5 arc-degree spatial resolution and 10-year time resolution for the period 2010-2050. Dataset contains: the AC penetration rate, the total population by grid cell and the electricity consumed for AC utilization by households at each grid cell. Since July 2024 the data has been downloaded 217 times. The output data of the sectoral final energy demand for adaptation and of supply-side impacts on generation power outages will be shared in open-access platforms following the project timelines.

The climate impacts and adaptation scenarios from the impact assessment modeling chain are also available and being used for the case study 3.1 Thaya River Basin and Ebro River basin.

2. Short Summary of results

ACCREU's estimates of climate impacts and adaptation in **agriculture and forestry** sector include:

1) Crop yields and input requirements for 18 crops at the global scale, with country-specific and subnational projections for the ACCREU scenarios in 2030, 2050, and 2100

2) Temperature stress on livestock productivity and feeding for ruminant livestock at the global scale, with country-specific and subnational projections for the ACCREU scenarios in 2030, 2050, and 2100.
3) Grassland productivity at the global scale, with country-specific and subnational projections for the ACCREU scenarios in 2030, 2050, and 2100

Adaptations in the agriculture sector include 1) **autonomous adaptation** which are decisions made by crop and livestock farmers based on changing conditions and market signals, without policy intervention and 2) **planned adaptations** which includes improved access to more technical options and investments and policies to further reduce barriers to trade. Low, medium/reference, and high adaptation scenarios are developed for the agriculture.

ACCREU's estimates of climate impacts and adaptation in **water sector** include:

1) Water demand estimates for domestic, industrial and agriculture at the global scale, with country-specific and subnational projections for the ACCREU scenarios in 2030, 2050, and 2100. Estimates for Europe are also available at the 5' resolution.
2) Aggregated runoff, environmental flow requirements, and surface water available to be used for irrigation at the global scale, with country-specific and subnational projections for the ACCREU scenarios in 2030, 2050, and 2100

Adaptations in the water sector include **autonomous adaptations** (irrigated area abandonment) and planned adaptations which includes increased water storage for irrigation and conjunctive use of surface water and groundwater.

ACCREU's estimates of climate impacts and adaptation in the **energy sector** include:

1) Energy demand for all fuels (electricity, fossil fuels) and sectors (residential, commercial, industry, agriculture) at the global scale, with country-specific and subnational projections for the ACCREU scenarios in 2030, 2050, and 2100.
2) Residential air conditioning adoption and air conditioning electricity use at the global scale, with country-specific and subnational projections for the ACCREU scenarios in 2030, 2050, and 2100.
3) Unplanned (forced) and planned power outages during extreme weather events for thermal (nuclear, coal, gas, and oil) and renewable (hydro) power generation across Europe in 2030, 2050, and 2100.

Adaptation in the energy sector is characterized in terms of 1) **autonomous adaptation (e.g.** adjustments made by households and firms through a more or less intensive use of energy-using appliances) and 2) planned adaptation (e.g. increased adoption of energy-using appliances, such as air conditioning, and planned changes in their power plant maintenance operations resulting in a **planned power outage** as a response to extreme weather events, in order to avoid the possibility to incur in more costly forced power outages). Low, medium, and high adaptation scenarios are identified for residential energy demand and residential air conditioning adoption and use.

3. Evidence of accomplishment

Manuscripts in preparation:

- Arbelaez-Gaviria J., Palazzo A., et al. Sustainable expansion of irrigation under climate change
- Fridman, D et al. Impacts of dynamic land use change on water balance modeling
- Palazzo, A., Arbelaez-Gaviria J, et al. Integrated Assessment of Cross-Sectoral Hotspots and Adaptation Options in the Water, Land, and Energy Nexus with Continental and Transboundary River Basin Perspectives
- Colelli F., Sue Wing I., Future temperature variability around climatic shifts exacerbates global energy demand impacts of warming.
- Sergio A., Colelli F., Resilience of Europe's Power Generation to Climate Change.

Published Manuscripts:

- Falchetta, G., Cian, E.D., Pavanello, F. et al. Inequalities in global residential cooling energy use to 2050. Nat Commun 15, 7874 (2024). *https://doi.org/10.1038/s41467-024-52028-8.*

Published datasets:

- Fridman, D., Burek, P., Palazzo, A., Wada, Y., & Kahil, T. (2024). SSP-aligned projected European water withdrawal/consumption at 5 arcminutes (0.9.1) [Data set]. Zenodo. *https://doi.org/10.5281/zenodo.13767595*
- Falchetta, G., Pavanello, F., De Cian, E., & Sue Wing, I. (2024). Global gridded scenarios of residential cooling energy demand to 2050 [Data set]. In Nature Communications. Zenodo. *https://doi.org/10.5281/zenodo.12697821*

Funded by
the European Union

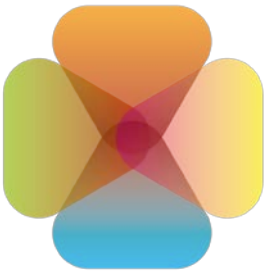

ACCREU
Assessing
Climate Change
Risk in EUrope

Table of Contents

Abstract

1. Introduction

This deliverable reports on the objectives outlined in ACCREU's Task 2.2 Impacts on food, energy, and water, providing a detailed account of the work conducted and the progress made towards achieving the task's objectives. This deliverable will present an overview of the significant advancements made under in the biophysical and economic modeling of climate impacts and adaptation on agriculture, bioenergy, and forestry as well as the climate change impacts on energy demand and supply. The agriculture and forestry sector are covered using the IIASA's impact assessment modeling chain and findings. The energy sector, analyzed by CMCC through statistical and econometric methods, provides new insights into the estimations of energy needs for adaptation, reflected in changes in final energy consumption across economic sectors, and the impact of extreme weather on the energy supply side (power generation interruptions). Additionally, this deliverable includes further analyses on household adoption rates and usage of air conditioning appliances, and provides estimates of electricity and gas expenditures by income quintile for the distributional analysis in WP4.

1) **Scenario Updates Based on CMIP6:**

The impact assessment modelling impact chain and the energy sector modeling was updated with the latest climate scenarios from the sixth phase of the Coupled Model Intercomparison Project (CMIP6). These updates enabled more accurate projections of climate impacts on European agriculture, forestry, and the energy sector, as well as on large regions outside Europe.

At the start of the project the planned task objective for the bioeconomic modeling was envisioned to focus on updating projections for crop yields, water availability for irrigation, and forest productivity under the CMIP6 scenarios. However, the scope was expanded to include additional areas of impact. We extended the climate impacts analysis to cover the effects of climate change on **grassland productivity**, as well as the impacts of **heat stress on livestock**. This broader approach allowed for a more holistic assessment of how climate change may affect the crop and livestock sectors as well as indirectly affecting the forestry sector, providing deeper insights into the challenges and adaptation needs across the land system.

We have also expanded the scope of updating the scenarios to include the 2023 revisions of the Shared Socioeconomic Pathways (SSPs) datasets used in the impact assessment modeling chain and in the energy sector projections, to reflecting updated projections for GDP and population growth.

The following sections are relevant to this task objective:

- **Section 2.1.1 Climate impacts and mitigation**
- **Section 2.1.2 Socioeconomic trends**

2) **Energy supply and demand:**

We developed econometric models providing new estimates for the climate change impacts on energy demand across fuels and sectors at global level and for the EU. The scope of this contribution was expanded to include gridded projection of air-conditioning electricity and AC.

As for energy supply, we develop an empirically-based model associating extreme weather conditions to power supply unavailability of thermal (nuclear, coal, gas, and oil) and renewable (hydro) power generation across Europe. While indicators based on temperatures are the main driver of energy demand changes, energy supply shocks include the impact of water stress indicators based on hydrological projections from the CWatM model.

The following sections are relevant to task objective:

Section 2.2.4 Energy models and ACCREU developments
Section 3.3 Energy supply and demand
Section 4.3 Adaptation costs

Our results provide a foundation for ACCREU model-based assessments and for developing policy recommendations aimed understanding the broader impact of climate change on energy systems.

3) Expanded Food System Indicators:

We developed and analyzed comprehensive set of indicators related to the food system. This includes measures of food security, availability, affordability, and price stability. We provide food security indicators of calorie availability, at the regional level for European regions as well as regions outside of Europe.
These enhancements provide a more holistic view of the potential disruptions to food systems under various climate scenarios.

The following sections are relevant to task objective:

- **Section 4.1 Expanded food security indicators**

4) Distributional Effects on Producers and Consumers:

The model was further refined to assess the distributional impacts of climate change across producers and consumers. This analysis highlights the varying degrees of vulnerability within the agricultural and bioenergy sectors and how adaptation benefits affect producers and consumers differently. This section also examines the role of trade as an adaptation mechanism.

The following sections are relevant to task objective:

- **Section 4.2 Distributional effect among producers and consumers**

5) Water Demand, Availability, and Scarcity:

In addition to the food system analysis, we evaluated the impacts of climate change on water demand, availability, and scarcity. Using the GLOBIOM model and our integrated assessment impact modeling chain, we analyzed how changing climate conditions affect agricultural water needs, providing a assessment of regional water use patterns.

The following sections are relevant to task objective:

- **Section 3.2.2 Aggregated Runoff**
- **Section 3.2.1 Water demand for domestic and industrial uses**
- **Section 3.2.3 Sustainable water for irrigation**

6) Improved hydrological modeling and sectoral water use assessments:

a) Sectoral water use

Water use across households, industries, and agriculture was assessed using CWatM at a 5-minute spatial resolution and daily time steps for Europe, offering high granularity in water use simulations. The integration of these sectoral demands allowed us to better understand the competing pressures on water resources in a changing climate.

The following section is relevant to task objective:

- **Section 3.1.1 Crop yields and irrigation water requirements**
- **Section 3.2.1 Water demand for domestic and industrial uses**

b) Gridded irrigation and land use change from GLOBIOM:

Irrigation and land use change projections from GLOBIOM were fed into the CWatM model to understand the impact of dynamic land cover maps on the water balances for Europe. This integrated approach enabled us to identify potential water scarcity hotspots in Europe, providing critical insights for water resource management and adaptation strategies under climate stress.

The following section is relevant to this task objective:

- **Section 5 Impacts of dynamic land use and land cover change in hydrological modeling, Two-direction soft coupling of CWatM-GLOBIOM**

Through these comprehensive modeling efforts, we have provided an in-depth assessment of climate change impacts and adaptation on both the food, energy and water sectors, offering valuable insights for policy development and future adaptation planning.

2. Methods and scenario protocol

This section presents the methodological approach used to conduct a cross-sector analysis of the impacts of slow-onset climate change on the agriculture and forestry sectors. The impact-chain approach integrates the simulation of climate impacts from sector-specific biophysical modeling with an economic land use model GLOBIOM to assess the biophysical impacts and market-driven adaptation options. The section provides an overview of the ACCREU scenario protocols, models included in the impact assessment chain and model developments undertaken throughout the project.

2.1. Scenario Protocol

This section provides an overview of the scenario protocol used in ACCREU to assess the impacts of future climate change and adaptation on the agriculture and forestry sectors. The protocol integrates both climate and socioeconomic projections to offer a comprehensive view of potential future global change conditions. This section will cover the climate projections (i.e., Global Climate Models (GCMs), Representative Concentration Pathways (RCPs), and mitigation scenarios), socioeconomic trends (i.e., gross domestic product (GDP) growth and population growth), and adaptation strategies included within the modeling for the agriculture and forest sector.

2.1.1. Climate impacts and mitigation

2.1.1.1. Climate forcing data

As a main part of Task 2.2 the models have been updated to use the bias-corrected climate data and impact modeling data from the ISIMIP project (https://protocol.isimip.org/), based on CMIP6 climate data. The models have considered the daily/monthly projections of temperature (minimum, maximum and average), precipitation, and solar radiation and we derived the number of frost days based on the minimum temperature (using a 0°C threshold) for the RCPs under the ACCREU scenario protocol. The ACCREU scenario protocol agreed by the consortium includes RCP 2.6, RCP 4.5, and RCP 7.0.

On average, by mid-century the RCPs represent **increases in annual average temperature from 0.83 to 2.06 °C in Europe** for RCP7.0, compared to the current climate, depending on the climate trajectory which can be seen for an the average of the GCM ensemble in Figure 1.

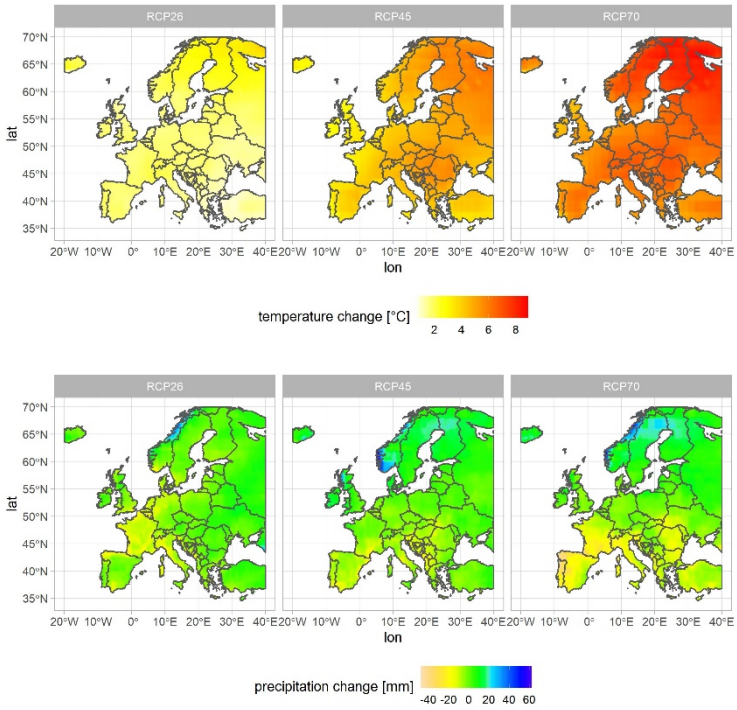

Figure 1 Precipitation and temperature change at mid-century for Europe for UKESM1-0-LL over different RCP assumptions Source: CMIP6 GCM results.

In our modeling protocol we used the climate projections from four GCMs (GFDL-ESM4, IPSL-CM6A-LR, MPI-ESM1-2-HR and UKESM1-0-LL). We adopt an ensemble approach for a more robust representation of climate variability and uncertainty in simulating future climate conditions. Some GCMs project higher than average mid and end of century temperature change (e.g., UKESM1-0-LL) while others project lower than average (e.g., MPI-ESM1-2-HR) (Figure 2).

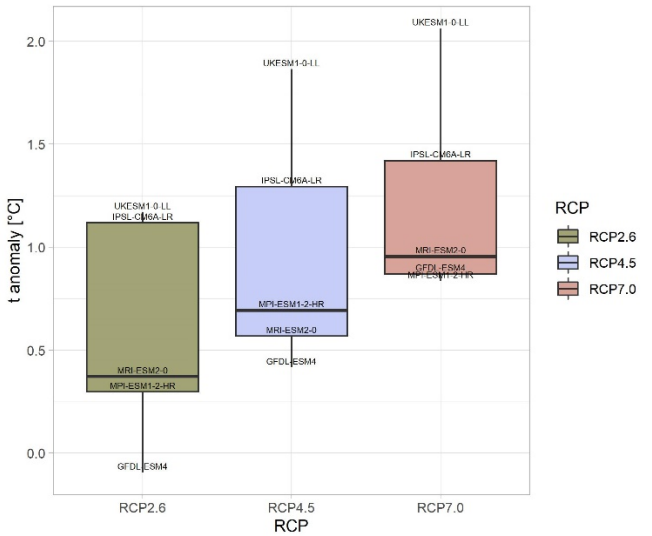

Figure 2 Projected mid-century temperature change from ensemble of CMIP6 GCMs for RCP 2.6, 4.5 and 7.0 Source: CMIP6 GCM results

2.1.1.2. Climate mitigation

The scenarios protocol includes both climate impacts and mitigation. The carbon price pathways, developed by the IAM community give a range of carbon prices that coincides with different levels of global GHG mitigation by all sectors of the economy to achieve certain levels of climate stabilization by 2100 conditional on the Shared-Socio-economic Pathways (Rogelj et al., 2018). MESSAGE provides a carbon price pathway and future projected demand for biomass and bioenergy that would be necessary to achieve the level of climate stabilization. Scenario specific carbon prices are implemented in GLOBIOM for CO2 and non-CO2 emissions on the entire agriculture, forestry and land use (AFOLU) sectors. The carbon price acts as a tax on emissions and as a subsidy for carbon sequestration and incentivizes in GLOBIOM the transition towards more GHG efficient production systems and the adoption of GHG mitigation technologies. The biomass demand is included as an exogenous demand for bioenergy from forest and other agricultural products.

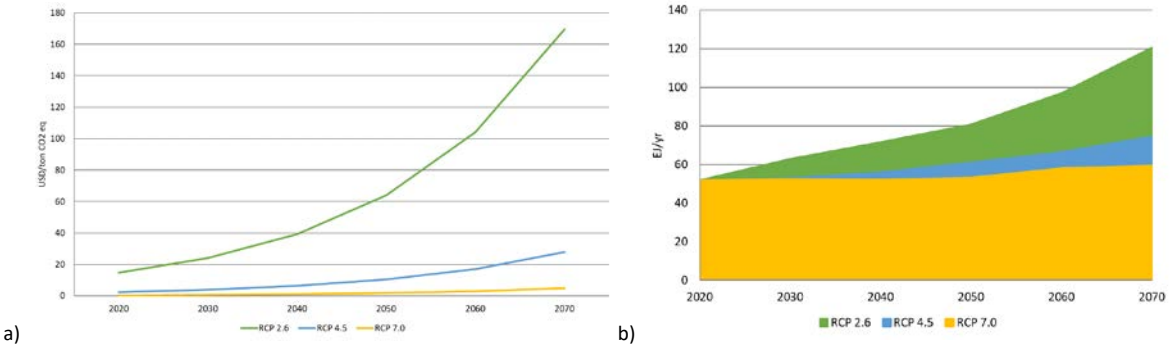

Figure 3 Carbon price (a) and biomass demand (b) projections from MESSAGE over time applied to each mitigation RCP scenario

2.1.2. Socioeconomic trends

The Shared Socioeconomic Pathways (SSPs) are five scenario narratives, developed between 2013 and 2017, that represent alternative trajectories for global socioeconomic development and climate change mitigation. These narratives, spanning a wide range of future development patterns and climate ambitions, were published in Global Environmental Change (O'Neill et al., 2017; van Vuuren et al., 2017) and have since become a widely used tool in the climate research community. Rather than predicting future trends, the SSPs provide "storylines" that explore how societal changes may unfold under different climate scenarios.

While the SSPs have been instrumental in climate scenario assessments over the past decade, their original framework assumes future projections starting from 2005. This has become somewhat outdated as the world nears 2025, with nearly two decades of developments unaccounted for in the 2005-2025 quantifications. To address this, the climate research community began updating the core elements and scenario quantifications of the SSPs in 2023.

In January 2024, version 3.0 of the SSP GDP and population projections was released after comprehensive internal and external reviews. These updates incorporate revised assumptions about technological, societal, and environmental factors. The updated population and GDP projections have been applied in ACCREU scenario modeling which ensure more relevant modeling of future socioeconomic trends. Figure 4 shows the comparison of the SSP assumptions for GDP and population from version 2.0 and version 3.0 for European countries. The comparison of the SSP2 assumptions for the rest of the major global regions are shared in the Annex of this report and also available for download from IIASA's SSP database explorer.

According to the revision of the SSPs, in the SSP2 middle of the road scenario, the global population is projected to increase 0.8% per year until 2030, 0.7% per year from 2030-2040, and 0.5% per year from 2040-2050, adding another 1.75 billion people to today's estimate of 7.7 billion people. This is slightly higher compared to the SSP2 V2 (+300,000 people) which estimated the world's population would reach only 9.0 billion. In the previous version of the SSP2, for Europe, the population was projected to increase from 520 million to around 541 million by 2050. In the SSP2 V3 the population of Europe is projected to slightly decline to around 509 million by 2050. The economic growth of Europe is projected to continue on much the same course as the SSP2 V2 projections (1.6% p.a growth) and the projections for the historical periods have been updated.

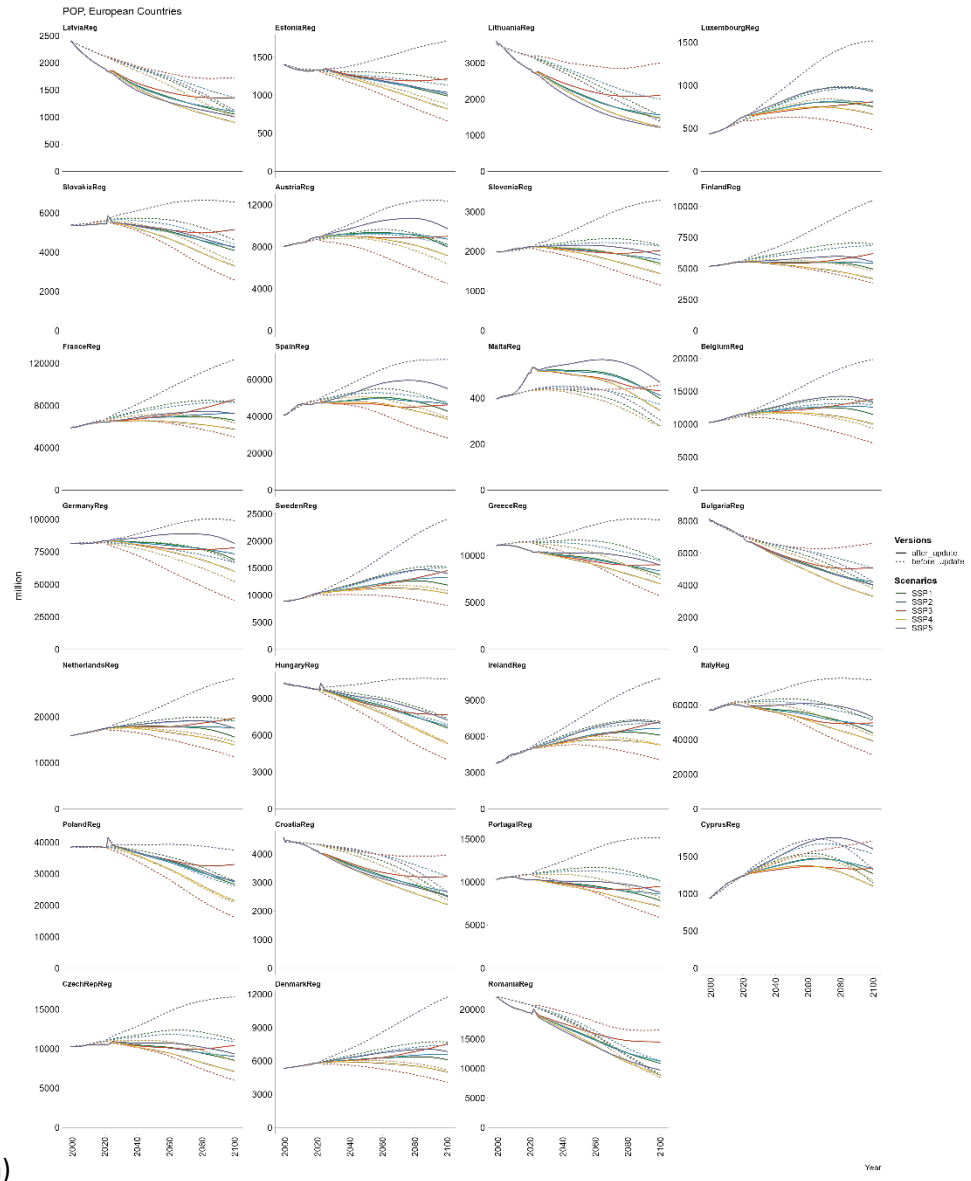

a)

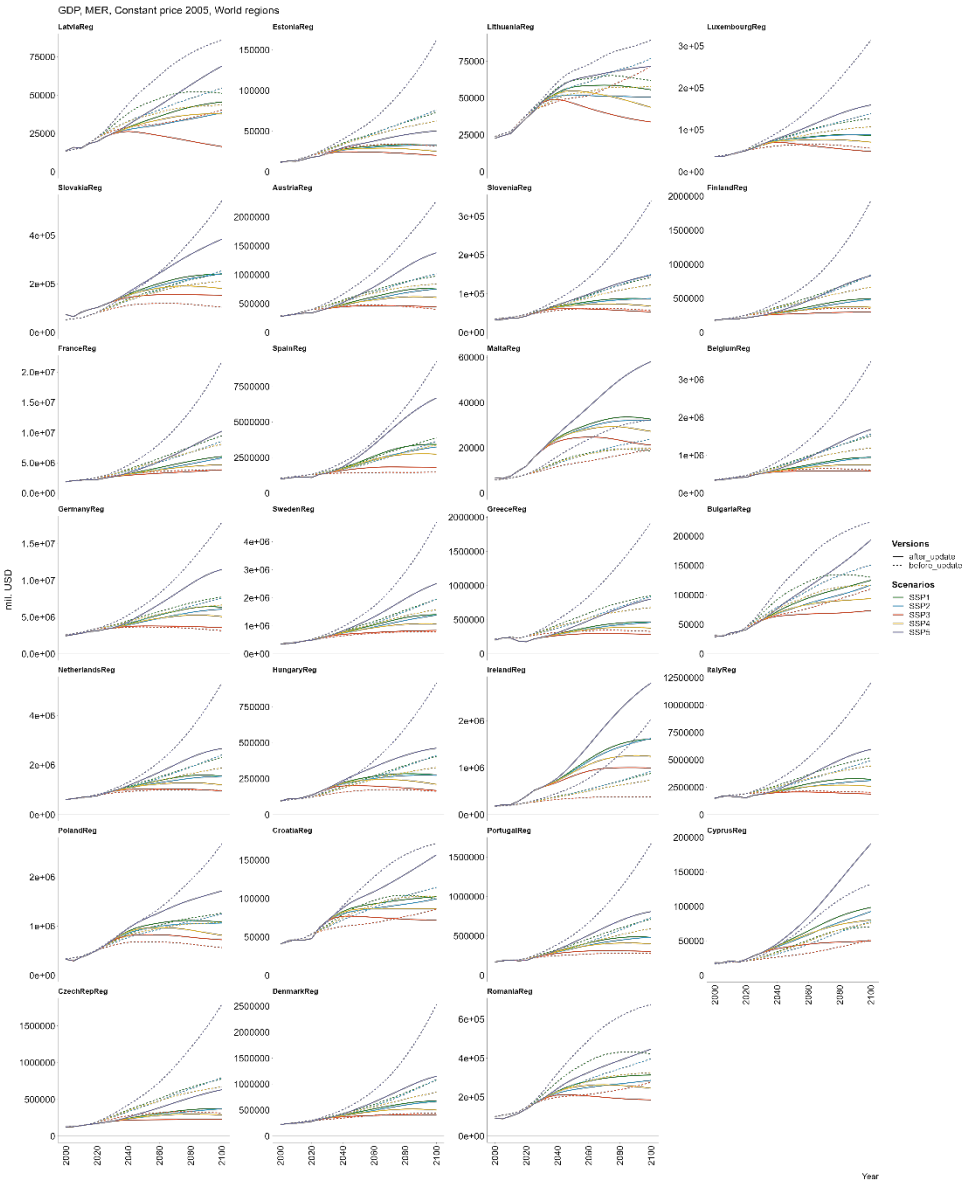

b)

Figure 4 Population (a) and GDP (b) growth for Europe by region for SSP 2023 revision and 2012 SSPs

2.1.3. Adaptation

In this section, we describe how autonomous and planned adaptation strategies are included in the agriculture, forestry and energy sector under different climate change scenarios—namely, the **high adaptation** and **low adaptation** pathways. Autonomous adaptation refers to the adjustments made by farmers based on changing conditions, without policy intervention. In GLOBIOM, these autonomous adaptations are incorporated in the model optimization that aims to maximize the producer surplus under given resource and production constraints. For example, if rising temperatures reduce the yields of a specific crop in a specific region, the model assumes that farmers may autonomously shift to a crop that has less impacted yields or to crops that are more profitable under the new climate conditions (**price-induced crop switching**). This choice is driven by market signals such as changing prices and the relative profitability. Energy demand changes are a form of adaptation, with responses varying by degrees of new technology adoption and economic capacity. Energy for adaptation can be categorized into three levels: low, where no new technology is adopted with respect to the historical baseline, and responses are limited to short-term adjustments (intensive margin); medium, where climate alone drives long-term technological changes; and high, where both climate and higher income drive greater technological adoption and adaptability over time. In the short run, households and firms mainly adjust **energy use** through the intensive margin, while long-term climate shifts lead to **changes in durable goods** (extensive margin).

The GLOBIOM model evaluates the potential for the agriculture sector to adapt to changing environmental conditions. In the **high adaptation** scenario, farmers have access to more technical options and have higher adaptive capacity, therefore more proactive measures are assumed, including the **adoption of advanced technologies** to increase yields under climate change, rehabilitate and update irrigation systems to increase efficiency, expand sustainable irrigation, and import crops from areas less climate effected areas. This scenario represents a future where significant investments are made to reduce the vulnerability of agricultural systems to climate impacts. In the **low adaptation** scenario, farmers have less access to technical options and have lower adaptive capacity and less ability to adjust to changes. Irrigation systems are poorly maintained, which lowers their efficiency. Crop switching and **land use adjustments** happen at a slower rate and on a smaller scale compared to the high adaptation scenario. This scenario represents a future where the agricultural sector's capacity to respond to climate change is limited. The reference scenario represents the medium adaptation scenario that aligns with the underlying assumptions for the development of the agriculture and forestry sector under the socioeconomic pathway SSP2 (Fricko et al., 2017).

Table 1 provides specific assumptions for the adaptation pathways as modeled by GLOBIOM, detailing the different technological and adaptive capacity measures included these adaptation pathways. Under these different scenario assumptions GLOBIOM can provide a comprehensive analysis of how different levels of adaptation can reduce the magnitude of the potential negative effects from likely climate futures.

Changes in energy demand are a consequence of different forms of adaptation across households and firms. In the context of energy demand, our focus is on **autonomous adaptation**, which refers to the adjustments made by households and firms, particularly through the more intensive use of adaptive appliances, and on **planned adaptation**, in terms of increased adoption of technologies and. Our empirical framework allows us to distinguish between two key forms of autonomous adaptation. First, people and firms respond to temperature shocks by adjusting their usage of energy-consuming goods like air conditioners. This immediate response, called the "intensive margin," reflects changes in the utilization of a fixed capital good. In the short-run, changes in the time allocation of a households

has also unintended consequences on energy use. The lack of intention makes this form of adaptation, which is identified by short term adjustments to unexpected weather shocks autonomous.

Over longer periods, agents perceive repeated temperature regimes as climatic shifts, prompting more significant adjustments, such as households without air conditioning purchasing one, which can also be classified as a **planned adaptation response**. This response, known as the "extensive margin," unfolds more gradually. Since capital goods are fixed in the short run, responses to unexpected weather shocks predominantly occur through the intensive margin. In the macro-level energy demand estimation, technologically-constrained adaptation is implicit in the difference between short-term and long-term coefficients, highlighting how immediate responses differ from those that evolve over time. In the micro-level AC ownership and use model, the intensive margin is directly estimated based on the change in household-level electricity consumption based on interannual weather changes, conditional on the presence of AC shock. Second, adaptive capacity is reflected in how GDP per capita modulates the long-term coefficients, indicating that wealthier societies may adjust more effectively. Both in the macro-level and micro-level energy demand estimations, this effect is captured by the modulating effects of per capita income on these responses.

We exploit macro and micro level evidence to identify how adaptation levels can vary. Under **low adaptation**, no additional technology is adopted with respect to the level chosen by households and firms without climate change, and energy responses are restricted to the intensive margin alone. In other words, existing technologies are assumed frozen at historical climate conditions**. Medium adaptation** involves long-term technological adoption driven by climate changes alone, allowing more flexible responses. **High adaptation** represents a scenario where additional, long-term technology adoption is driven by climate shifts and amplified by higher income, reflecting an enhanced adaptive capacity to future climate risks. Table 2 below shows the underlying framework for the definition of adaptation scenarios in the energy sector.

In the context of energy supply, **planned adaptation** refers to the adjustments made by power system generator through the change in their power plant maintenance operations resulting in a **planned power outage** as a response to extreme weather events, in order to avoid the possibility to incur in more costly forced power outages. Adaptation costs in this setting are computed as the forgone profit. The assessment of the economic and energy system implications of autonomous and **planned adaptation** strategies in the context of both energy demand and supply will be developed in the Deliverable 2.6 through the energy system model OSeMOSYS.

Table 1 Adaptation options included in GLOBIOM for the Agriculture sector

Adaptation options	Short description	Autonomous/ planned	How included in GLBIOM	Key Impact Assessment Impact Chain model Sources and references
Ag. R&D	Investments to improving crop resilience and increase crop yields	Planned	**High adaptation:** High levels of R&D (0.8% p.a growth-SSP1 yields) **Reference adaptation:** Medium R&D (0.7% p.a growth-SSP2 yields) **Low adaptation:** Low levels of Agricultural R&D (0.5% p.a growth-SSP3)	(Herrero et al., 2014) (Rosegrant et al., 2017)
Irrigation	Investments to expand sustainable irrigation to ensuring proper growth and adequate water supply when rainfall is insufficient. Investments can include large scale public infrastructure costs to improve water availability, on-farm system expansion costs, system upgrades and rehabilitation to improve water use efficiency, microtanks to provide sustainable water storage,	Planned	**High adaptation:** Reduced water supply costs, 5% increase in the irrigation efficiency per decade, improved local water supply for irrigation **Reference:** 1.5% increase in the water use efficiency per decade (Hanasaki et al., 2013) **Low adaptation:** 3% decrease per decade due to poor maintenance in systems and conveyance losses (Howell, 2005; Hsiao et al., 2007)	(Palazzo et al., 2019) (FAO, 2008; Inocencio et al., 2007, 2005; Sauer et al., 2010; Schmidhuber et al., 2009; Toan, 2016; Van Koppen et al., 2005)
International trade	The model employs the spatial equilibrium approach to international trade and assumes homogenous goods (considering initial trade patterns).	Autonomous and planned	Decrease in the trade costs between regions	(Guerrero et al., 2022; Janssens et al., 2022; Mosnier et al., 2014)
Change in agricultural management: agricultural land expansion and agricultural land conversion/system transition	Land expands depending on the relative profitability of converting land to different use types and land expansion constraint. Agricultural land will convert to a higher yielding or more intense system (i.e., from rainfed to irrigated or from extensive livestock to intensive/mixed systems livestock) depending on the relative profitability of converting land to different use types	Autonomous	**High adaptation:** Irrigation expansion limited to historical trends from 2000-2020 and allowed to expand beyond the observed historical trends for future years (i.e., 2000-2020) **Reference:** Irrigation expansion limited to historical trends from 2000-2020 then limited to 30% beyond the previous period irrigated area totals in future periods **Low adaptation:** Irrigation expansion limited to historical trends from 2000-2020 and then limited to expand only 10% beyond the previous period irrigated area totals in future periods	(Havlik et al., 2015; Leclère et al., 2014) (Pastor et al., 2016; Palazzo et al., 2019)

Change in agricultural management: crop choice	Cropland will switch to higher yielding crops depending on the relative profitability (taking into account the climate effect on crop productivity)	Autonomous	Crop choice is fully autonomous across all scenarios	

Table 2 Representation of adaptation in the energy sector impact estimations

Adaptation options	Short description	Autonomous/ planned	How included in Energy models	Key Impact Assessment Impact Chain model Sources and references
Intensive use of appliances/services	More intensive use of cooling/heating appliances and of broader energy-intensive services (e.g. irrigation) in response to temperature changes.	Autonomous	• **Low adaptation:** Variation in the intensive use of fixed capital stock (under historical climate) due to climate change. • **Reference adaptation:** Intensive use changes due to the underlying variation in energy-intensive capital stock under future climate. • **High adaptation:** Intensive use changes due to the variation in per capita income, affecting energy-intensive capital stock on top of future climate.	ACCREU analyses Colelli and Sue Wing (in prep.); (Falchetta et al., 2024)
Extensive adoption of new appliances/services	Long term, technological adoption, driven by climate and per capita income shifts.	Autonomous and planned	• **Low adaptation:** No additional technological adoption, frozen technology at historical climate. • **Reference adaptation:** Variation in energy-intensive capital stock due to future climate. • **High adaptation:** Variation in energy-intensive capital stock due to a variation in per capita income, on top of future climate.	-
Scheduling of generation interruptions	Power system operators can deliberately plan to reduce or interrupt the generation schedule in anticipation of adverse weather conditions.	Planned	• **Low adaptation:** no planned response of operators, exposure to extreme weather results in forced outages (i.e. sudden generation interruptions). • **Reference adaptation:** frequency of planned outages follows historical patterns. • **High adaptation**: when needed, operators always respond to extreme weather exposure though planned outages, reducing to zero the occurrence of forced outages.	ACCREU analysis Sergio and Colelli (in prep.).

2.2. Model development and improvement along the impact assessment modelling chain

We developed and improved IIASA's impact assessment modeling chain to examine the anticipated biophysical impacts of slow-onset climate change on agriculture and forestry sectors and examine the autonomous and planned adaptation solutions with a focus on the EU. In order to conduct the impact assessment on the energy sector, CMCC developed novel econometric and statistical models that capture the role of adaptation on the changes in energy-intensive appliances (AC stock) and final energy demand by sectors, as well as energy supply-side responses to extreme weather in the form of planned and forced power generation outages.

Figure 5 illustrates IIASA's impact assessment modeling chain that integrates various models and data sources to assess the impacts of climate change and adaptation on agriculture, forestry, and the environment. Most of the activities along the impact assessment modeling chain are conducted under ACCREU Task 2.2, however the link to biodiversity modeling (under ACCREU Task 2.4) are included here for completeness.

At the top of the chain, the data from CMIP6 GCMs serves as the foundation for projecting future climate, providing essential climate inputs for the entire modeling process. The sectoral models then use the different climate scenarios and simulate growth in forests, crops, livestock, grassland and changes in runoff to capture the direct effects of climate on the change in productivity, input requirements, or resource availability.

Serving as the core of the modeling chain, GLOBIOM integrates outputs from the sectoral models to assess their interactions and provide a comprehensive analysis of the market implications of climate impacts on different sectors and potential adaptations to climate impacts on the land systems. offers a holistic view of how climate change affects livelihoods and resource allocation.

The results from GLOBIOM are then downscaled provide results at a high spatial resolution. The downscaling facilitates two-way coupling between economic modeling and hydrological modeling. This connection allows for an examination of the impacts of land use change and irrigation expansion on water balance as well as the implications of land use change on biodiversity.

Overall, this impact assessment modeling chain aims to provide a thorough understanding of the complex interactions between climate change, land use, water resources, and economic systems. By integrating various models and simulating changes under different climate scenarios, the framework facilitates informed decision-making and policy development, ensuring that climate adaptation and mitigation strategies are effectively tailored to address the multifaceted challenges posed by climate change.

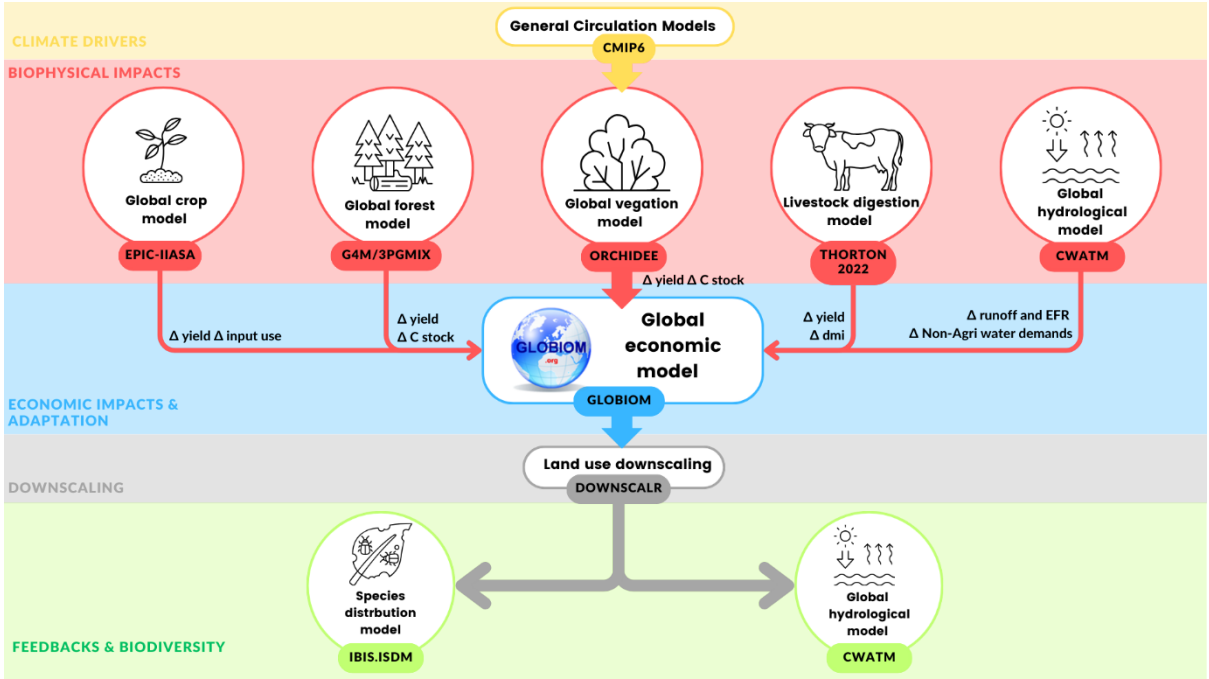

Figure 5 Schematic of the impact assessment modelling chain

2.2.1. Models of the impact assessment chain

An overview of the models included in the impact chain is found in Table 3 Biophysical Impact model overview. Process-based crop models (e.g, EPIC-IIASA) simulate how factors like weather, plant genotypes, environmental conditions, and management practices influence plant growth. In our modeling framework we employ 3PGmix to model the productivity effects of the forest. 3PGmix is a simplified process-based model that predicts forest productivity based on the absorbed photosynthetically active radiation (APAR) and canopy quantum efficiency.

Based on the simulation protocol, we selected the corresponding output from the impact models or if it was unavailable from ISIMIP3b (e.g., RCP4.5) we conducted additional modeling simulations for the biophysical, hydrological, and other process-based models using the monthly or daily projections of temperature (minimum, maximum and average), precipitation, and solar radiation available for CMIP6. These additional simulations are noted in Table 3 as “ACCREU”.

These simulated the changes in the climatic conditions and changes in the productivity and resource requirements forms a basis for connecting our biophysical models with the economic models later on in the impact assessment modeling chain. We connect these models via growth shifters of the various productivity and resource factors in relation to the reference period.

We use a 30-year average to assess slow-onset climate shocks because it helps distinguish the long-term climate trends from short-term weather variability. Climate changes often occur gradually, and short-term variability, such as annual or decadal weather extremes, can mask these trends. A 30-year period smooths out these temporary fluctuations (the "noise") and highlights the underlying long-term changes (the "signal")[1].To calculate this 30-year average for a given year we take the model simulation parameter from that year and average it with the 15 years prior and 15 years following. This gives a smoothed 30-year average which we use to calculate the 30-year shifter. These 30-year shifters are computed as the ratio between different attributes under climate change (e.g., crop yield,

[1] https://www.noaa.gov/explainers/understanding-climate-normals

forest mean annual increment, grassland net primary productivity, livestock dry matter intake) and the same attributes under current climate (Eq. 1).

$$\Delta X = \frac{X_{climate\_change}}{X_{current}} \quad \text{(Eq. 1)}$$

ΔX: shifter of biophysical forest, crop, grassland parameter X (for forest: mean annual increment MAI, soil carbon, standing stock; for crop: yields, irrigation water requirement: for livestock: dry matter intake requirement; for grassland: net primary productivity)
$X_{climate\_change}$: value of biophysical parameter X under climate change averaged over 30 year period
$X_{current}$: value of biophysical parameter X under current climate averaged over 30 year period

Table 3 Biophysical Impact model overview

Sector covered	Model	Model type	Model inputs	Model outputs	Source of data	RCPs
Agriculture -crop	EPIC-IIASA (Balkovič et al., 2013a)	Biophysical crop model	Temperature (tmin, tmax), precipitation, radiative forcing	crop productivity (yields), fertilizer and water requirements	ISIMIP3b	Simulated: RCP 2.6, 7.0 Estimated: RCP4.5
Agriculture-livestock	Livestock Heat Stress	Livestock digestion model	Temperature (tmin, tmax), precipitation, radiative forcing	Dry matter intake, meat and milk production	Thorton et al. 2022 and **ACCREU**	
Agriculture – water	CWatM (Burek et al., 2019)	Hydrological and water demand	Temperature (tmin, tmax), precipitation, radiative forcing	Water available for irrigation (aggregated runoff and non-ag water demand)	ISIMIP3b and **ACCREU**	Simulated: RCP 2.6, 4.5, 7.0
Agriculture - grassland	ORCHIDEE	Vegetation model	Temperature (tmin, tmax), precipitation, radiative forcing	Change in net primary productivity	ISIMIP3b	Simulated: RCP 2.6, 4.5, 7.0
Forest	3PG-Mix (Lessa Derci Augustynczik et al. In prep)	Forest growth model	Temperature (tmin, tmax), precipitation, radiative forcing	Mean annual increment and standing carbon stock.	**ACCREU**	Simulated: RCP 2.6, 7.0 Estimated: RCP 4.5
	ORCHIDEE For countries outside of	Vegetation model	Temperature (tmin, tmax), precipitation, radiative forcing	Change in net primary productivity	ISIMIP3b	Simulated: RCP 2.6, 4.5, 7.0

2.2.2. CWatM model and ACCREU developments

The Community Water Model is an open-source large-scale integrated hydrological and channel model which calculates water availability (surface and groundwater) and environmental flow requirements, as well as the socio-economic water demands and impacts from water infrastructures such as reservoirs, groundwater pumping, and irrigation (Burek et al., 2019). A further description of the open source model and its source code is available at https://cwatm.iiasa.ac.at. Figure 6 shows an overview of the included hydrological process groups into the model.

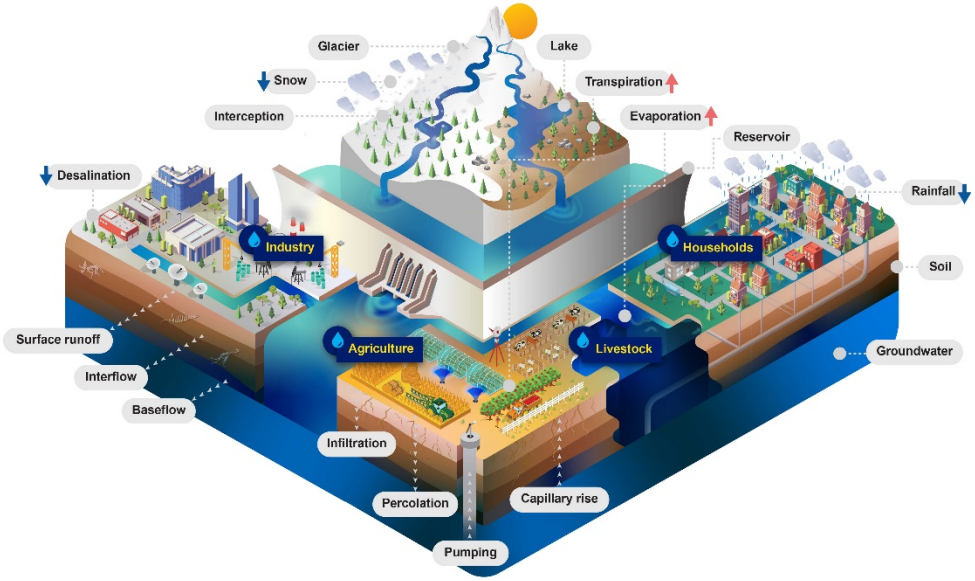

Figure 6 CWATM - Water related processes included in the model design

The model is based on a 0.5°grid aggregating from 30 arc seconds based on the topography and land cover. The hydrological conceptual framework and structure of CWatM are similar to that of other large-scale hydrological models such as H08 (Hanasaki et al., 2010, 2008, 2006), WaterGAP (Alcamo et al., 2003; Flörke et al., 2013), LPJmL (Bondeau et al., 2007; Rost et al., 2008), LISFLOOD(Burek et al., 2013; De Roo et al., 2000), PCR-GLOBWB (van Beek et al., 2011; Wada et al., 2014), VIC (Xu et al., 1994), MHM (Samaniego et al., 2011; Kumar et al., 2013), and HBV (Bergström and Forsman, 1973; Lindström, 1997).

The model was primarily run using CMIP6 climate data, as provided under the ISIMIP3b protocol. This allowed for consistency with widely accepted climate impact projections. CWatM participates in the ISIMIP community and the results from their CMIP6 scenarios for RCP8.5, RCP7.0, and RCP2.6 are available here: https://www.isimip.org/impactmodels/details/257/

Model developments as a part of ACCREU

As a part of the ACCREU project, we also conducted simulations under the RCP 4.5 climate projections, which was not included in the ISIMIP3b protocol. Incorporating RCP 4.5 enabled us to explore a broader range of potential climate outcomes, providing additional insights into the medium-level mitigation pathway that balances emissions reductions and climate impacts. These results will be published as part of the ACCREU scenario explorer. The results from the analysis for RCP 4.5 and the other RCPs is found in Section 3.2.2.

CWatM also projects future water demands based on socioeconomic change. As a part of the ACCREU project CWatM has incorporated new projections for population, GDP per capita, and urbanization

patterns from the latest SSP database (v3.0.1; available at https://data.ece.iiasa.ac.at/ssp/) and developed and published a dataset providing annual water withdrawal and consumption estimates for Europe at a spatial resolution of 5 arcminutes, covering the period from 2020 to 2100 for four SSPs (1, 2, 3, and 5) (Fridman et al., 2024). The dataset is available open-access: 10.5281/zenodo.13767595 The findings from the analysis are found in Section 3.2.1.

2.2.3. GLOBIOM model and ACCREU developments

GLOBIOM is a global partial equilibrium model that is used to model the supply and demand of agricultural products at a high spatial resolution in an integrated approach that considers the impacts of global change (socioeconomic and climatic) on food, feed, and fiber markets (Havlík et al., 2011a). GLOBIOM models the supply and demand for various agricultural and forestry products using regional level and spatially explicit data inputs (Figure 7). In GLOBIOM, land is allocated or converted to production activities in the agricultural and forestry sector in order to maximize the sum of producer and consumer surpluses, subject to market equilibrium and resource, technological, and policy constraints. The equations of the model are linear or have ben linearized so that the model can be solved using a linear programming method. The model is recursive-dynamic and run on ten year time steps, meaning that endogenous model solutions depend on the solutions found for the previous period.

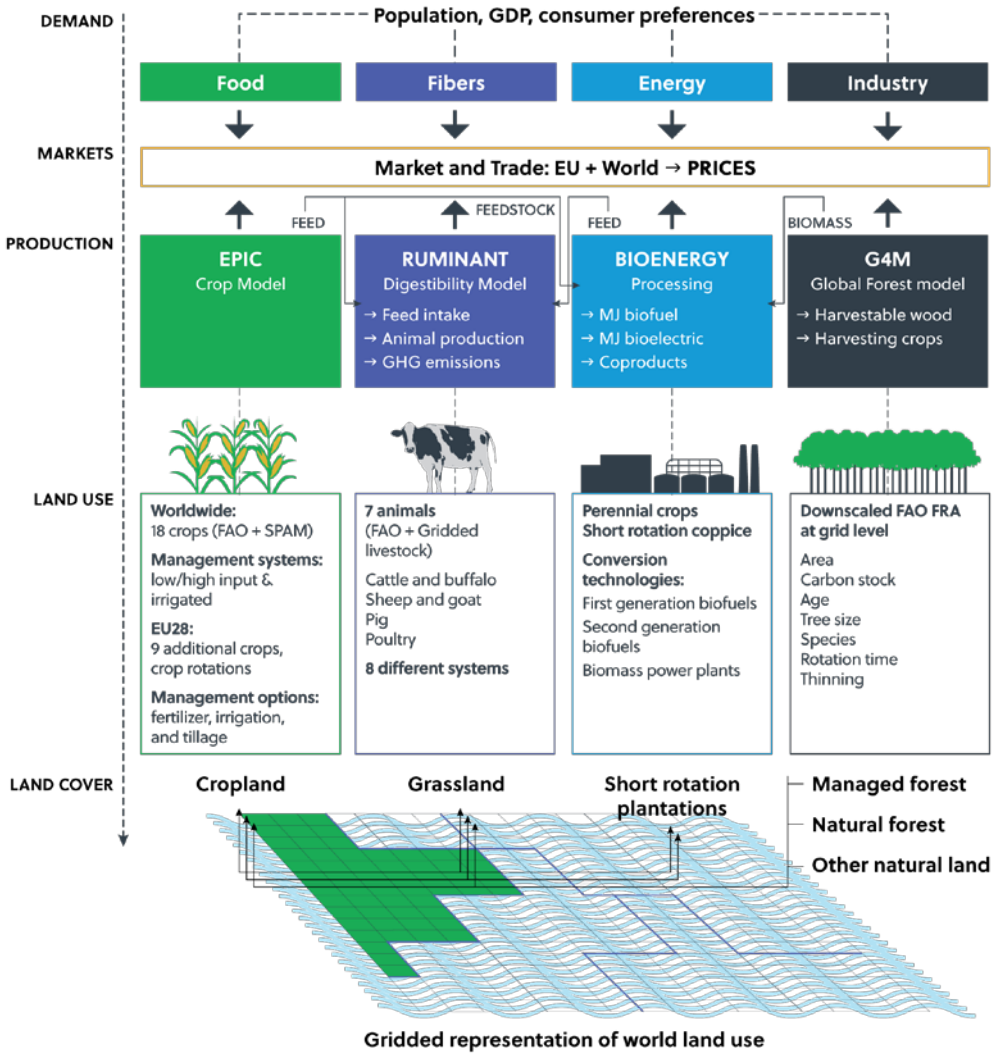

Figure 7 Illustrative representation of the bottom-up structure of GLOBIOM (Source: updated from Havlík et al. (2011a) and GLOBIOM.org)

Model developments as a part of ACCREU

Within the scope of the ACCREU task 2.2, the GLOBIOM model was improved to enable a more comprehensive analysis of the climate impacts across various agricultural and forest sectors. The model incorporated the latest revisions of the Shared Socioeconomic Pathways (SSP) data which directly affect the changes in food demand, well as changes in water demand from non-agricultural sectors as modeled by CWatM. Section 3.2.3 provides additional details on how the water for irrigation and sustainable irrigation is considered within GLOBIOM. GLOBIOM was improved to include the full suite of climate impacts on different agriculture and forest sectors as well as on the water balances. The inclusion of heat stress impacts on livestock and grassland productivity impacts were not initially foreseen at the beginning of the project, but were implemented to enable a more holistic representation and the most advanced representation of cross-sectoral climate impacts on the land sector.

Additionally, model developments were made to better represent agricultural adaptation strategies, particularly the inclusion of irrigation as a viable climate adaptation option. This involved representing the change in water available for irrigation under a changing climate (i.e., water from hydrological modeling) and also accounting for the investments required for implementing irrigation systems as part of the adaptation strategy, including the costs associated with improving efficiency and improving water supply though local/on-farm water storage solutions. These improvements enhance the model's ability to assess the economic feasibility and potential benefits of adopting irrigation in response to climate challenges. Section 0 provides more details on how the adaptation scenarios are considered within GLOBIOM.

2.2.4. Energy models and ACCREU developments

2.2.4.1. Sectoral final energy demand

As a part of the ACCREU project, **we developed an econometric model aimed at providing** new estimates for the climate change impacts on **energy** demand across fuels and sectors at global level and for the EU. We exploit a panel dataset of annual observations across 134 countries and 50 years (1970-2019), comprising: i) population-weighted annual Cooling Degree Days (CDDs, with thresholds alternatively 18°C and 24°C) and Heating Degree Days (HDDs, with thresholds alternatively 15°C and 18°C) from gridded ERA5 data; ii) per capita energy consumption in four sectors (residential, commercial, industrial, agriculture) and for two energy carriers (electricity and fossil fuels) from the IEA statistics; iii) economy-wide per capita GDP and total capital stock per capita from the OECD dataset. We decompose accumulated temperature exposures, in the form of heating and cooling degree days (HDDs and CDDs, respectively), into decadal moving averages and annual anomalies from those slowly-varying means. We use these data to empirically model associations between final demands for electricity and fossil fuels in four economic sectors (residences, services, industry and agriculture) and high-frequency anomalies, which we attribute to intensive margin responses to weather fluctuations, and low-frequency trends, which we attribute to extensive margin responses to climate change, and interactions between the two. We measure the location-specific climate shifts as the 10-year moving average of the variable of interest. For each of the two alternative weather variables, we compute the climatic exposure combining the information of the weather realizations of the previous 10 years in that same location. We compute the vectors of weather anomalies by taking the difference between the observed annual level of CDDs and HDDs and the climate normal.

- Climatic Cooling Degree Days (CDD^{C})
- Climatic Heating Degree Days (HDD^{C})
- Positive and Negative Weather anomaly in CDDs (CDD^{A+}; CDD^{A-})

- Positive and Negative Weather anomaly in HDDs (HDD^{A+}; HDD^{A-})

We estimate a set of fixed-effects (FE) models where the dependent variable is the sector-specific natural logarithm of per capita final energy demand ($q_{i,t}$) and our key meteorological variables are the slowly-moving climate norms ($CDD_{i,t}^{C}$ and $HDD_{i,t}^{C}$) and the vector of hot and cold anomalies ($CDD_{i,t}^{A}$ and $HDD_{i,t}^{A}$). Location (μ_i) and time (λ_t) fixed effects are included to flexibly control for unobservable variable biases resulting from unit-specific time-invariant characteristics and year-specific global shocks, while the level of income per capita is included as a control (Eq. 2) or, in an alternative model, as a modulation effect of the weather impacts (Eq. 3).

$$q_{i,t} = \alpha\, CDD_{i,t}^{C} + \beta HDD_{i,t}^{C} + CDD_{i,t}^{A}\left(\gamma + \delta CDD_{i,t}^{C}\right) + HDD_{i,t}^{A}\left(\theta + \vartheta HDD_{i,t}^{C}\right) + \rho\, y_{i.t} + \mu_i + \lambda_t + \varepsilon_{i,t} \qquad \text{(Eq. 2)}$$

$$q_{i,t} = CDD_{i,t}^{C}(\alpha + \alpha^{y}\overline{y_i}) + HDD_{i,t}^{C}(\beta + \beta^{y}\overline{y_i}) + CDD_{i,t}^{A}\left(\gamma + \delta CDD_{i,t}^{C}\right) + HDD_{i,t}^{A}\left(\theta + \vartheta HDD_{i,t}^{C}\right) + \rho\, y_{i.t} + \mu_i + \lambda_t + \varepsilon_{i,t} \qquad \text{(Eq. 3)}$$

Through this approach, we provide an empirically-grounded decomposition of final energy demand into changes associated with slowly evolving climate trends and high-frequency meteorological anomalies, while controlling for the modulating effects of per capita income on these responses.
The decomposition of observed weather realizations between climatic CDDs and HDDs - and hot and cold anomalies shows that --- over the 50 years of our panel --- the global, population-weighted, climatic CDDs (HDDs) have steadily increased (decreased) (Figure 8, Panel a). Hot weather anomalies can magnify the long-term warming trend: while the mean global population weighted additional unexpected CDDs is 23 CDDs (or 4% of the median climatic CDD level), the maximum observed global hot anomaly reached around 100 CDDs (or 17% of the median climatic CDD level). The relatively homogeneous level of exposure to anomalies across climatic conditions is an important source of variation allowing us to evaluate empirically the interaction effects between short- and long- term adjustments (Figure 8, Panel b). Importantly, the within-country variation in the slowly moving climatic CDDs and HDDs is affine in magnitude to the short-term variations in CDDs and HDDs (Figure 8, Panel c), suggesting that meaningful within-country climatic information can be extracted from an empirical setting based on panel data with fixed-effects.

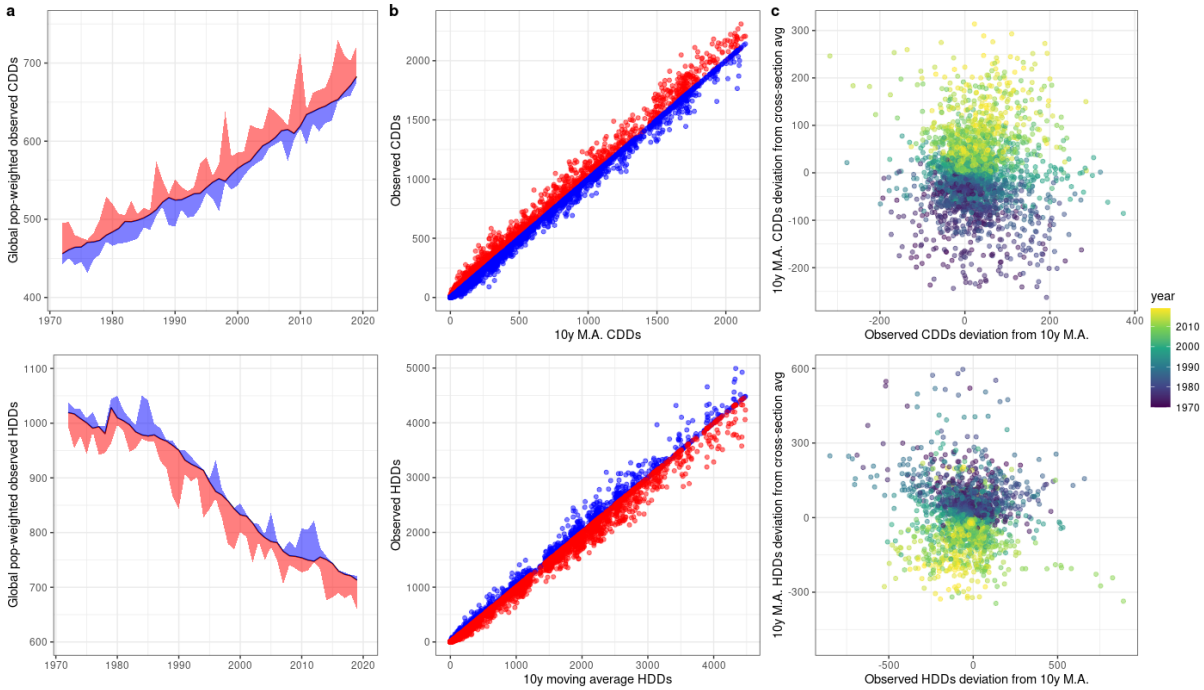

Figure 8 Decomposition between climatic and anomalies CDDs or HDDs.

(a) Population-weighted global level trends in climatic CDDs and HDDs (black line) and short-term hot and cold anomalies (red and blue shades), resulting in the actual observed weather exposure. (b) Population-weighted country level climatic CDDs and HDDs (black line) and short-term hot and cold anomalies (red and blue shades), resulting in the actual observed weather exposure. (c) Population-weighted country level relationship between the within-country long-term changes in the climatic CDDs and HDDs (computed as the difference in the yearly climatic CDDs and HDDs with respect to the average country-level climatic CDDs and HDDs) and the short-term changes in CDDs and HDDs (computed as the difference in the yearly observed CDDs and HDDs with respect to the climatic CDDs and HDDs).

2.2.4.2. Residential air-conditioning stock and demand

Besides estimating climate-change impacts on the macro energy demand indicators, we also developed a global-level household microdata-based Random Forest non-parametric statistical model to predict **cooling appliance ownership** and **household cooling electricity consumption** at the household level, and provide prediction and projections on a global gridded scale. The methodology is extensively documented in Falchetta et al. (2024). Figure 9 below shows the underlying framework and estimated prediction space.

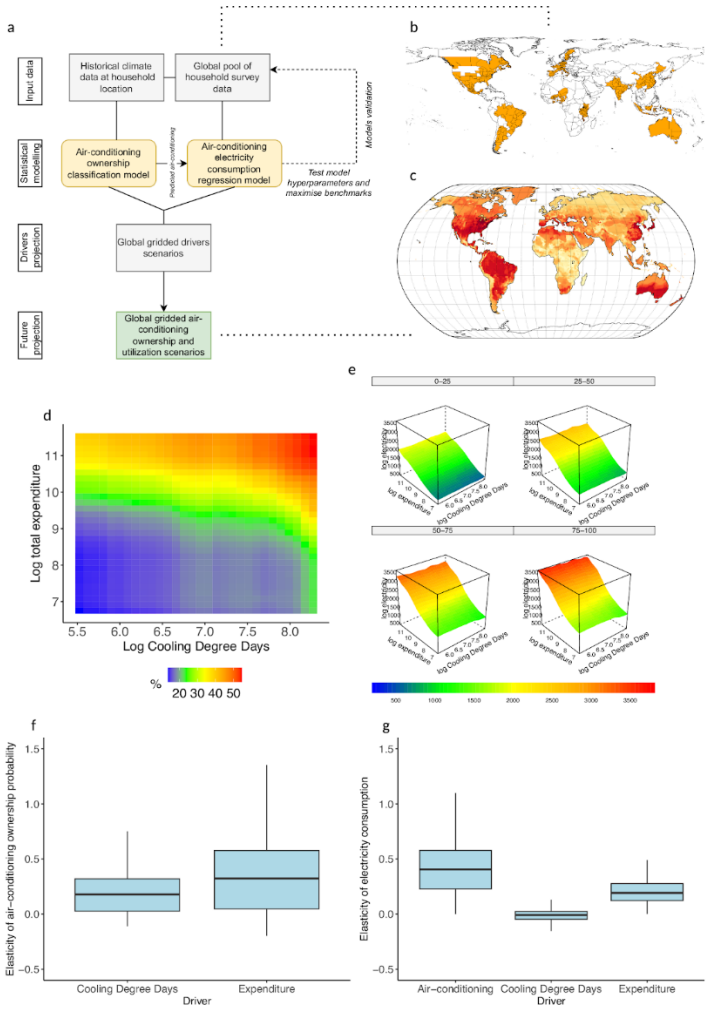

Figure 9 Statistical framework and estimated prediction ranges of the analysis presented in this paper.

(a) Flowchart of the residential air-conditioning (AC) analysis; (b) Countries covered in the household survey global pool database; (c) Representative example of output gridded projections; (d,e) Partial dependence plots (conditional probabilities for the 1st stage AC ownership model; expected values for the 2nd stage electricity consumption model, by AC ownership probability bins); (f,g) Box plots of the distribution of the estimated partial elasticities derived from the models' partial dependencies.

The first stage model predicts household-level AC penetration as a function of a vector X of climate and socio-economic drivers for household *i* in country *c fixed effects*:

$$AC_{i,c} = f(X_{i,c}) + i + c \qquad \text{(Eq. 4)}$$

where the vector of variable *X* includes: CDD, Cooling Degree Days; HDD, Heating Degree Days; HURS, Relative Humidity; Total yearly household expenditure; Household head gender; Household head age; Household head education; Household size; Household home ownership status; Household sampling weights; Urbanization status. Then, the second stage model predicts household-level electricity consumption as a function of the predicted air conditioning penetration in the first stage, as well as the same vector X of climate and socio-economic drivers.

$$ELY_{i,c} = f(AC_{i,c} + X_{i,c}) + ic \qquad \text{(Eq. 5)}$$

We trained the two random forest models on the pooled household sample (trimming the tails of the within-country distributions at the 1st 99th percentiles for all variables). The first model is a classification probability model to assess whether a household owns at least an AC unit. The second

model is a regression model to predict household yearly electricity consumption as reported from the survey data. The model is validated both on the training data (household level) and at the country level by aggregating predictions and comparing them against the household survey-based statistics as well as other sources of recent national AC statistics (see Falchetta et al. 2024 for details and accuracy metrics). The cross-validation procedure demonstrates that the model performs well on unseen data, while the aggregated prediction validation shows that the model predictions at the grid-cell level are internally consistent with national-level statistics.

To conduct the study, we assembled a globally-relevant household micro data database covering more than 500 sub-national administrative units from 25 countries. Together, these countries represent 62 percent of the world's population and account for 73% of the global electricity consumption. For each survey we gather information on annual electricity expenditure (also on quantity when available), air-conditioning ownership, total household expenditure, electricity prices, and several socio-economic and demographic variables. We limit our sample to non-missing air-conditioning and non-missing electricity data. This means that our data set excludes households that did not have access to electricity during the survey year.

Historical climate data is drawn from the European Centre for Medium-Range Weather Forecasts's ERA-5 historical climate reanalysis data product, covering the period 1970-2019, and having a spatial resolution of 0.25 arc-degrees. We obtain daily average temperature to calculate Cooling and Heating Degree Days (CDDs and HDDs) at each year and pixel, adopting the temperature threshold of 18C. Moreover, we also include climate relative humidity (*HURS*), which is a further input to the model given its crucial importance for heat perception and impacts. Household data are then merged with this information using the most disaggregated geographical information available (e.g. provinces or districts) in each survey, and the year in which the survey is conducted. Particularly, we collapse across grid cells within each administrative unit using population weights in order to represent temperature exposure for the average person within a unit.

2.2.4.3. Power generation supply

Within the ACCREU project we empirically analyzed how extreme weather conditions affect thermal (nuclear, coal, gas, and oil) and renewable (hydro) power generation across Europe. By matching high-frequency data on power outages with detailed weather exposure at the power plant level from 2017 to 2023 across 20 European countries, we investigated both unplanned (forced) disruptions and planned outage decisions during extreme weather events. We use panel data from the ENTSO-E Transparency Platform at the power plant level, detailing both forced and planned outages from 2017 to 2023 across 20 European countries. The dataset includes detailed characteristics of 929 power plants, encompassing different technologies: nuclear, coal, gas, and three hydro types (reservoir, run-of-river, pumped storage), along with their geographical coordinates (latitude and longitude) and nominal power capacity (see Figure 10, panel a). The dataset includes 44,637 recorded forced outages and 62,672 planned outages. Planned outages stem from maintenance schedules and operational strategies, while unplanned outages occur due to technical failures. From this data, we construct a panel dataset at the power plant and daily level, where a binary variable indicates the occurrence of an outage (1 for an outage, 0 for no outage), resulting in over 1.4 million observations. The original hourly outage data has been aggregated to a daily level to simplify analysis by matching it with daily level weather data. At the European level, the total number of daily outages shows both an upward trend and significant seasonal variation, particularly for planned outages (see Figure 10, panel b). The average frequency of these events varies by technology and outage type (forced vs. planned). Planned outages are slightly more common than forced ones, with hydro-power pumped generators

experiencing the highest likelihood of outages, while nuclear power has the lowest (see Figure 10, panel c). Both forced and planned outages tend to be concentrated in days where the power plant experiences uncommon exposure to weather, although the type of outage affects the correlations (see Figure 10, panel d).

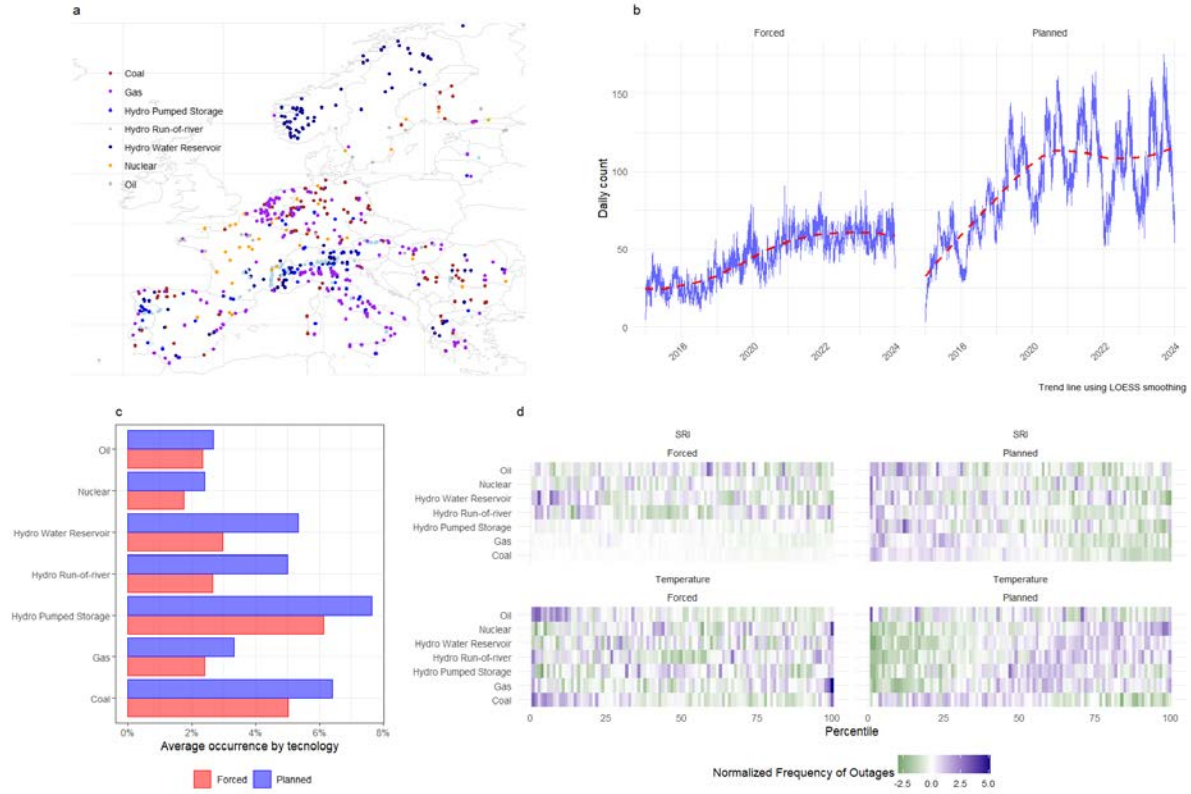

Figure 10 Planned and forced outage data.

(a) Map showing the geographical distribution of the power plants considered in the study, colored by technology type. (b) EU-level daily sum of outages (blue line) and its smoothed trend (red line). (c) Observed average outage probability by technology and outage type. (d) Heatmap of the normalized EU-level frequency of outages ordered by the percentiles of temperatures and Standardized Runoff Index (SRI) computed at the power-plant level.

To conduct the empirical analysis, we compile a dataset of weather variables, including temperature, precipitation, and water runoff, sourced from the Copernicus ERA5 reanalysis data. Hourly data is used to calculate daily maximum and minimum temperatures, while water runoff is used to compute the Standardized Runoff Index (SRI), a common indicator for floods and droughts. To assess the impact of extreme temperatures on energy systems, we apply a binning strategy based on percentiles at the power plant level. The l-th upper percentiles of maximum temperatures ($Tmax_{i,t}^{l}$) span from above 98th, 95th–97th, 90th–94th percentile intervals, and represent heatwave exposure, while the k-th lower percentiles of minimum temperatures ($Tmin_{i,t}^{k}$) pan from the 10th–6th, 5th–3rd, and below 2nd percentile and indicate cold spells. Our primary model uses 1-month and 3-month SRI time spans, as shorter periods capture recent conditions that more accurately affect plant operations. To ensure robustness, we also test other SRI periods. Finally, we classify drought and flood conditions into three levels—Moderate, Severe, and Extreme—according to standard threshold values (Svoboda et al., 2012).

We use a fixed-effects logistic regression model to analyze the impact of extreme weather events on power plant outages. This model has the advantage of not requiring restrictive assumptions about the relationship between unobserved heterogeneity and observed covariates. We use plant-by-month and country-year fixed effects to control for both spatial and temporal heterogeneity:

$$\Pr(outage_{i,t} = 1) = \alpha^l(Tmax_{i,t}^l) + \beta^k(Tmin_{i,t}^k) + \gamma^z SRI_{i,t}^z + \delta_{i,m} + \theta_{j,y(t)} + \varepsilon_{i,t} \quad \text{(Eq. 6)}$$

Where i is the power plant, t is the day, $\delta_{i,m}$ is the power plant by month fixed effect and $\theta_{j,y(t)}$ is the year by country j fixed effect. We use Conley standard errors (Conley, 1999)to account for spatial and temporal correlations in our error terms, as power plants nearby or experiencing similar weather conditions may have correlated errors. This correction improves the accuracy of our standard errors by accounting for potential spillover effects of extreme weather across plants within a certain distance or time window.

3.1. Agriculture and Forestry

This following section provides a comprehensive analysis of the projected climate change impacts on various agricultural and forestry sectors. By examining a range of crops, livestock, and forest ecosystems, we assess how different climate scenarios, which are represented by changes in temperature, precipitation, and radiative forcing, affect productivity and input requirements of forest and agriculture sector activities.

The analysis in this section focuses on the direct impacts (e.g., yield changes) on staple crops (e.g., maize, wheat) in Section 3.1.1, livestock in Section 3.1.2, grassland productivity in Section 3.1.3 and forest productivity in Section 3.1.4.

3.1.1. Crop yields and irrigation water requirements

Crop yields

The direct impacts of climate change on yields have been examined at mid and end-of-century using a multi-model ensemble from CMIP6 data by Jagermeyr et al. (Jägermeyr et al., 2021). The study found that variability in crop yields were due to different climate models, CO2 fertilization effects, and other climate factors, though there was good model agreement in the direction of impacts for several crops in the European context. For the ACCREU project, we use the climate-induced crop yield and irrigation water requirement changes modelled at a high spatial resolution by IIASA's globally gridded crop model, EPIC-IIASA). From the multi-model assessment, EPIC-IIASA was found to perform well in simulating crop responses to climate change, particularly in capturing CO2 fertilization effects and water stress impacts. Its projections aligned with the broader ensemble of models, showing both yield increases for certain crops like wheat under lower emissions and yield declines for water-sensitive crops like maize and soybean under high-emission scenarios. For CMIP6 EPIC-IIASA directly simulated yields for four crops: maize, soybean, wheat and rice. To model climate change impacts for the rest of the crops in GLOBIOM, we map the crop yield impacts from the four simulated crops to the other crops in a similar way as the mapping used by Müller and Robertson (2014) for DSSAT (Table 4).

Table 4 Mapping of corn, wheat, rice and soya yield simulations from EPIC to all crops in GLOBIOM. Source: Janssens et al. (2020)

GLOBIOM crop	Mapping
Corn	Corn yield is directly simulated
Rice	Rice yield is directly simulated
Soybean	Soybean yield is directly simulated
Wheat	Wheat yield is directly simulated
Millet, sorghum	Millet and sorghum are represented by modified corn yield simulations: only half of the negative effects are applied due to better drought tolerance
Sugar cane	Sugar cane yield is represented by corn yield simulations

Other grains (barley)	Barley is represented by modified wheat yield simulations: only half of the negative effects are applied due to better drought tolerance
C3 crops (cassava, groundnuts, rapeseed, sunflower, palm, chickpeas, cotton, potatoes, sweet potatoes, beans)	C3 crops are represented by the average climate impact on the three C3 crops that are directly simulated (wheat, rice and soybean)[2]

Of the directly simulated crops, maize and wheat are the most important for Europe so this section will focus the results on these crops unless otherwise noted.

Table 5 Country aggregation for major European regions

Central and Eastern Europe	Austria, Czech Republic, Hungary, Poland, Romania, Slovakia, Slovenia
Northern Europe	Denmark, Estonia, Finland, Ireland, Latvia, Lithuania, Sweden
Southern Europe	Bulgaria, Croatia, Cyprus, Greece, Italy, Malta, Portugal, Spain
Western Europe	Belgium, France, Germany, Luxembourg, Netherlands
Rest of Europe	Albania, Bosnia and Herzegovina, Greenland, Iceland, Macedonia, Montenegro, Norway, Serbia, Switzerland, and United Kingdom

Maize yields are projected to decline over time which could lead to a decrease in production of, on average, **9.8 M tons dry matter (-15% of the 2020 production levels)** and **34.5 M calories** in RCP 7.0 (assuming no change in management or areas) (Figure 11). For RCP 2.6, the losses by 2050 could still be on average, 7.7 M t dm (-12% of the 2020 production levels). The magnitude of these losses depends on the specific climate model, RCP, and region. On average, the production gaps from climate change under RCP 7.0 will likely be seen in Western and Southern Europe (around 39% and 36% of the total European regional gap, respectively), and 16% for Central and Eastern Europe and 10% for the rest of the countries in the wider European area, when weighted by the historical cropland area under maize production. The regions with the least GCM agreement in direction of the impact on maize yields (i.e., the most uncertainty variability) was Northern Europe (Table 6), because there is very little maize grown in these countries. In Table 6, the symbol "+" indicates three of four GCMs indicate positive change, "-" indicates negative change and no agreement indicates that the GCMs were split with half indicating positive and half indicating positive change.

Table 6 Average climate impact on crop yields and the direction of GCM agreement in 2050 for Europe and major subregions of Europe based on EPIC-IIASA CMIP6 projections

Wheat	**Average of the GCM ensemble yield / direction of GCM agreement Yields in 2050**[3]			
	RCP 2.6		**RCP 7.0**	
Northern Europe	-2.0%	No Agreement	-8.0%	No Agreement
Western Europe	-1.3%	No Agreement	-2.5%	No Agreement

[2] Using an average of wheat, rice and soybean impacts weighted by base year area x yield

[3] At least 75% GCM ensemble agreement, in this case 3 of 4 GCMs

Central and Eastern Europe	-2.0%	No Agreement	-1.0%	+[4]
Southern Europe	-0.8%	No Agreement	-0.7%	-
Rest of Europe	-2.9%	-	-6.4%	-
Europe	-1.6%	No Agreement	-2.7%	No Agreement
Coarse Grains	**RCP 2.6**		**RCP 7.0**	
Northern Europe	0.0%	No Agreement	-2.6%	No Agreement
Western Europe	-5.0%	-	-6.9%	-
Central and Eastern Europe	-4.3%	-	-3.8%	-
Southern Europe	-4.9%	-	-6.7%	-
Rest of Europe	-3.7%	-	-6.7%	-
Europe	-4.3%	-	-5.6%	-

Wheat yields have more mixed impacts over time largely driven by the CO2 fertilization effect. Two GCMs (UKESM1-0-LL and GFDL-ESM4) show European production gap from the impacts of climate change, reducing production by up to 18 M tons dry matter in 2050. Two GCMs (IPSL-CM6A-LR and MPI-ESM1-2-HR) show a positive impact from climate change that could add up to 3 M tons try matter in 2050. In regions with agreement in the negative direction of the impacts (e.g, Southern Europe and Rest of Europe), the decrease at a European level would be, on average, **1.5 M ton dry matter,** again assuming no change in management or areas (Figure 11). The magnitude of these losses depends on the specific climate scenario and region, management system and crop. For the average GCM, the impacts on rainfed yields were most negative in Southern Europe (e.g., France, Spain and Italy). The regions with the least GCM agreement in direction of the impact on wheat yields (i.e., the most uncertainty variability) was Northern and Western Europe (Table 6). In the Annex there is an additional figure of the climate impacts on maize and wheat yield as modeled by EPIC-IIASA weighted by harvested area in 2000 by European country under RCP 2.6 and RCP 7.0.

[4] The average GCM ensemble is negative but the direction of agreement is positive due to one GCM (UKESM1-0-LL) with a larger negative impact than the other 3 GCMs with positive impacts.

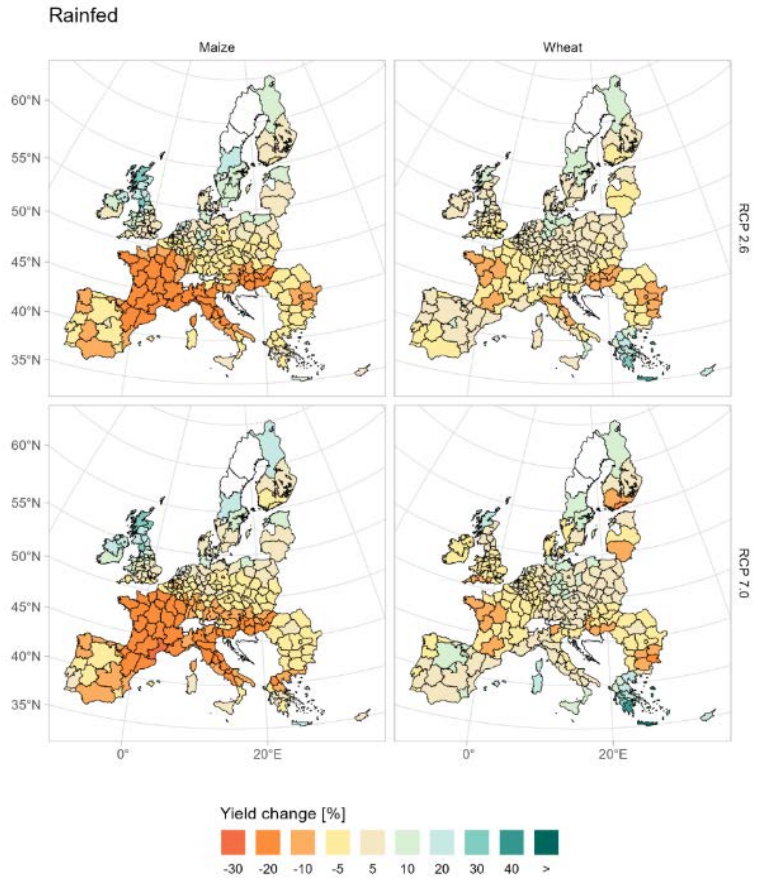
Rainfed
Maize
Wheat
60°N
55°N
50°N
45°N
40°N
35°N
0°
20°E
RCP 2.6
RCP 7.0
Yield change [%]
-30 -20 -10 -5 5 10 20 30 40 >

a)

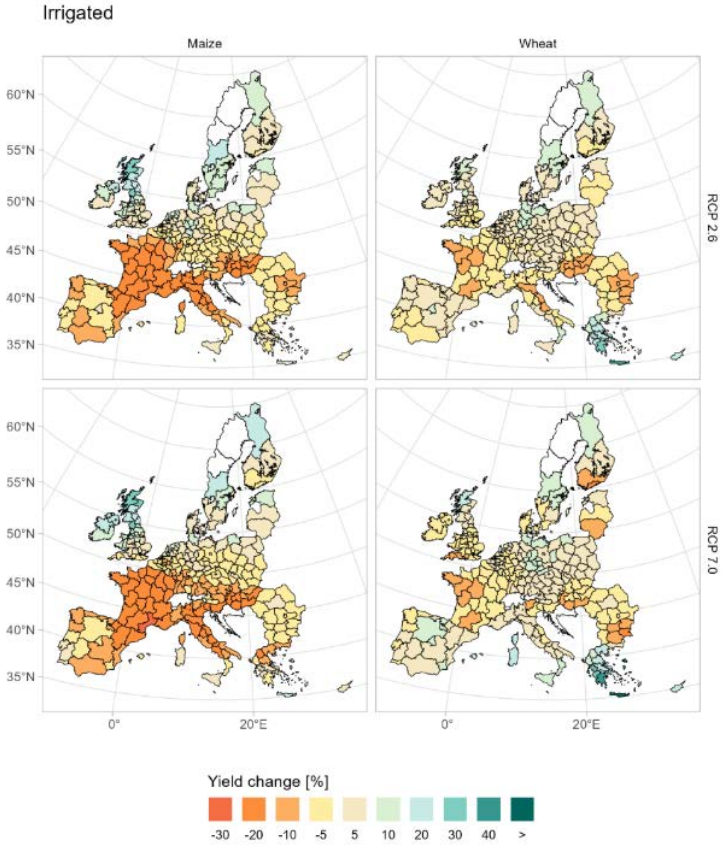
Irrigated
Maize
Wheat
60°N
55°N
50°N
45°N
40°N
35°N
0°
20°E
RCP 2.6
RCP 7.0
Yield change [%]
-30 -20 -10 -5 5 10 20 30 40 >

b)

Figure 11. Projected mid-century (2035-2065) climate change impacts on rainfed (a) and irrigated yields (b) in Europe by mid-century. Percentage change with respect to yields under current climate.

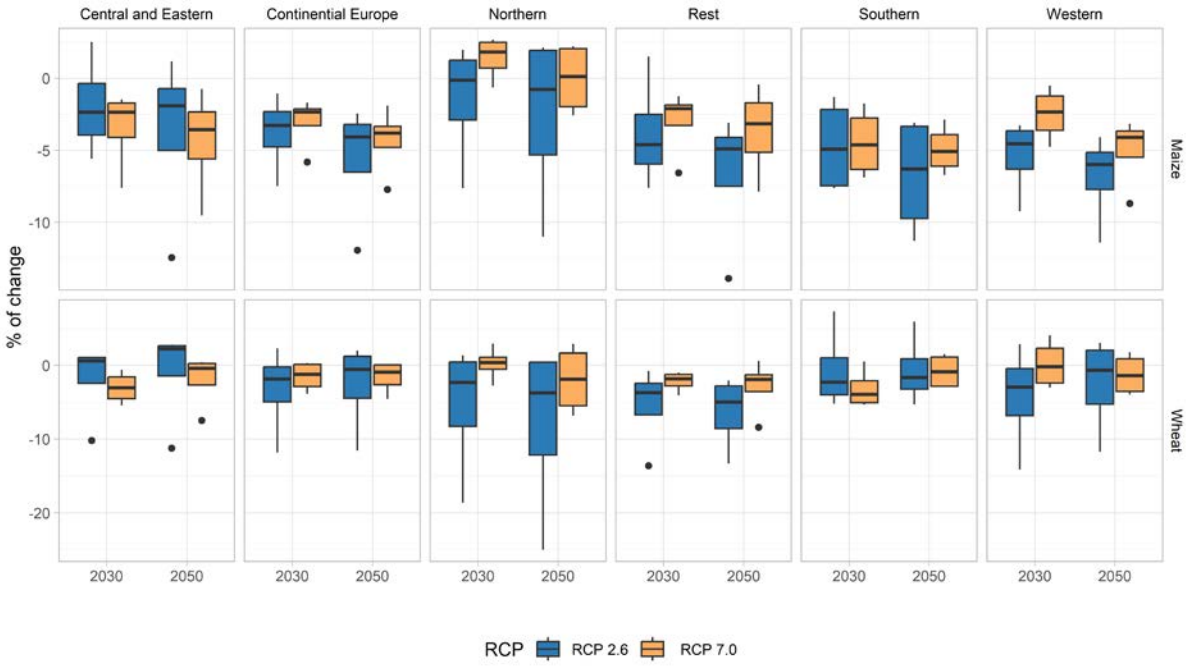

Figure 12. Relative change in crop yields under climate change compared to reference period of no climate change for aggregate regions in Europe. Percent change with respect to current climate.

Irrigation water requirement

Irrigation water requirements as modeled by EPIC-IIASA for CMIP6 fluctuate in response to the shifts in the crop productivity, with increased crop productivity generally increasing the water demand, while lower productivity may reduce it. This relationship reflects how more water is often required to support the increase in productivity, whereas in less productive regions, the demand tends to decrease accordingly.

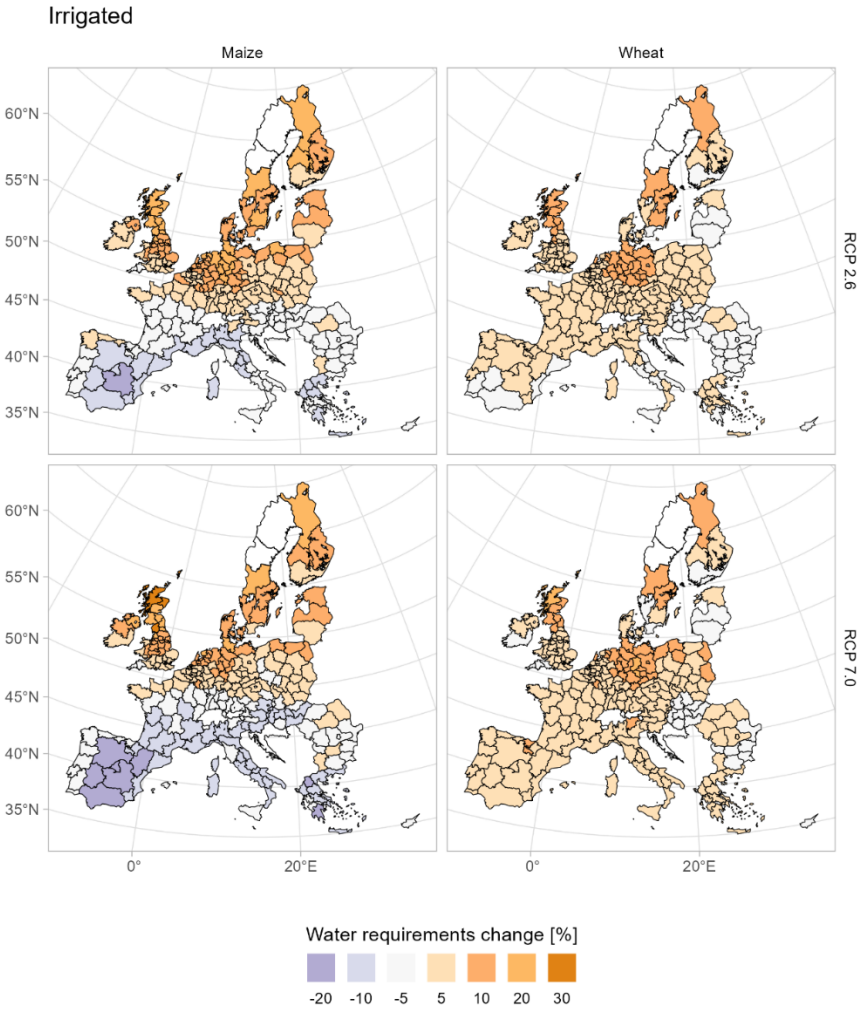

Figure 13. Projected mid-century (2035-2065) climate change impacts on crop irrigated water requirements in Europe

3.1.2. Temperature stress on livestock feeding and productivity

Temperature stress is an increasingly critical issue for livestock production systems worldwide, particularly as climate change leads to rising global temperatures. This phenomenon significantly impacts the health and productivity of ruminants, affecting their dry matter intake (DMI), weight gain and milk yield (Thornton et al., 2022). Thorton et al (2022) found that future temperature extremes may cause animals struggle to maintain their thermoneutral zone, and that their ability to consume feed decreases in cases of heat stress, which in turn diminishes productivity and can lead to economic losses for producers. We utilize the livestock temperature stress effects from Thorton et al. (2022) to assess how rising temperatures directly influence feed demand and productivity to understand how climate change affects agricultural productivity and food security. As many ruminants are fed by grasslands, the impacts from climate change on livestock dry matter intake are intrinsically linked with the climate impacts on grasslands (Section 3.1.3 Grassland productivity impacts).

The change in dry matter intact includes both the grass and crop feeds and also affects the productivity including meat and milk of livestock. These changes in dry matter intact also consider diet structure of the different livestock production systems. The changes in dry matter intake around mid-century

are relatively limited but the decrease in dry matter intake can be seen in the regions facing the greater anticipated temperature changes with respect to present climate (e.g., Southern Europe and Northern Europe).

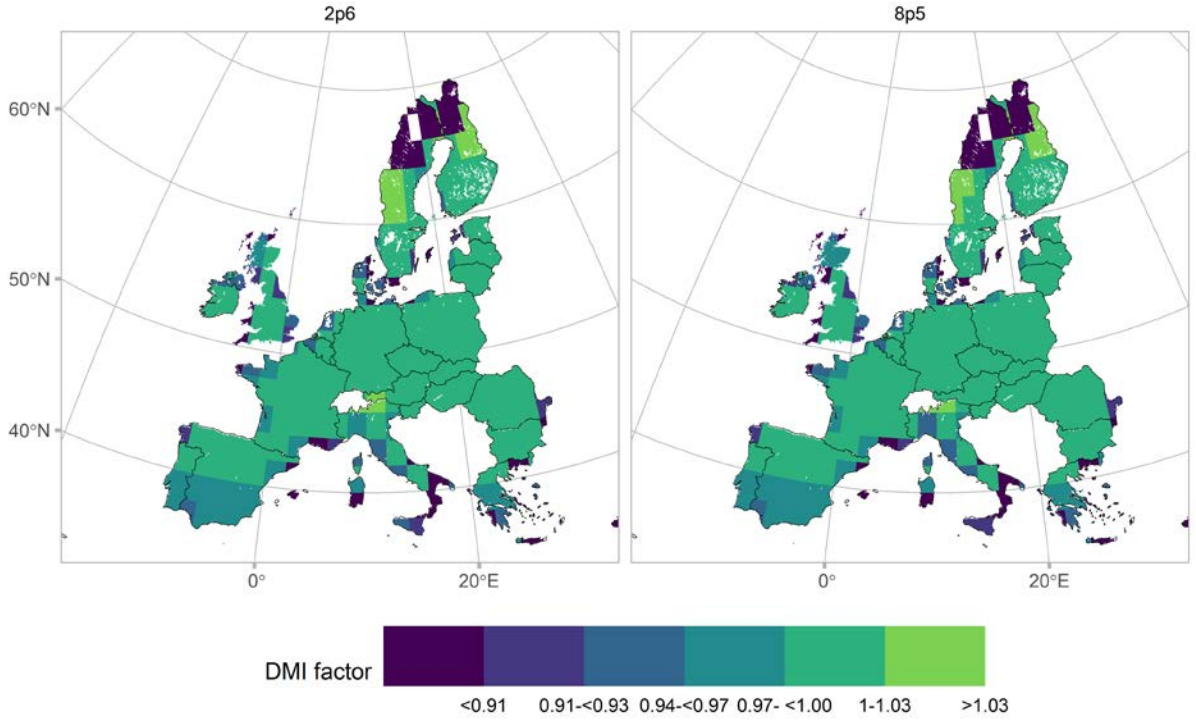

Figure 14. Projected mid-century (2035-2065) climate change impacts on productivity for ruminant animals in Europe

3.1.3. Grassland productivity impacts

The ORCHIDEE model, which stands for "Organizing Carbon and Hydrology in Dynamic Ecosystems," is a process-based vegetation model used to simulate carbon, water, and energy exchanges between land surfaces and the atmosphere. Developed at the Laboratoire des Sciences du Climat et de l'Environnement (LSCE) in France, it is part of the IPSL (Institut Pierre-Simon Laplace) Earth system model framework and integrates modules for plant growth, soil processes, hydrology, and nutrient cycling. It is often used for studying the impacts of climate change on ecosystems, including grasslands, forests, and croplands.

In ORCHIDEE, grassland productivity is modeled by capturing the physiological processes that drive growth, such as photosynthesis, respiration, and allocation of carbon to leaves, stems, and roots. The model incorporates environmental factors like temperature, solar radiation, soil moisture, and atmospheric CO_2 levels, which influence photosynthetic rates and, consequently, biomass production. Grassland productivity in ORCHIDEE is highly responsive to climatic conditions and resource availability. For example, under adequate water and nutrient supply, higher temperatures or elevated CO_2 can boost productivity, while drought conditions or nutrient limitations can lead to reductions.

From the vegetation model ORCHIDEE we modelled the impacts on the net primary productivity. The NPP reflects the rate at which a plant converts atmospheric carbon dioxide into biomass through

photosynthesis, indicates grassland productivity, with higher values suggesting greater growth potential. Figure 15 shows the projected changes in grassland net primary productivity (NPP) across Europe under the three different pathways: RCP2.6, RCP4.5, and RCP7.0. Most of Europe sees minor to moderate increases in grassland productivity, particularly in central and southern regions (shown in light green to teal colors). Under higher warming levels the positive productivity impacts are more pronounced. The strong negative impacts in Scandinavia are likely an artifact of the vegetation modeling.

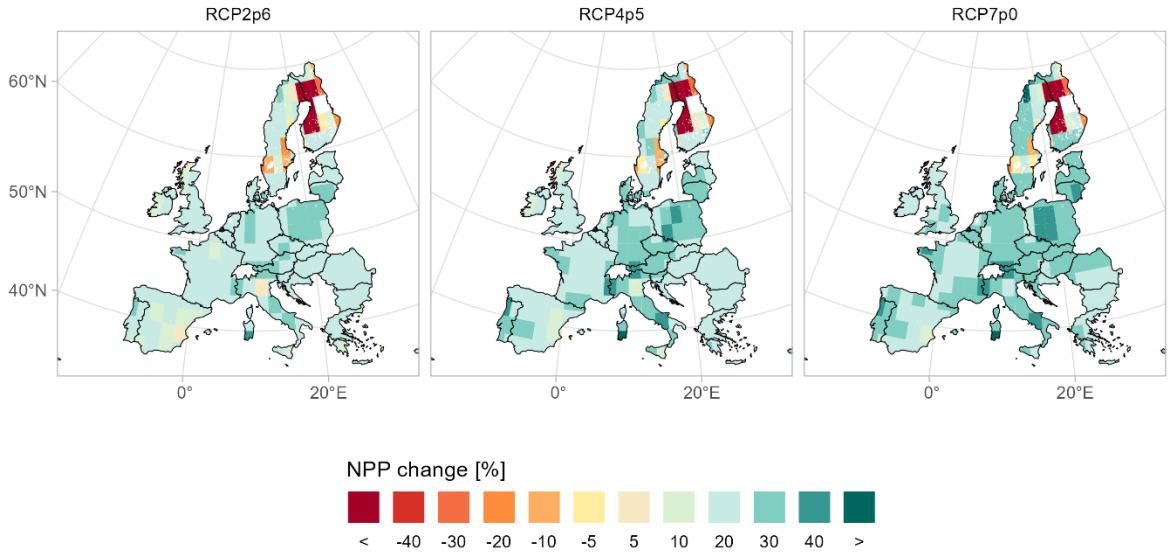

Figure 15. Projected mid-century (2035-2065) climate change impacts on grassland productivity in Europe

In the Annex there is a further information on the change in grassland productivity as modeled by ORCHIDEE for European countries under RCP 2.6, RCP 4.5, RCP 7.0.

3.1.4. Forest productivity impacts

From the forest growth model 3PGmix we modelled the impacts on the mean annual increment. The MAI reflects the average wood production at a certain reference age and is a basis for the harvesting potentials. The standing stock refers to the total living biomass which can depend on the age class dynamics.

Figure 16 shows the projected change in the mean annual increment across Europe under the three different pathways: RCP2.6, and RCP7.0. We can observe the regional variations in climate change effects; where the highest increase occurs in the boreal zone, especially central Sweden and Finland, as well as mountainous areas in central Europe. Moreover, Mediterranean forests displayed decreases in standing stocks due to the increase in aridity in the region, with lower precipitation and higher temperatures.

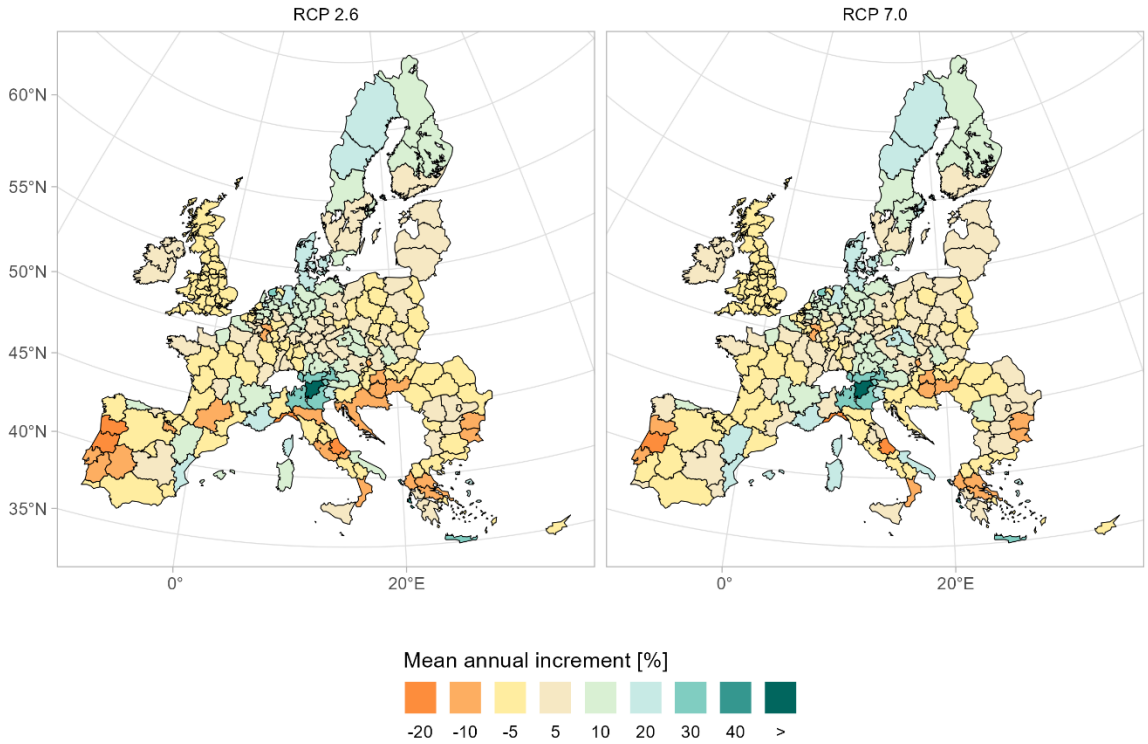

Figure 16. Projected mid-century (2035-2065) climate change impacts on forest productivity in Europe

3.2. Water

The following section examines the water resources. We present the water demand for domestic and industrial use driven by socioeconomic changes (e.g., population and GDP), the changes in aggregated runoff patterns due to climate change. Additionally, we present the availability of sustainable water resources for use by irrigation.

3.2.1. Water demand for domestic and industrial uses

High-resolution (5 arcminute) projected water withdrawal and consumption for Europe were produced in for the ACCREU project. We followed the methodology outlined by Wada et al. (2011a, 2011b) and incorporates new projections for population, GDP per capita, and urbanization patterns from the latest Shared Socioeconomic Pathways (SSP) database (v3.0.1; available at https://data.ece.iiasa.ac.at/ssp/) (Fridman et al., 2024).

Since the SSP update is still in progress as of October 2024, some necessary input data are sourced from an earlier version of the SSP data (SSP 2013, see Table 7). The dataset provides annual water withdrawal and consumption estimates for Europe at a spatial resolution of 5 arcminutes, covering the period from 2020 to 2100 for four SSPs (1, 2, 3, and 5). Below, we outline the procedure used to downscale the population projections to a 5-arcminute resolution and describe the main equations applied to project water withdrawal and consumption under different SSPs.

Table 7: Data availability in different versions of the SSP database as of October *2024.*

Data	SSP Database Version	Water demand module

Population	SSP v3.0.1 2024	Domestic
GDP per capita	SSP v3.0.1 2024	Domestic/industrial
Energy use per capita	SSP 2013	Industrial
Electricity use per capita	SSP 2013	Industrial

Water withdrawal and consumption for the domestic and industrial sectors is projected at the national level, based on GDP per capita (for both domestic and industrial sectors) as well as energy use and the proportion of electricity in total energy use (for the industrial sector). The projected population grids are derived from the SSP national population estimates and country-specific population allocation weights.

Historical water withdrawals

Historical water withdrawal and a common baseline for future projections. The calculation of the historical domestic and industrial water withdrawal follows the approach developed by Wada et al. (2011) and used by the PCR-GLOB hydrological model in the Water Futures and Solutions (WFaS) project. An extensive description of the procedure can be found in Wada et al. (2016).

Domestic water withdrawals per capita, used as a baseline for the historical water withdrawal workflow, were extracted from the World Bank Data Bank[5]. The water withdrawal per capita for the reference period (~2020) and a country i ($wwcap_{REF,i}^{DOM}$) is calculated in Eq. 7 as:

$$wwcap_{REF,i}^{DOM} = \sum_{t=2015}^{2020} \frac{{ww_{t,i}}^{TOT} \times fDom_{t,i}}{P_{t.i}} \quad \text{(Eq. 7)}$$

where ${ww_{t,i}}^{TOT}$ is the national total annual water withdrawal in country i during year t (m3 per year), $fDom_{t,i}$ is the fraction of domestic water withdrawal relative to the national total withdrawal (ranges between 0 -1), and $P_{t.i}$ is the national population size in country i and year t (number of people).

Industrial water withdrawal per grid cell, used as a baseline for the historical water withdrawal workflow, was compiled by Wada et al. (2011a) based on multiple sources (Shiklomanov, 1998; Vorosmarty et al., 2005). The baseline grid represents the year 2000 and aligns with the global industrial water withdrawal figure extracted from the AQUASTAT database (FAO, 2024).

Future projections of water withdrawals

We have used the simulated historical values for 2020 as a baseline to project both domestic and industrial water withdrawal into the future. This approach assures a consistent and smooth transition between the historical and future water withdrawal, yet it introduces errors in the projections. Figure 1 and Figure 2 show the correlation between the simulated and registered (or observed) annual domestic and industrial water withdrawal, respectively, indicating an overall good model performance. The observed data was extracted from the World Bank Data Bank. All data was extracted for all world countries and every year between 1970 -2020. Additional details are given in Table 8.

Table 8 Indicator codes, description, and units for calculating the baseline domestic water withdrawal per capita and validating the simulated historical water withdrawal.

Indicator code	Description	Units
ER.H2O.FWTL.K3	National annual total water withdrawal	Cubic kilometer

[5] https://databank.worldbank.org/ ; accessed 6/9/2024

ER.H2O.FWDM.ZS	Percentage of water withdrawal used by the domestic sector	% (0-100)
ER.H2O.FWIN.ZS	Percentage of water withdrawal used by the industrial sector	% (0-100)
SP.POP.TOTL	Annual national population counts	No. of people

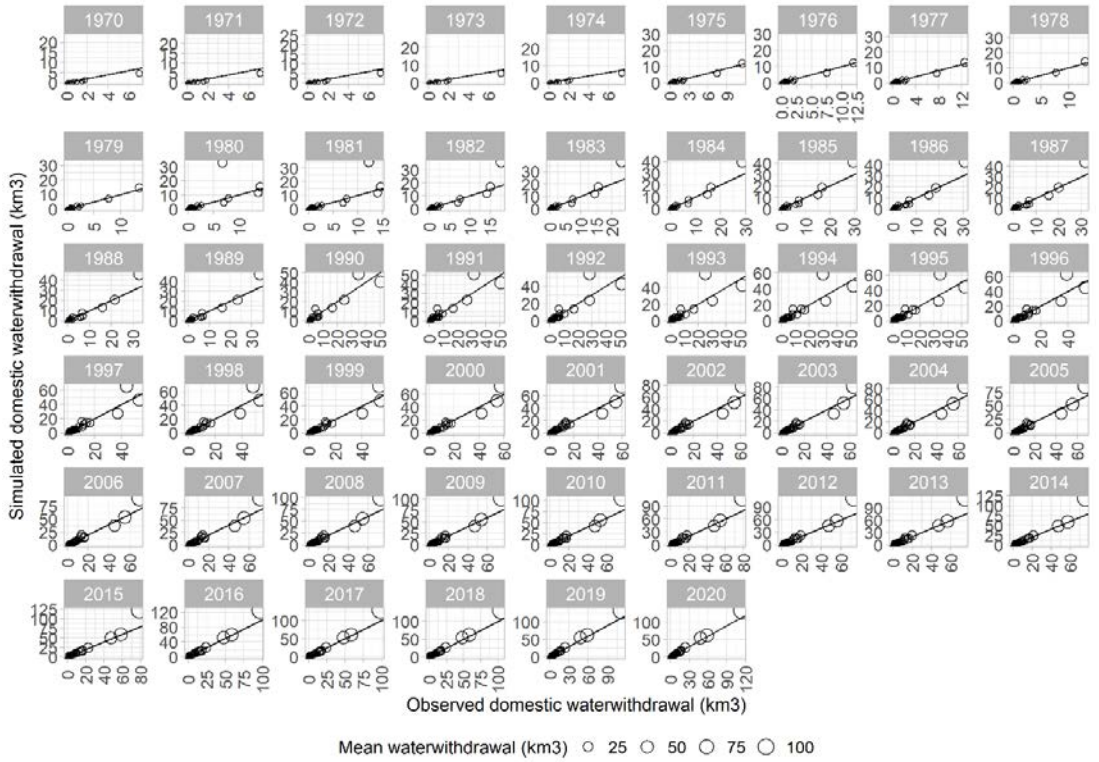

Figure 17. Correlation between annual observed and simulated domestic water withdrawal between 1970 -2020. Each circle

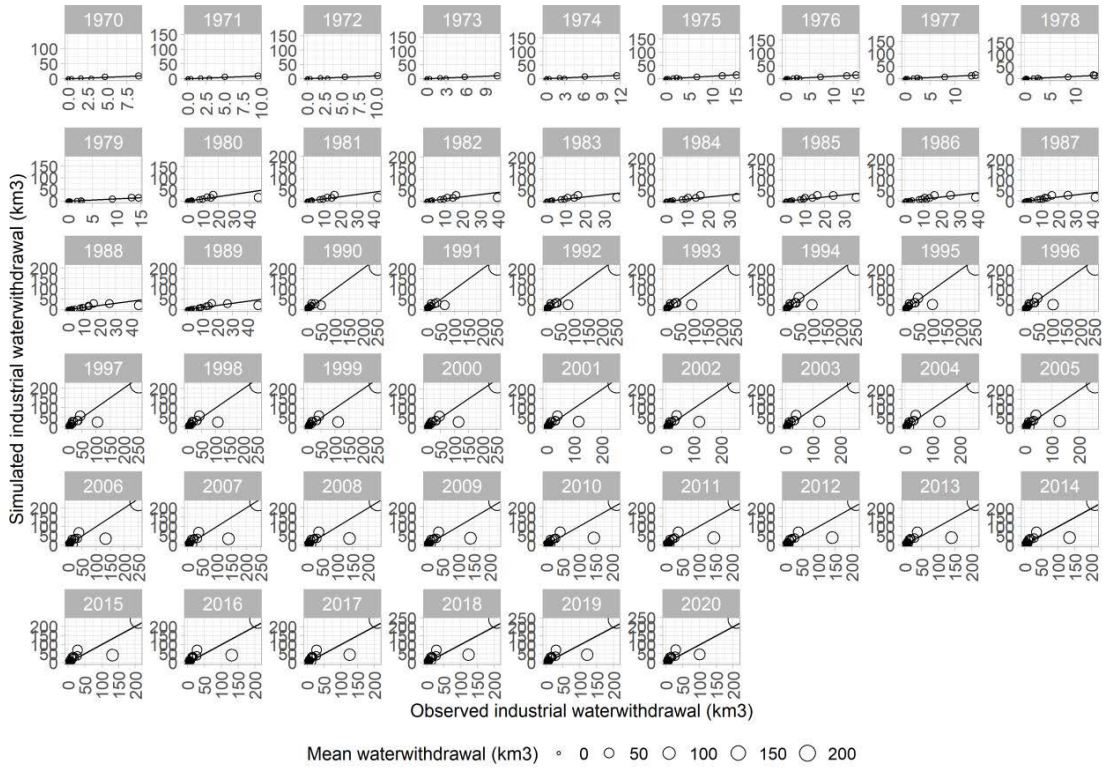

Figure 18. correlation between annual observed and simulated industrial water withdrawal between 1970 -2020. Each circle represents a country, and the size of the circle stands for the average (simulated and observed) water withdrawal.

Water withdrawal and consumption for the domestic and industrial sectors are projected at the national level, based on GDP per capita (for both domestic and industrial sectors) as well as energy use and the proportion of electricity in total energy use (for the industrial sector). Data on energy demand and the share of electricity is not yet available in the SSP database v3.0.1 but will be updated in the future.

Projecting Domestic Water Withdrawal and Consumption

Domestic water withdrawal projections are based on the following equation (Eq. 8):

$$ww_{t,r}{}^{dom} = totPop_{t,r} \times wwc_r^{dom} \times econFunDom_{t,r} \times techImpDom_{t,r} \qquad \text{(Eq. 8)}$$

Where $ww_{t,r}{}^{dom}$ is the total domestic water withdrawal in year *t* for the region *r* (e.g., a specific country); $totPop_{t,r}$ is the total population; wwc_r^{dom} is the baseline water withdrawal data; and $econFunDom_{t,r}$ and $techImpDom_{t,r,}$ are the relative increase in water withdrawal due to economic growth, and decrease due to increasing water use efficiency.

The economic function is affected by GDP per capita and is calculated by the following equation (Eq. 9):

$$econFunDom_{t,r} = \frac{GDPCap_{t,r}}{GDPCap_r}^{econCoeff} \qquad \text{(Eq. 9)}$$

$GDPCap_{t,r}$ is the projected gross domestic product per capita in a given year and country, and $GDPCap_r$ is the baseline gross domestic product per capita (baseline year is set to 2020). The $econCoeff$ varies based on SSP and is set to 0.6 for SSP1, 0.85 for SSP2, 0.8 for SSP3, and 0.8 for SSP5.

The technological improvement, originally modeled as a linear process, was modified to account for diminishing rates of technological improvement and increasing efficiency. The $techImpDom_{t,r}$ is formulated as a fraction of the projected water withdrawal which is required after accounting for technological improvement (e.g., better use of water and reduced leakage) and is within the range (0, 1), whereas zero means no water withdrawal, and one means no efficiency improvement.

The equation (Eq.10) used to calculate the technological improvement is given as:

$$techImpDom_{t,r} = 1 - \ (1 - r_r)^{t-2020^{-effCoeff}} \qquad \text{(Eq. 10)}$$

Where$techImpDom_{t,r}$ is the projected share of actual water withdrawal relative to the projected volume; r_r is the regional annual efficiency reduction term (standing for annual efficiency gains); t is the projected year; and $-effCoeff$ is a calibration parameter set to align the range of efficiency gains with the result of the former linear approach (see Table 9).

Table 9 Efficiency coefficients as a function of annual efficiency reduction rate (r)

Range of r	Efficiency coefficient (effCoeff)
>= 0.997	0.25

0.993 -0.997	0.35
< 0.993	0.45

Industrial water

Industrial water withdrawal is projected using the following equation (Eq. 11):

$$ww_{t,r}{}^{ind} = wwb_r^{ind} \times econFunInd_{t,r} \times techImpInd_{t,r} \quad \text{(Eq. 11)}$$

Where wwb_r^{ind} is the baseline industrial water withdrawal (million m3 year-1), the economic function is calculated as in equation (Eq. 12):

$$\text{econFunInd}_{t,r} = \begin{cases} \text{gdpFunc} \times \text{techFunc} : \text{gdpFunc} > 0 \text{ and techFunc} > 0 \\ \text{gdpFunc} : \text{gdpFunc} > 0 \text{ and techFunc} = 0 \\ \text{echFunc} : \text{gdpFunc} = 0 \end{cases} \quad \text{(Eq. 12)}$$

t

The GDP function uses the formula used in the domestic water withdrawal projection. The techFunc is the ratio between a projected and present technological function, the ratio of per capita energy use to per capita electricity use (baseline year is 2015). For more information about the calculation of the consumptive versus withdrawal of water for domestic and industrial use see Fridman et al. (2024).

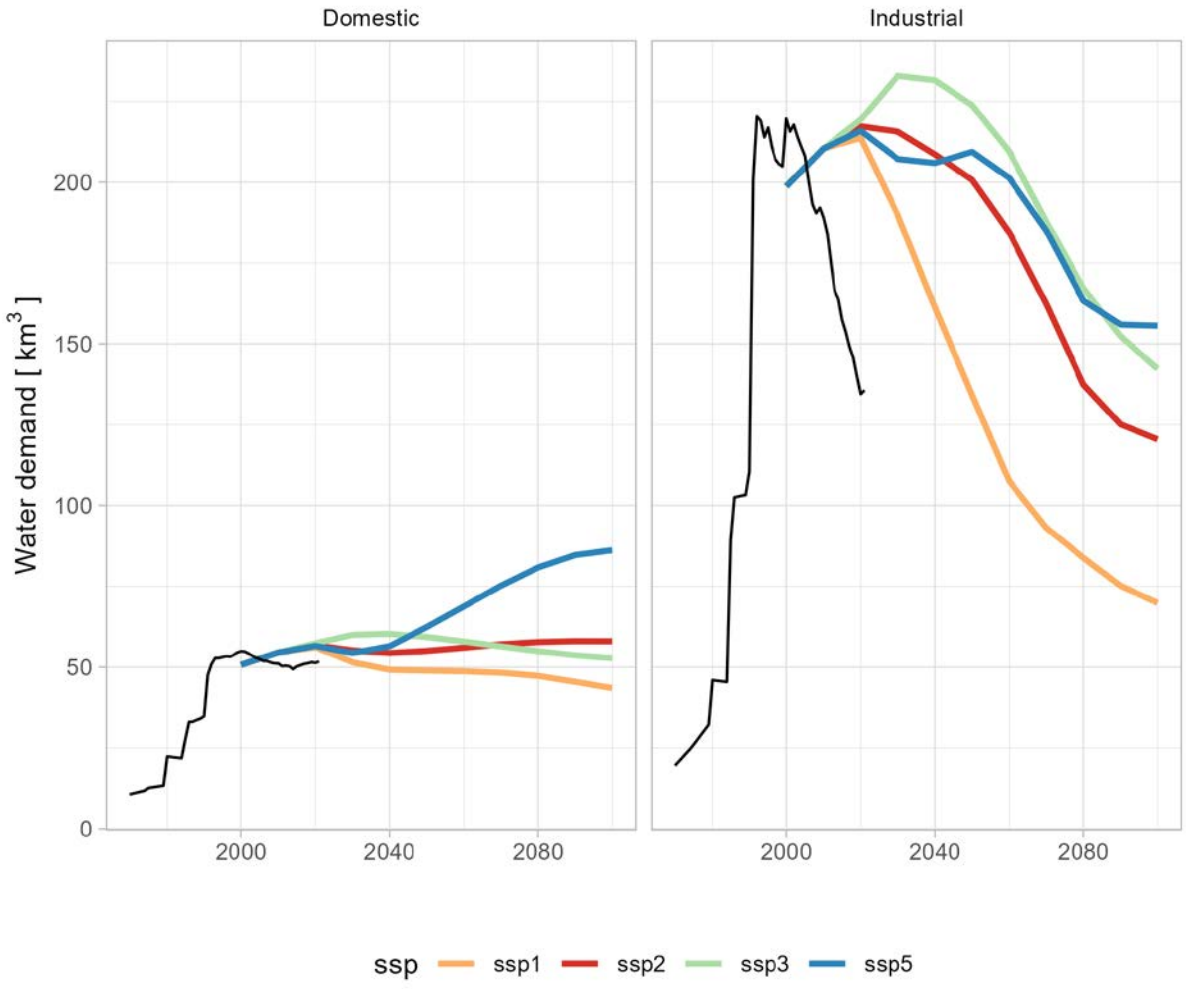

Figure 19. Comparison of water demand projections for domestic and industrial use based on SSPv3 data for Europe for with historical water demands from FAO AQUASTAT (2024) *and* Fridman et al. (2024)

In the long run, the total water withdrawal is largest for SSP5, followed by SSP2, and smallest for SSP1 (Figure 19). There are some differences between the per capita and absolute water withdrawal, particularly when comparing SSP2 and SSP3 between 2070 and 2100. As the per capita water withdrawal according to SSP2 is much higher than that of SSP3, it is partially compensated due to the higher technological improvement rate in SSP3.

The projected industrial water withdrawal following the SSP v3.0.1 shows similar decreasing trends for SSP1, SSP2, and SSP3 compared to the SSP 2013 version, though industrial water withdrawals for SSP5 and SSP1 are higher over the long term. Another clear difference between these two datasets is the observed inconsistency between the historical and projected water withdrawal estimates for the SSP 2013 version, which was corrected in the current release (Figure 19 and Figure 20).

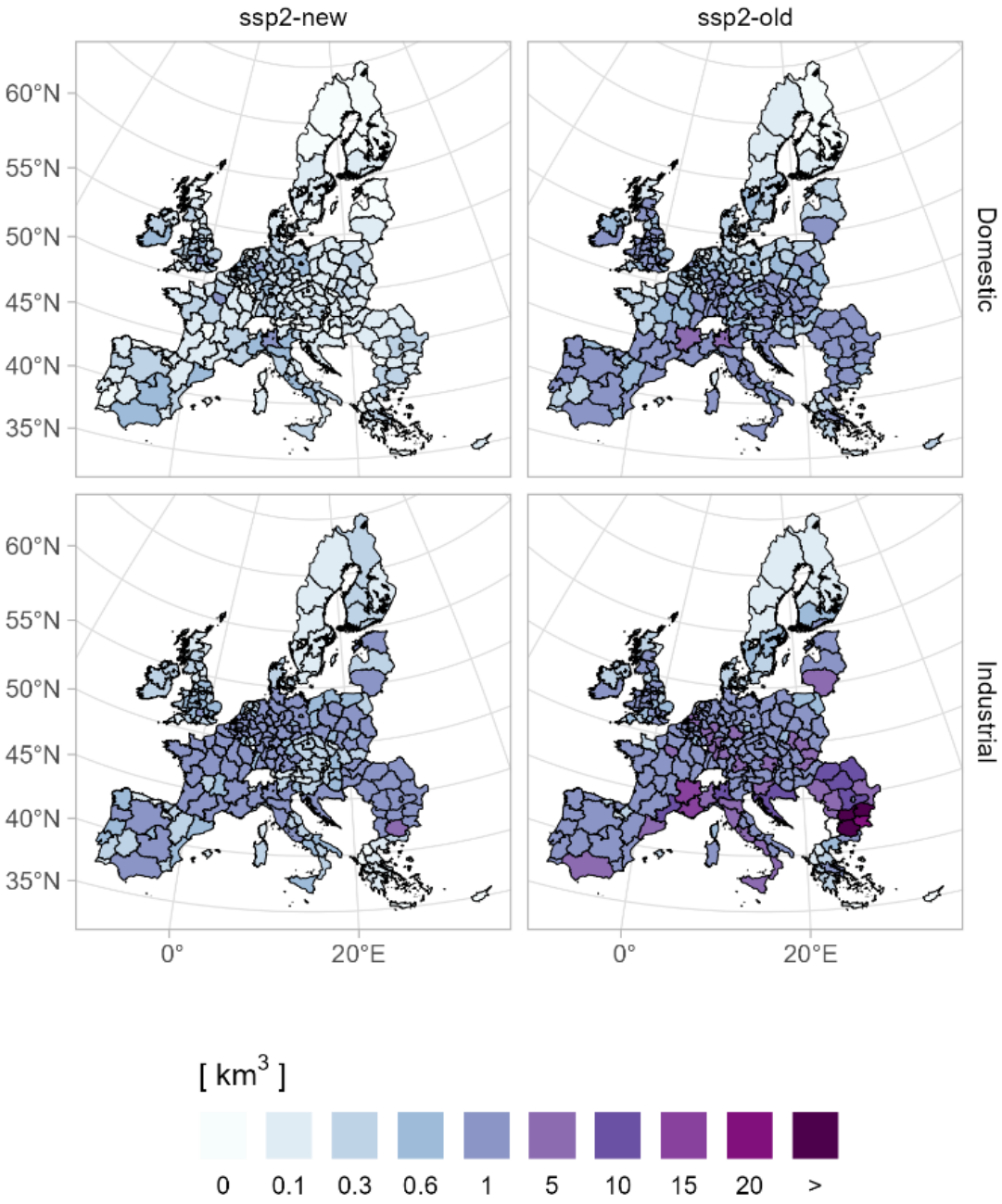

Figure 20. Comparison of mid-century (2035-2065) water demand projections in Europe for SSPv3 and SSPv2 based on (Fridman et al., 2024)

Data useability and limitations

These data have been made available on Zenodo and can be used as model inputs (e.g., for hydrological modeling with the Community Water Model, CWatM) and to calculate water scarcity metrics. The following Section 3.2.3 details how the data is included and used in the GLOBIOM model. The provided data include both water withdrawal and water consumption. The latter accounts for the consumptive use of water, and the water withdrawal represents both consumptive use and the (potential, subject to water availability) return flows. The gridded data format allows aggregation at different spatial scales, e.g., NUTS divisions or river basins, to advance policy-relevant water accounting at an administrative unit scale.

As the temporal resolution is coarse, this data does not represent seasonal variation (e.g., due to temperature changes), and the user shall assume a monthly uniform water withdrawal. Further, per capita water consumption (and withdrawal) is projected nationally. Thus, this data does not represent subnational variation that might be associated with the GDP per capita and built-up land density. Finally, some non-irrigation water withdrawal sources are not included in these data, e.g., aquaculture and livestock.

3.2.2. Aggregated Runoff

The climate impact on can be seen in at an annual level in Figure 21 which shows the change in the total annual aggregated runoff for the GCM ensemble as modeled by IIASA's hydrological model CWatM for the CMIP6 simulations. The results show that under all RCPs most countries in Southern Europe will have moderate to significantly less aggregated runoff at an annual level. Under higher warming levels (RCP 7.0), this finding holds for many of the countries in other regions as well with the exception of some countries in Western Europe (e.g., Germany, Netherlands, Belgium) and most countries in Northern Europe which have more aggregated runoff available in RCP 7.0 than under other lower warming levels. In Central and Eastern European countries, the countries that are further south (e.g., Hungary, Slovakia, Slovenia, Romania) face less aggregated runoff under all RCPs, while Poland, Czech Republic and Austria will have more aggregated runoff.

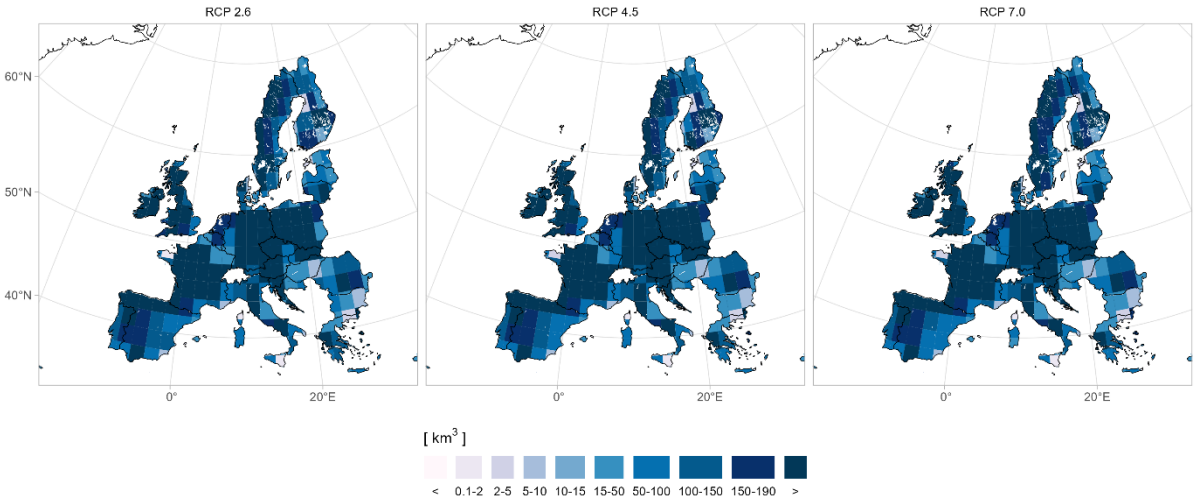

Figure 21. Aggregated runoff at mid-century (2035-2065) for an average of 4 GCMs from CWatM simulations based on CMIP6 data. Source: ISIMIP3b and ACCREU simulations

Figure 22 presents the monthly average river runoff (measured in million cubic meters) for four major European rivers—the Danube, Po, Rhine, and Tagus—at mid century, with each line representing a different general circulation model (GCM) as well as the GCM ensemble. The figure shows the distinct seasonal trends in river runoff, with peaks in spring or early summer and low points typically in late summer to early autumn for each river. For instance, the Danube experiences high runoff in May and June, while the Rhine peaks around April and May. Each river shows variability among the GCMs models, especially during peak flow periods, indicating uncertainty in projected runoff patterns under future climate projections. The differences in runoff patterns across the rivers and models emphasize the importance of considering a range of climate models to understand potential impacts on water resources in these regions.

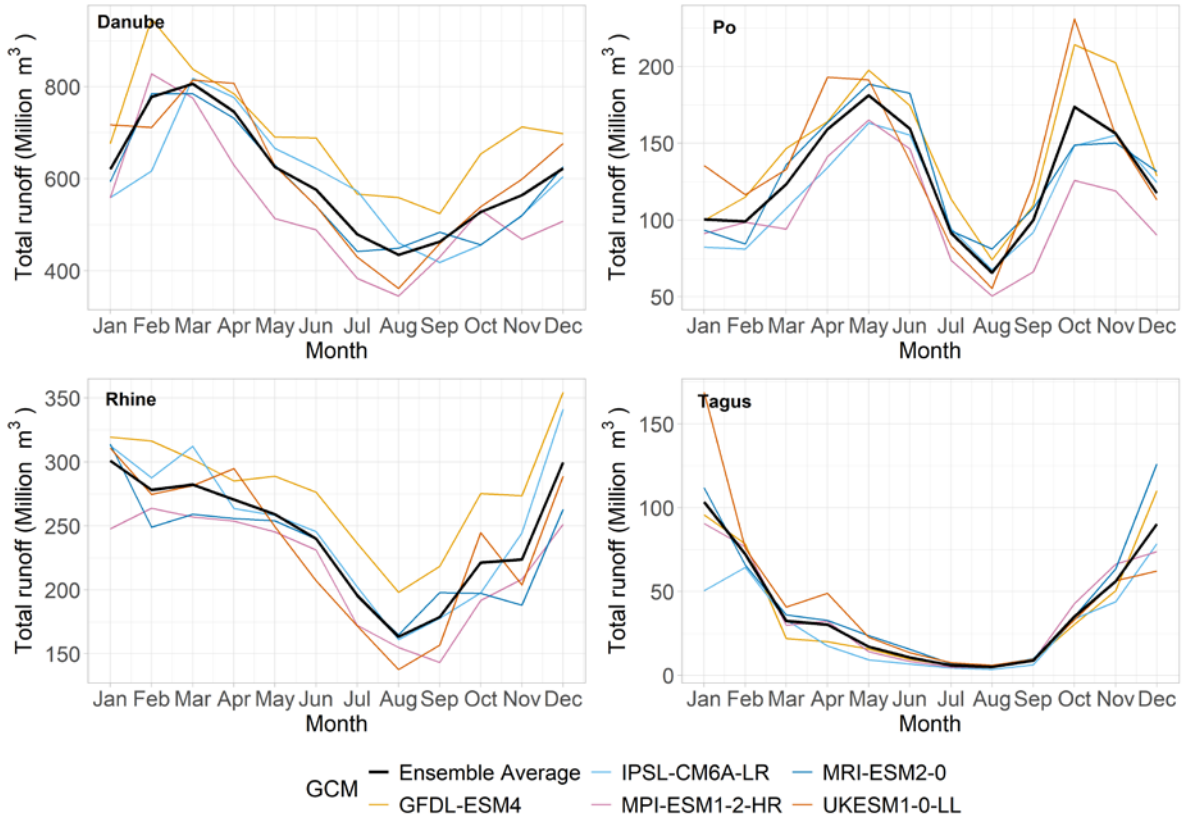

Figure 22 Differences in the monthly total runoff at mid-century by GCM compared to the ensemble average for select European Basins (Danube, Po, Rhine, and Tagus)

3.2.3. Sustainable water for irrigation

In this section we describe how the sustainable water available for irrigation is calculated and then used by GLOBIOM.

CWatM uses the historical climate data generated by each GCM to run historical scenarios of water balances. We use this to calculate the average aggregated runoff in each land unit i and each month m for the 30-year period around each year in the time period t of the historical period (2000-2020) to give us the historical climate monthly aggregated runoff available in each land unit, $SF_{i,m}$. The same is done to calculate the average aggregated runoff for the projection period (2030-2100). The surface water for irrigation use in GLOBIOM, $SWAI_{i,m,t}$ is calculated in Eq. 22 by subtracting aggregated runoff by the water demand from non-agricultural sectors (e.g., domestic and industrial) also calculated by CWatM (See Section 3.2.1) and when applicable the environmental flow requirement available in cropland as shown below in km^3

$$SWAI_{i,m,t} = SF_{i,m,t} - OTHDEM_{i,m,t} - EFR_{i,m,t} \quad \text{(Eq. 22)}$$

t	time period
i	land unit
m	month
$SWAI_{i,m,t}$	surface water available for irrigation in km^3 used in GLOBIOM
$SF_{i,m,t}$	aggregated runoff by CWatM in km^3
$OTHDEM_{i,m,t}$	non-agricultural water demand (e.g., domestic and industrial) by CWatM in km^3
$EFR_{i,m,t}$	environmental flow requirement based on the variable change in flow by CWatM in km^3

GLOBIOM then uses the surface water available for irrigation, $SWAI_{i,m,t}$ as a constraint on water available for irrigation water use. Irrigation can only occur in land units were water is available in the month, *m*, when water is available (Eq. 23). Based on the initial crop distribution maps of irrigated area $A_{i,c}$ and the irrigation water requirements from EPIC $I_{i,c,m}$the total irrigation water demand for each crop. When aggregated, we have the total irrigation water demand $CID_{i,m}$.

The total irrigation water demand expressed in Eq. 24 cannot exceed the water available for irrigation, $WAI_{i,m}$. The water available for irrigation is split into the surface water available for irrigation, $SWAI_{i,m,}$ and groundwater available for irrigation, $GWAI_i$ in Eq. 25. The groundwater available for irrigation is currently calculated as the residual of the total water demand for irrigation from the surface water available for irrigation in the year 2000. Siebert et al. (2010) estimate that more than 40% of irrigated areas are irrigated by both groundwater and surface water. The water available for groundwater in this case is used conjunctively, as a stopgap when surface water is limited (Eq. 26). Therefore, we allow the annual groundwater stock of water to be used in any months when surface water is insufficient. When the monthly water available for irrigation constraint is binding in any given month, then the total irrigation water demand cannot increase which means total irrigated area must remain constant or the crop choice must change (less water intensive crops).

$$\sum_c A_{i,c} * I_{i,c,m} = CID_{i,m} \quad \text{(Eq. 23)}$$

$$CID_{i,m} < WAI_{i,m} \quad \text{(Eq. 24)}$$

$$WAI_{i,m} = SWAI_{i,m,} + GWAI_i \quad \text{(Eq. 25)}$$

$$GWAI_i = \sum_m GWS_m \quad \text{(Eq. 26)}$$

Some land units have an excess of water available for irrigation in months of the growing season (e.g., when the $WAI_{i,m}$ is greater than the $CID_{i,m}$). Figure 23 and Figure 24 show the excess water available for irrigation by mid-midcentury with and without the consideration of environmental flow requirements. These figures aim to show the change in water available for irrigation and therefor use

a static irrigated area (year 2000). With environmental flows respected, there is very little and in most cases too little water available for irrigation expansion.

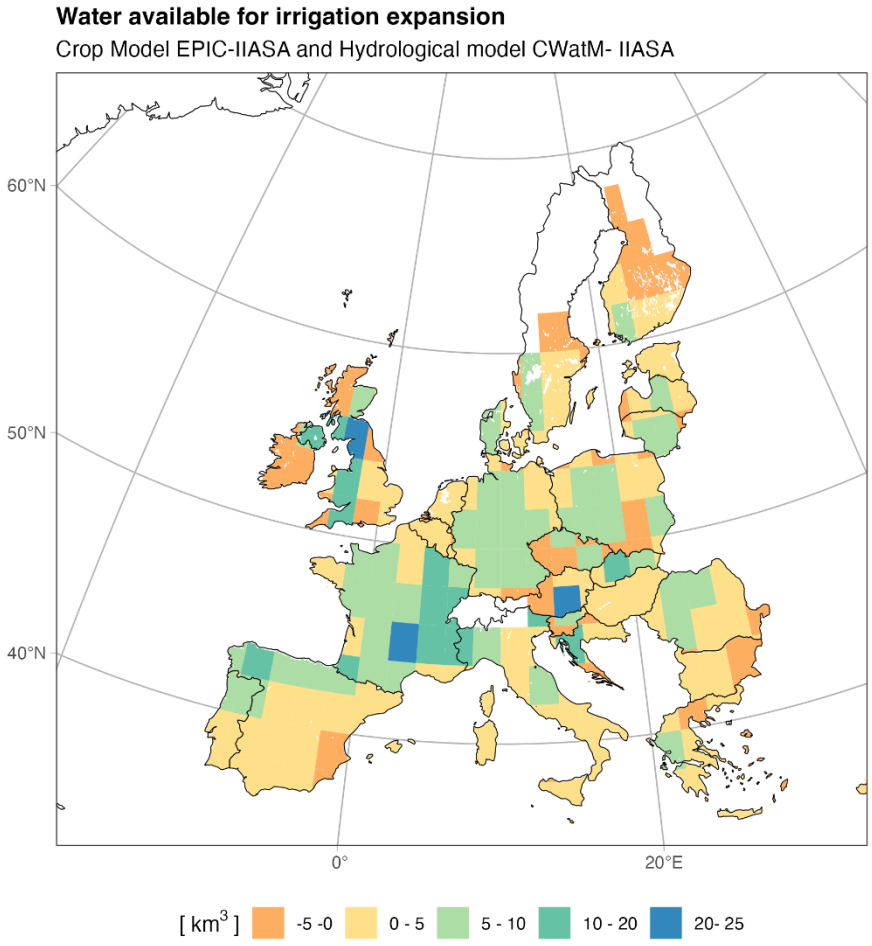

Figure 23. Projected change in water available for irrigation expansion in mid-century (2035-2065) based on water demand projections from (Fridman et al., 2024)*, irrigation crop water requirements from EPIC-IIASA* (Balkovič et al., 2013b) *and projected aggregated runoff from CWatM* (Burek et al., 2020) *Source: Arbelaez-Gaviria and Palazzo, in prep*

Table A 1 presents the GCM agreement in the direction of change of surface water available for use by irrigation. The symbol "+" indicates three of four GCMs indicate positive change, "-" indicates negative change and no agreement indicates that the GCMs were split with half indicating positive and half indicating positive change.

This is based on the aggregated runoff and the water demand from other sectors.

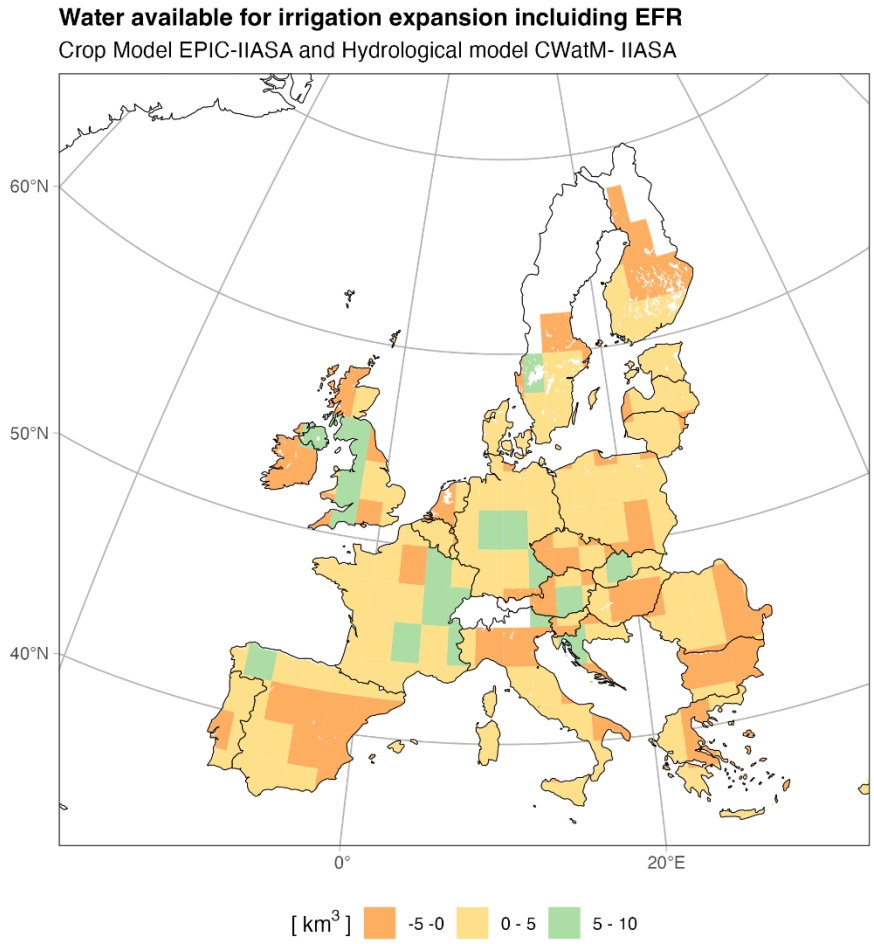

Figure 24. Projected change in water available for irrigation expansion in mid-century (2035-2065) based on water demand projections from (Fridman et al., 2024)*, irrigation crop water requirements from EPIC-IIASA* (Balkovič et al., 2013b) *and projected aggregated runoff and environmental flows from CWatM* (Burek et al., 2020) *Source: Arbelaez-Gaviria and Palazzo, in prep*

3.3. Energy supply and demand

3.3.1. Sectoral final energy demand

Both changes in hot and cold exposure result in additional energy being consumed across sectors. Differences in the response functions of the climatic versus idiosyncratic exposure provide empirical evidence that adaptive actions characterize the response of actors when faced by permanent slowly evolving climatic changes with respect to their own past climatic exposure. Inspecting sector-specific shocks, we find considerable heterogeneity in both the long- and short-run responses (Figure 25). The positive and statistically significant long-run electricity demand response to CDDs is shared by all sectors - with the residential sector accounting for around 45%, services and industry accounting for around 25% and agriculture for the remaining 5% of the total aggregated demand response, respectively. The electricity demand of the residential and service sectors is sensitive to HDDs, pointing to a small but significant contribution of electric-heating. On the other hand, changes in fossil fuel demand due to HDDs are mostly driven by the residential sector, and by a minor share by industry. Furthermore, we find a statistically significant negative effect of long-run CDDs on agriculture fossil fuel demand, suggesting fuel switching and possibly reductions in agricultural production - and hence energy use - under permanently hotter conditions. As for the short-term effects, we find a statistically significant and non-negligible effects of electricity consumption in response to hotter-than expected

CDDs for the residential and industrial sectors, with the latter being higher than the former - and of fossil fuel consumption to colder-than expected HDDs in the residential sector. Finally, we find evidence of a significant amplification effect of per capita income on the electricity and fossil demand response to heat and cold exposure.

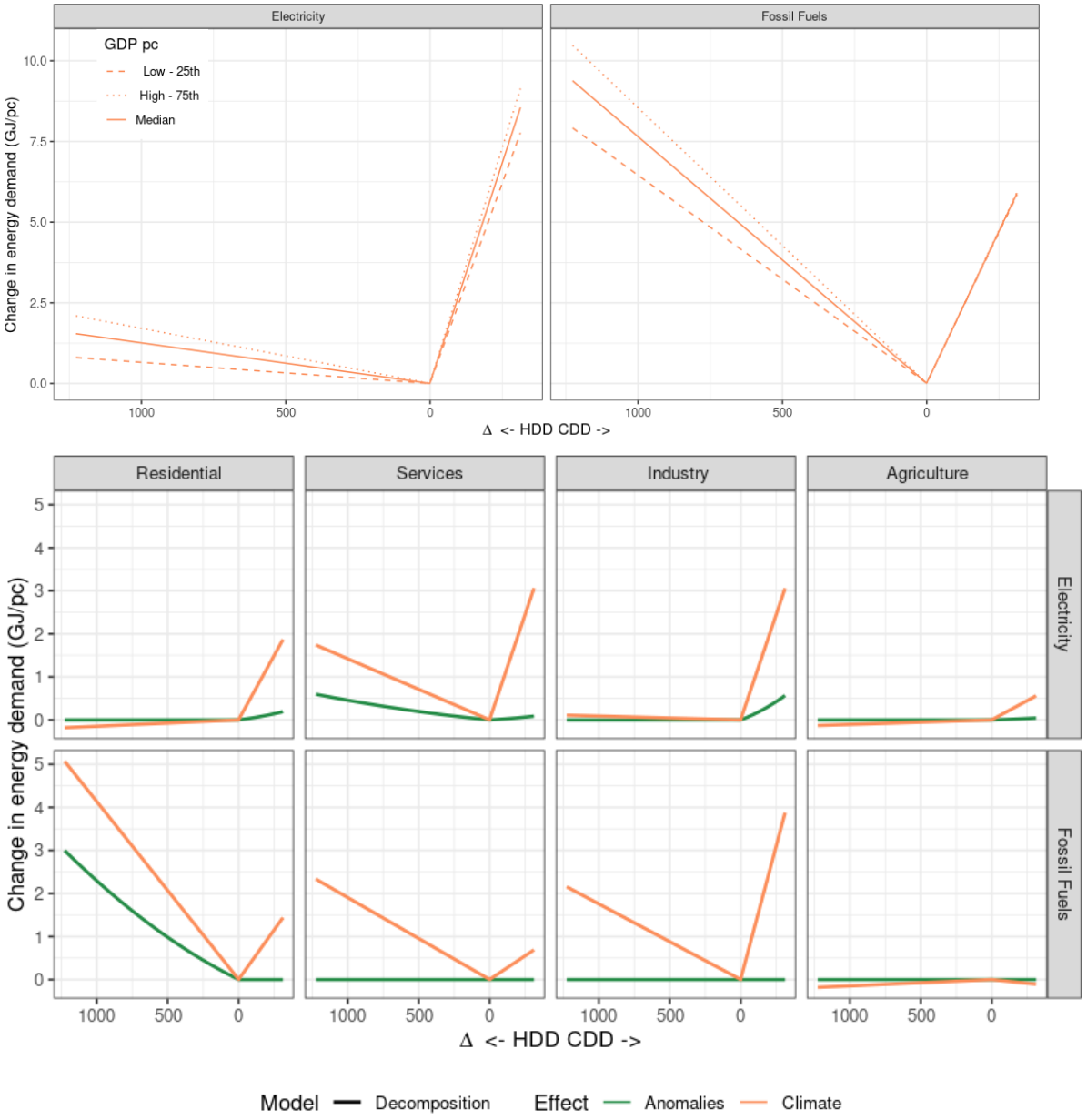

Figure 25 Estimated semi-elasticities of final energy demand response to CDDs and HDDs.

(a) Total long- (climate) and short-term (anomalies) semi-elasticities, including the modulation effect of per capita GDP, aggregated for all sectors. (b) Estimated semi-elasticities by sector and fuel.

We adopted the method described in section 2.1.1 to develop grid cell-level projections of future energy demand adjustments along the intensive and extensive margins, due to climate change. Note that the semi-elasticities quantify the relative effects of future climatic shifts on energy demand by assuming that today's structure of the energy markets is maintained in 2030, 2050 and 2100. Our projections furthermore depend on the assumption that the historical evolution of energy demand and per capita income can be an appropriate measure of the evolution of sectoral dynamics in the future. The adoption of more efficient adaptation measures (e.g. energy efficient cooling appliances, zero energy buildings, green-based solutions) at a rate higher than the historical one, as well as

breakthrough technological changes, can lower the energy demand required to satisfy heating and cooling needs as well as economic impacts of climate change. We also do not account for the dynamic implications of adaptation costs and benefits on the energy sector and other economic activities, as well as on carbon emissions, all of which will be evaluated by coupling the shocks estimated in this work with integrated assessment models and energy models of WP4.

Figure 26 shows the projections aggregated at the country-level of the final energy demand change in percentage (left) and EJ (right), with respect to a scenario with no climate change and current socioeconomic conditions, for RCP 4.5 and 2050. Aggregating all sectors' contributions (residential, commercial, industry and agriculture), we find that electricity demand tends to increase by 20%-30% in Southern Europe (e.g. Greece and Spain) under the "Reference" adaptation scenario, while Central European countries exhibit increases between 5% to 15% in 2050. On the one hand, the electricity demand changes in the "Low" adaptation scenarios are negligible, due to the low implicit adoption rate of cooling technologies under the historical climate. On the other hand, the electricity demand changes in the "High" adaptation scenario do not differ substantially from the "Reference", because in Europe adaptive capacity measured though per capita income levels is already high enough in the Reference case to enable effective long-term adjustments in response to the future climate (see also results of the section 2.5.2). Furthermore, aggregated electricity demand changes take into account both increases in cooling due to hotter summers and decreases in electric heating due to milder winters, resulting in a net effect that tends towards relatively small differences between the "High" and "Reference" scenario in Northern Europe. As for fossil fuel demand, the "Reference" adaptation scenario points to reductions around -15% to -25% in Northern European countries in 2050. Changes under the RCP 2.6 (7.0) point to electricity increasing up to 15% (40%) in Southern Europe and decreasing by up to 10% (30%) in Northern Europe in the same year. Over the end of the century relative changes are amplified, with electricity demand increasing up to 90% in Southern Europe and fossil fuel demand decreasing by as much as 30% in Northern Europe in the same year under RCP 7.0. The sectoral contribution to these changes is mixed: the majority of reductions in fossil fuels final energy come from households, with and EU-level sector-specific reduction of over 25% and 45% in 2050 and 2100 under the RCP 4.5. On the other hand, electricity demand increases are shared by the residential, commercial and industrial sector, with the latter contributing for around 50% over the total increase in demand (average across different scenarios, as shown in Figure 27). Importantly. We find that industrial sectors increase gas consumption as a response to a hotter climate, given in this sector some cooling options (e.g. cooling absorption) involve the use of fossil fuels. This increase only partially compensates for the decrease in buildings' gas demand due to lower heating needs. Maps for the other combinations of years and scenarios are shown in the Annex.

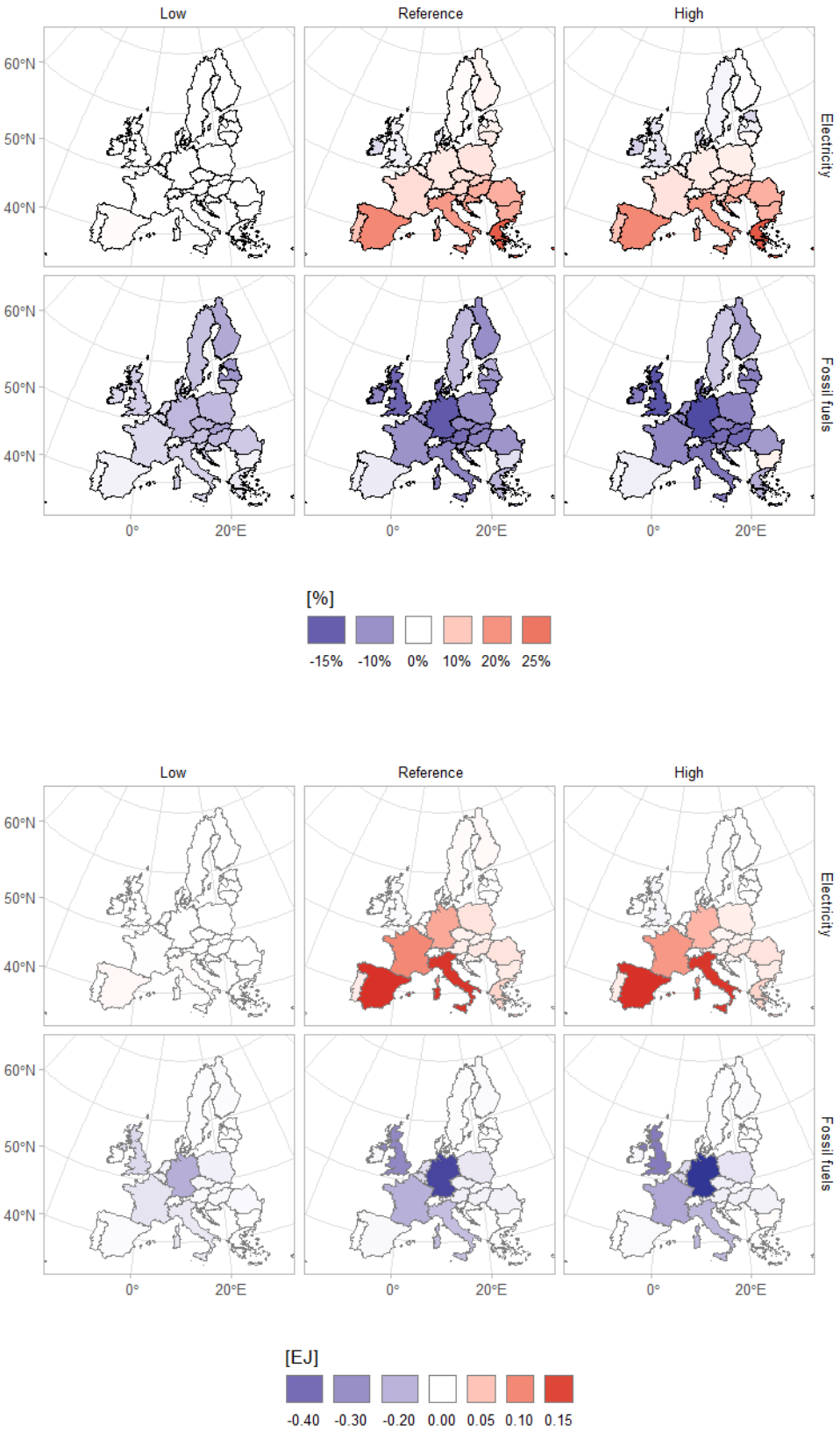

Figure 26 Country-level final energy demand change in percentage (upper panel) and EJ (lower panel) by adaptation scenario.

Projections are displayed for RCP 4.5 and year 2050, aggregating all sectors' contributions. Changes are relative to the climatic and income conditions of 2000-2014.

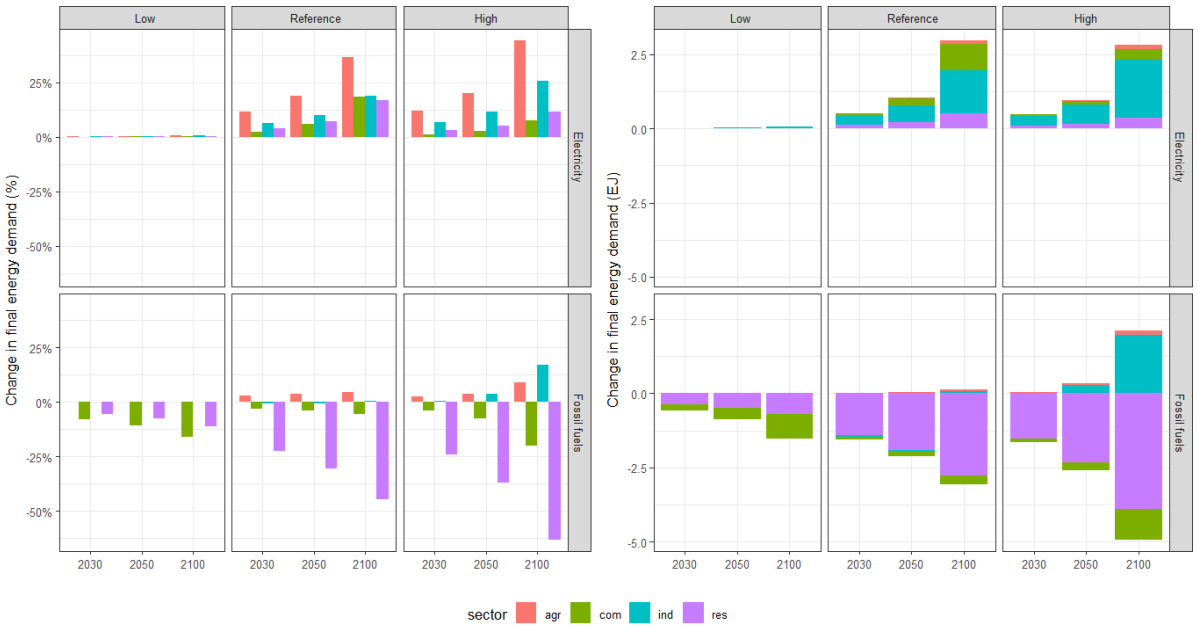

Figure 27 EU-level final energy demand change in percentage (left panel) and EJ (right panel) with respect to a scenario with no climate change and current socioeconomic conditions. Projections are displayed for RCP 4.5 and year 2050.

3.3.2. Residential air-conditioning stock and demand

To project future AC adoption and electricity consumption, we consider the scenario framework and method described in sections 2.1.1, adopting the 1995-2014 time period for the historical and the 2021-2040, 2041-2060 and 2081-2100 time periods for projections around 2030, 2050 and 2100, respectively. In addition, to estimate future growth in household expenditure we use yearly per-capita GDP growth rates based on gridded GDP projections compatible with the SSPs. When it comes to country-wide projections data, we draw information on future distribution of households among age, education and gender groups based on the SSP scenarios (for details see Falchetta et al., 2024). Based on the trained model, we produce predictions at the grid cell level for the globe and make projections along the SSP-RCP combinations as defined by the ACCREU scenario matrix. While the **medium adaptation** scenario considers the effect on AC ownership and use due to climatic shifts, the **low adaptation** variant considers the effect of climate change on the use of current AC stock. The **high adaptation** variant considers the growth in AC stock and use due to both climate and income changes.

Then, based on the granular projections, we can then compute AC penetration rates and electricity consumption levels for different income quantiles (with each quintile defined in the base year 2020). These inputs can go into CGE models to analyze unequal shocks and their cascade effects on socio-economic inequalities.

Our model-based predictions for 2020 for the world show a high heterogeneity in the distribution of AC across and within regions and countries based on sub-national units defined over a regular global grid with a spatial resolution of 0.5 arc-degrees, reflecting the interaction of different climatic conditions and the distribution of population and its socio-economic attributes. Existing areas of high concentration of household AC ownership (>50%) are clearly visible in North America, Southern Europe and North Africa, the Middle East, South Africa, Southern Latin America, Japan, Eastern China, and Australia. Looking at 2050, areas with high AC ownership rates will expand as a result of a warmer climate, rising affluence levels and socio-demographic change. Such growth is particularly strong in areas with currently low levels of AC penetration, such as South-East Asia (+96 million households, scenario mean), e.g. Indonesia, and Eastern Asia (+41 millions), e.g. Northern India, sub-Saharan Africa (+72 millions), while it will grow more slowly in Central Europe (+30 millions), North Africa and the

Middle East (+24 millions) and portions of Latin America (+33 millions) because of already higher current AC prevalence rates (North America), climate heterogeneity and low propensity to use AC (Europe). When aggregated to the global level, gridded projections (weighted by the number of households per grid cell) for the middle-of-the-road scenario result in a global projected AC penetration rising from the current 27% to a scenario-median of 41%. Households equipped with an AC unit would increase from 620 millions to an estimated median of 900 million by 2050. Greater AC availability growth translates into a surge in the use of energy and the related environmental impacts.

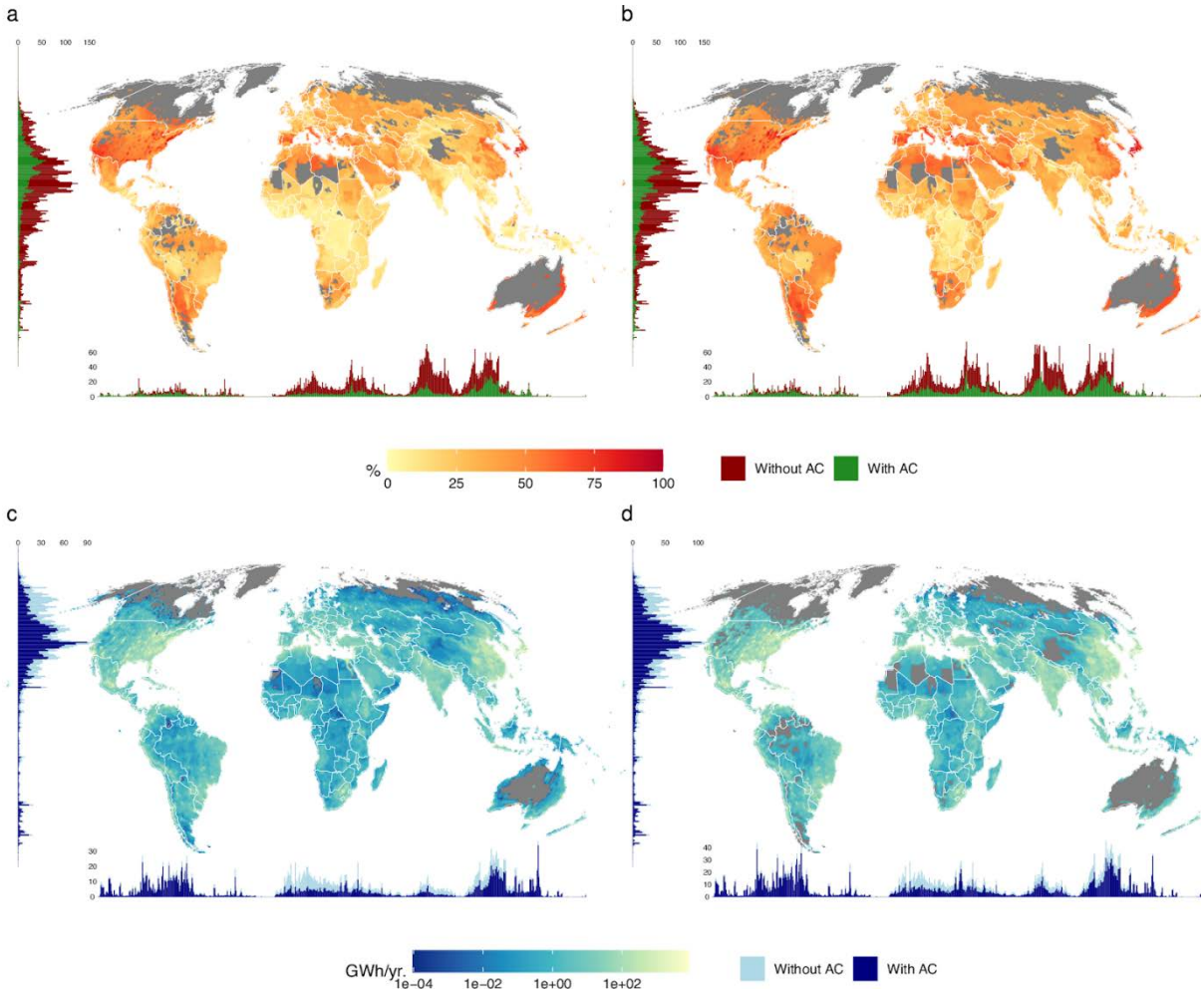

Figure 28 Global gridded projections for residential air-conditioning (AC) ownership and use inequality. (a,c) prediction for year 2020; (b,d): projection for year 2050 in SSP245

To better identify the dynamics of AC adoption in Europe for the ACCREU project, we compute the ownership rate at the NUTS2 level. Access to AC evolves rapidly from the "Low" adaptation to the "Reference" and the "High" scenarios, with several NUTS 2 regions in Southern Europe reaching ownership rates > 70% in 2050 and > 90% in 2100 in the two latter scenarios. Several areas in Central and Northern Europe reach penetration rates of 40%-50%, substantially above current average levels around or below 10%. Similarly to what we found in the macro-level demand estimation, differences in adaptation levels for the energy sector are more pronounced when evaluating the "Low" scenario with respect to the "Reference" scenario, while the gap between the "Reference" and the "High" scenario is negligible, given that in Europe current per capita income is already sufficiently high to justify an increase in adoption of AC as a response to climate change.

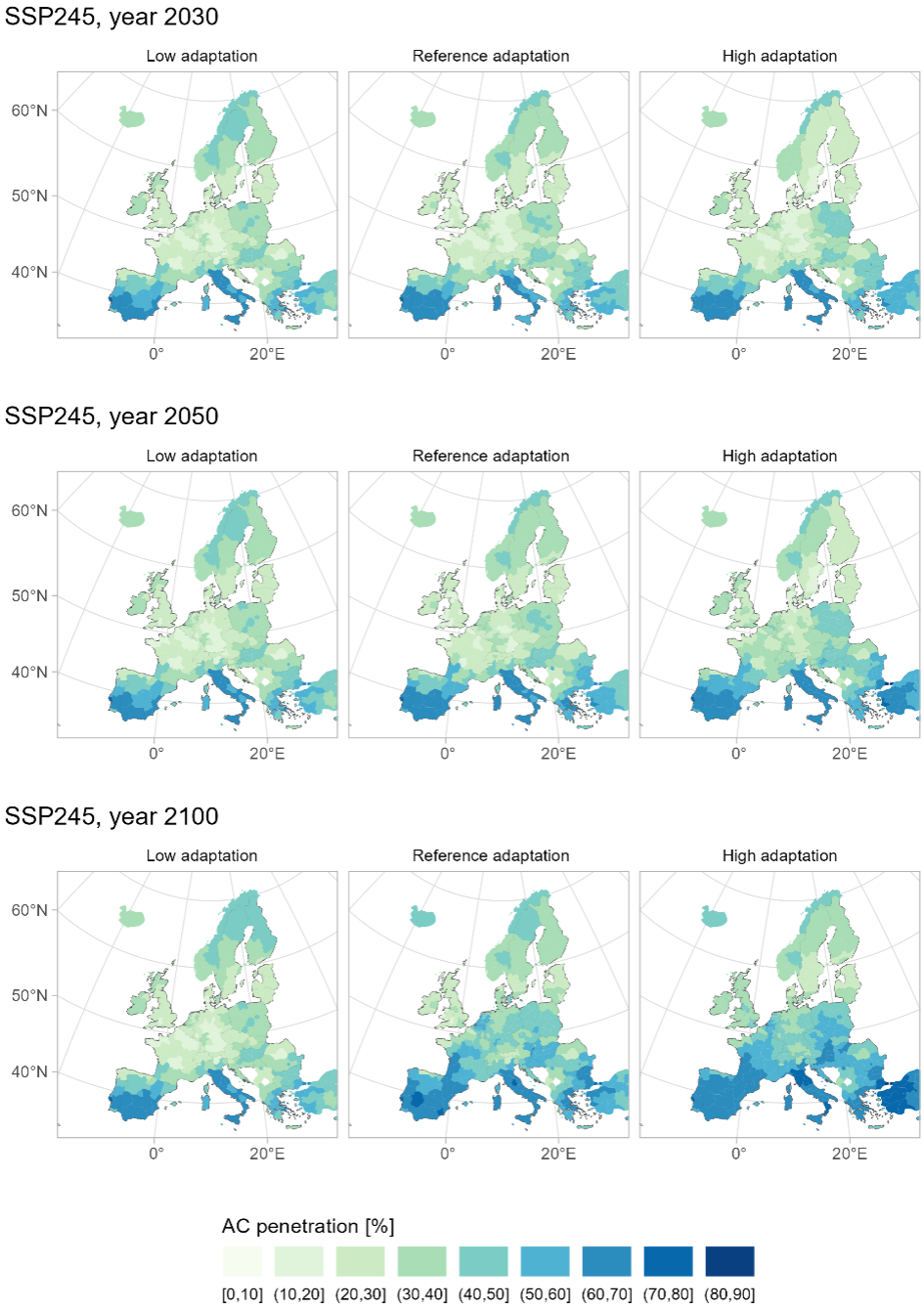

Figure 29 European, NUTS- projections for residential air-conditioning (AC) ownership and use.

3.3.3. Power generation supply

The empirical analyses conducted shed light on the impacts of extreme weather on European power supply. Thermal power technologies experience significant forced and planned outages due to extreme weather, with notable differences between technologies and types of outages. Fossil-based technologies exhibit a U-shaped response to extreme temperatures, confirming our hypothesis. Drought and flood conditions do not significantly affect forced outages for coal and gas but increase forced outages in oil-fired generation under extreme droughts. Planned outages of fossil-based

technologies are less influenced by extreme temperatures and are more sensitive to extreme drought conditions. Nuclear power presents a unique response among thermal technologies. Outages increase monotonically with temperature, especially the forced outages, indicating greater resilience than fossil-based technologies. However, this reverses when considering planned outages during drought conditions. Planned nuclear outages increase significantly during extreme droughts, with the probability rising by up to 45% [30%–60% confidence interval]. These findings support our hypothesis that planned outages align with predictable events like droughts, allowing operators to schedule maintenance proactively and indicating non-linear effects that suggest tipping points in the drought-outage relationship (Figure 30, upper panel).

We found furthermore that hydro-power plants are more affected by extreme variations in water runoff levels than by extreme temperatures (Figure 30, lower panel). Exposure to extreme hot or cold temperatures does not significantly increase outage probabilities across storage, run-of-river, and reservoir plants, with only minor effects of cold temperatures on storage forced outages and reservoir planned outages. In all cases, marginal effects on outage probabilities do not exceed 2 percentage points, resulting in total probabilities between 3% and 6%. In contrast, extreme drought conditions increase the likelihood of forced outages in pumped storage plants from 5% to around 10% [7%–13% confidence interval]. Run-of-river plants exhibit a U-shaped response, where both floods and droughts are associated with increased probabilities of forced and planned outages. However, significant effects are observed only for floods on forced outages and droughts on planned outages. This can be explained by three mechanisms: First, run-of-river plants are directly impacted by immediate river flow changes and are less flexible in managing water resources. Second, floods may be harder to anticipate, leading to a greater impact on forced outages. Conversely, managers may anticipate extreme droughts and plan for production halts. Third, they might schedule maintenance during dry periods when water availability is limited. Reservoir plants are the least affected by extreme runoff conditions, which is somewhat surprising given their reliance on consistent water inflows that can be disrupted by changes in precipitation and runoff patterns.

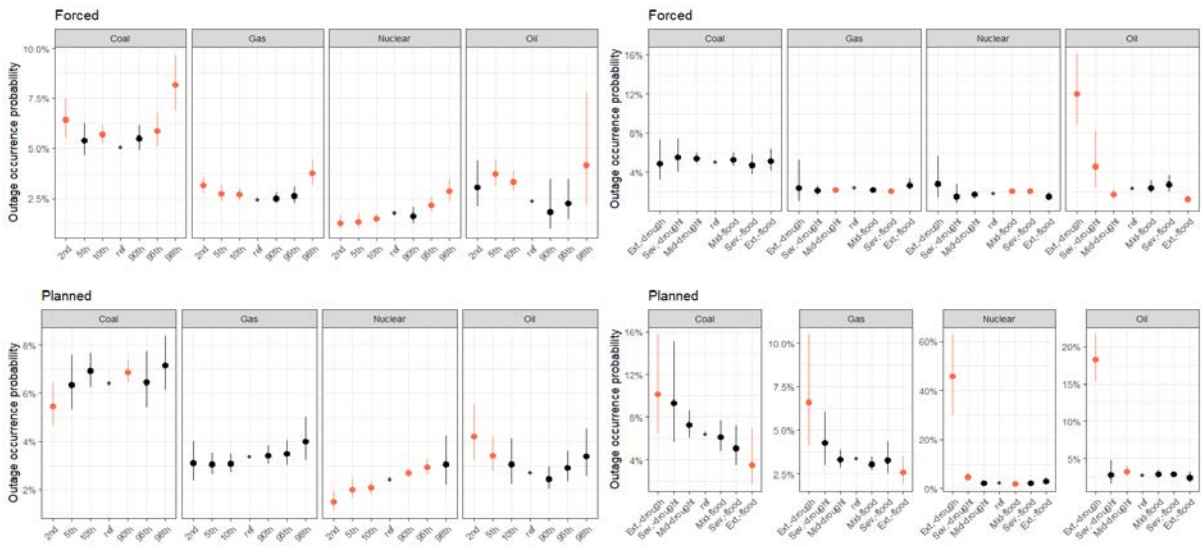

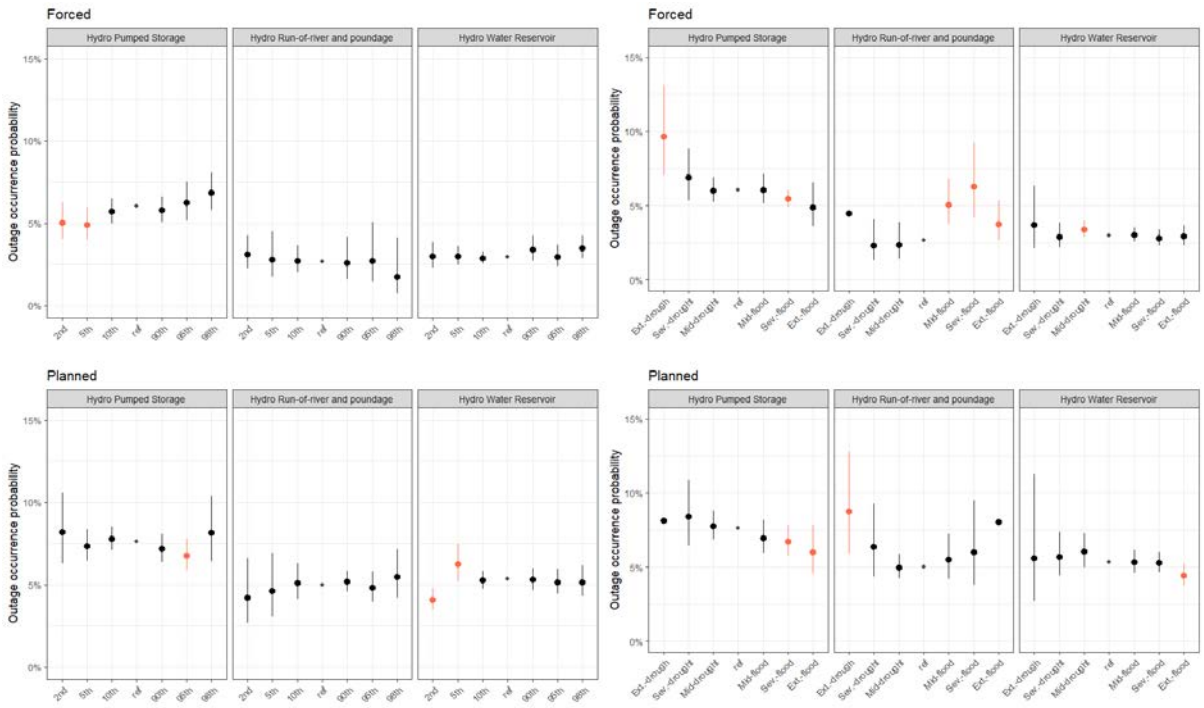

Figure 30 Estimated semi-elasticities of thermal and hydropower generation to extreme temperatures, drought and flood events.

We project separately the effects of extreme high and low temperature changes, as well as drought and flood events, based on future projections of CMIP6 models of daily minimum, daily maximum temperatures and water runoff levels, computing the future value of the variables identified in the empirical model (temperature quantiles and SRI categorical variables), coherently with the method outlined in section 2.1.1.

The projections developed for WP2 focus on the identification of future occurrences of extreme weather events in the locations of the power plant studied in this assessment, and therefore are indicative of changes in the exposure of power generation infrastructure under the future climate. The assessment of the occurrence of the planned and unplanned outages following such change in exposure, evaluating the vulnerability of the generation infrastructure and the adaptation actions that ensure an adequate provision of power during the outages, will be evaluated though the use of the energy model Osemosys in ACCREU's Deliverable 2.6.

Figures 31-32 present the total number of extreme droughts, extreme floods and extreme temperatures occurrences over a year in a location where a power plant is located, across various European countries and for different types of power plants. The indicator is computed taking the average of all GCMs' in the decade 2041-2050. Given the relatively low number of oil-fired generation plants in Europe, the following projections focus on nuclear, gas, coal and hydropower technologies. Overall, extreme flood conditions result to be events happening more frequently than extreme droughts in the locations of the European power plants, but the econometric analysis shows that with the expectation of hydropower run-of-river, the latter are associated with a higher likelihood of occurrence of power interruptions than the former. Notable cases where exposure to floods appears relevant are in France, where power-plant and day level exposure to such events surpasses 200 occurrences on average in 2050. Italy and Spain are instead the countries in which gas and coal power plants are more exposed to extreme temperatures, respectively.

Coal plants exhibit a significant exposure across Europe under RCP 245 in 2050: Hungary shows the highest mean drought occurrence, with an average of 100 events over a year, indicating that Hungarian coal infrastructure may be especially vulnerable to such conditions. Greece, Spain and Italy following at around 90, 80 and 70 occurrences per year, respectively, reflecting frequent impacts on coal infrastructure in southern Europe. Spain's coal infrastructure is also affected by extreme high temperatures with an average of 125 occurrences per year.

Gas plants show distinct patterns, with the Netherlands displaying the highest mean exposure of power plant-days count around 300, suggesting a considerable frequency of drought-related stress on gas infrastructure. Italy and Belgium follow with substantial mean values of 192 and 101, respectively, indicating a heightened susceptibility to extreme droughts in these areas as well. Furthermore, the Italian gas infrastructure is highly exposed to extreme high temperatures, with occurrences surpassing a mean value of 150. Hydro Reservoir plants, prominent in Scandinavian countries, show mean event counts of 84 in Sweden and 72 in Norway, suggesting frequent drought-related impacts in these northern hydro facilities. Hydro run-of-river plants, particularly in France, display a high mean of 141, while Italy and Austria show moderate averages of 53.2 and 66.3, respectively. Finally, nuclear plants emerge as highly affected, particularly in Western Europe, with Belgium showing the highest mean drought occurrence at 163, followed by France at 114. In contrast, nuclear plants in Finland display a notably lower mean (37.3), indicating that northern European nuclear infrastructure may be comparatively less affected by such events.

As for single location exposures (Figure 33), under RCP 245 the highest recorded number of days with Extreme Droughts is associated with a nuclear plant in northern Germany (around 73.60). Certain locations, such as in Austria and in the Netherlands, show multiple event values associated with different plant types. For example, in the Vienna area, both hydro run-of-river and coal plants experience a similar event intensity (66.33). Likewise, in the Netherlands, both coal and gas plants register an identical event intensity (55.82). This suggests that regional droughts may be impacting all plant types in these areas similarly, highlighting the shared vulnerability of multiple plant types in these locations. Overall, exposure to extreme droughts is high for all type of thermal power plants across central and northern Europe, with nuclear plants in northern Germany showing the highest average exposure. Conversely, gas and coal plants in central Europe, such as those near Belgium and the Czech Republic, tend to have moderate exposure. The power plants more exposed to Extreme Floods are instead gas and coal plants clustered around Germany and the Netherlands, and hydropower run-of-river pants in South-Eastern France and in Northern Italy. Both coal and hydropower plants in Southern Spain are highly exposed to extreme high temperatures, while vulnerability of Italian gas infrastructure comes from an exposure of less than 15-20 days per year in each specific plant, coupled by a high number distinct power plants exposed (Figure 35).

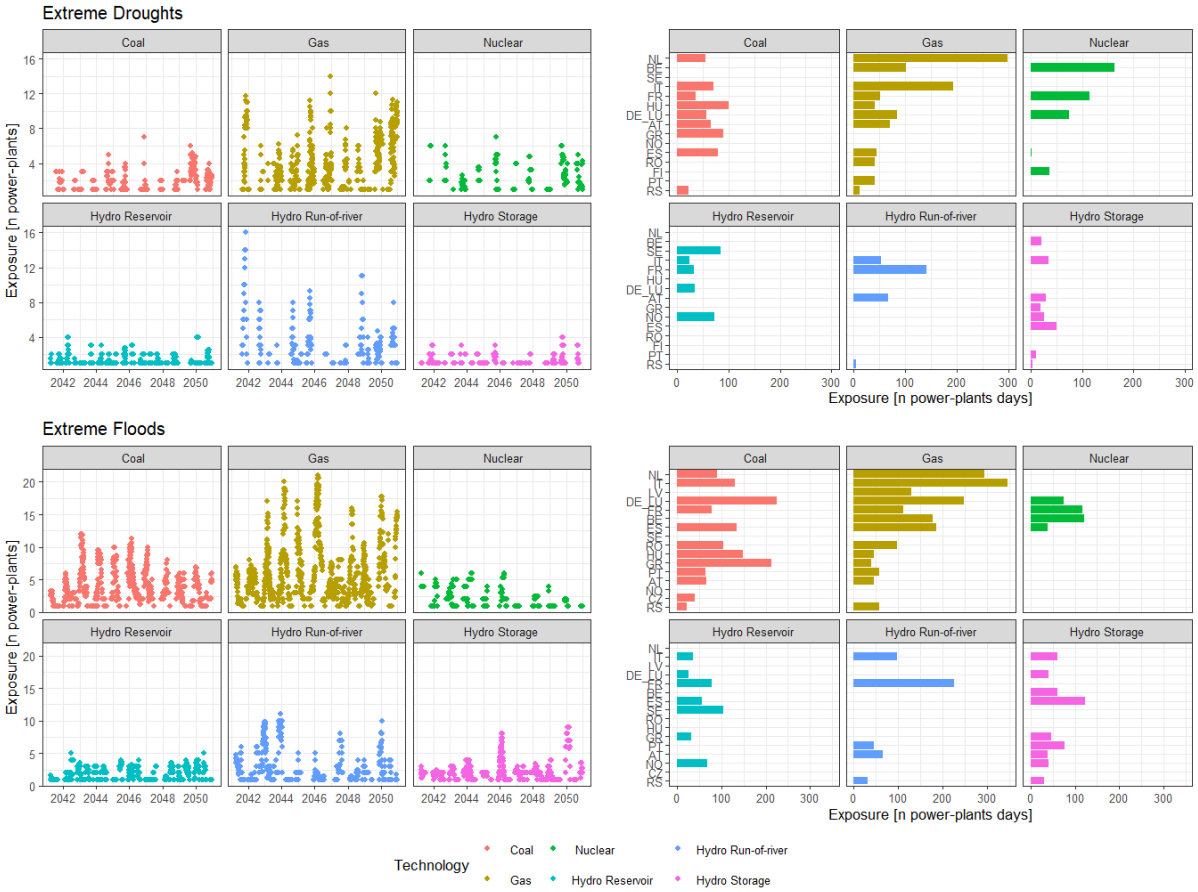

Figure 31 Left panel: EU-level daily number of power plants exposed to extreme droughts (SRI < -2) and extreme floods (SRI >2), average of GCM output for RCP 245. Right panel: Country-level annual number of power plant-days with exposure to extreme droughts and floods, average of GCM output for RCP 245.

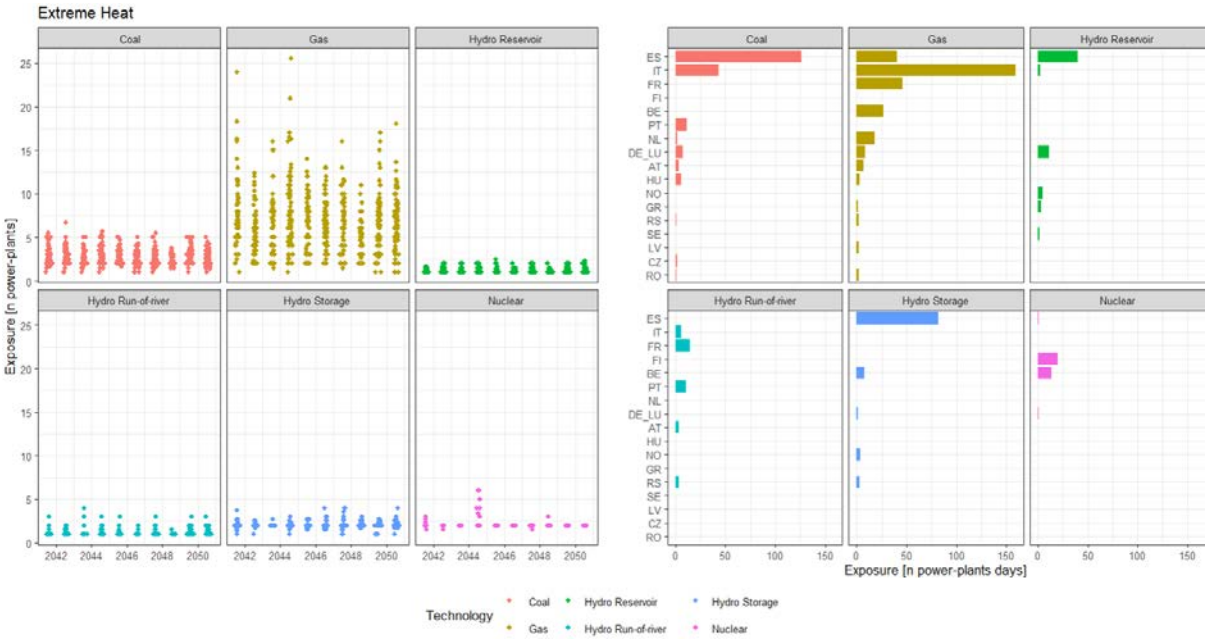

Figure 32 EU-level daily number of power plants exposed to extreme heat (maximum temperatures > local 98th percentile of 2000-2014 temperatures). Right panel: Country-level annual number of power plant-days with exposure to extreme heat, average of GCM output for RCP 245.

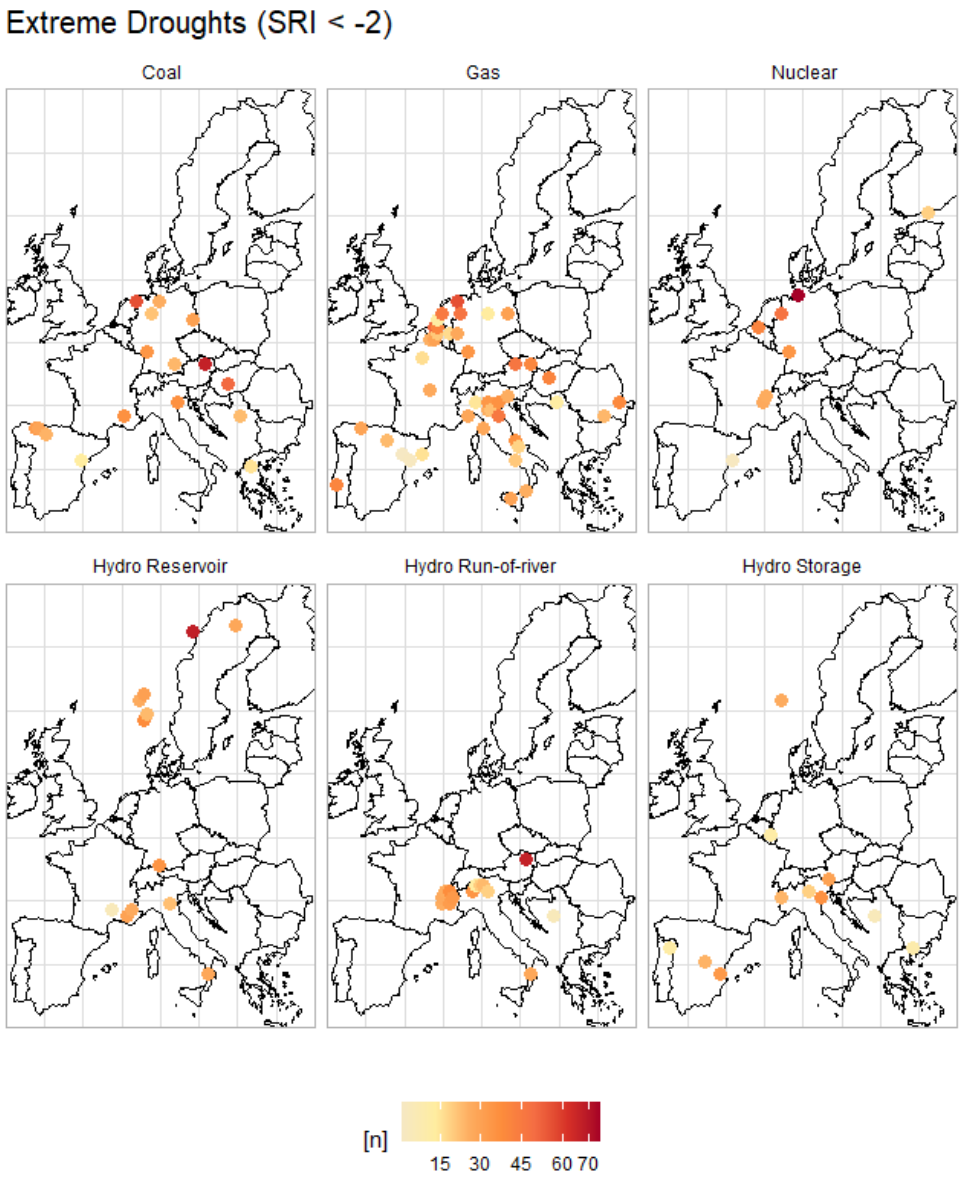

Figure 33 Location specific annual number of power plant-days with exposure to extreme droughts, average of GCM output and of 2041-2050, for RCP 245.

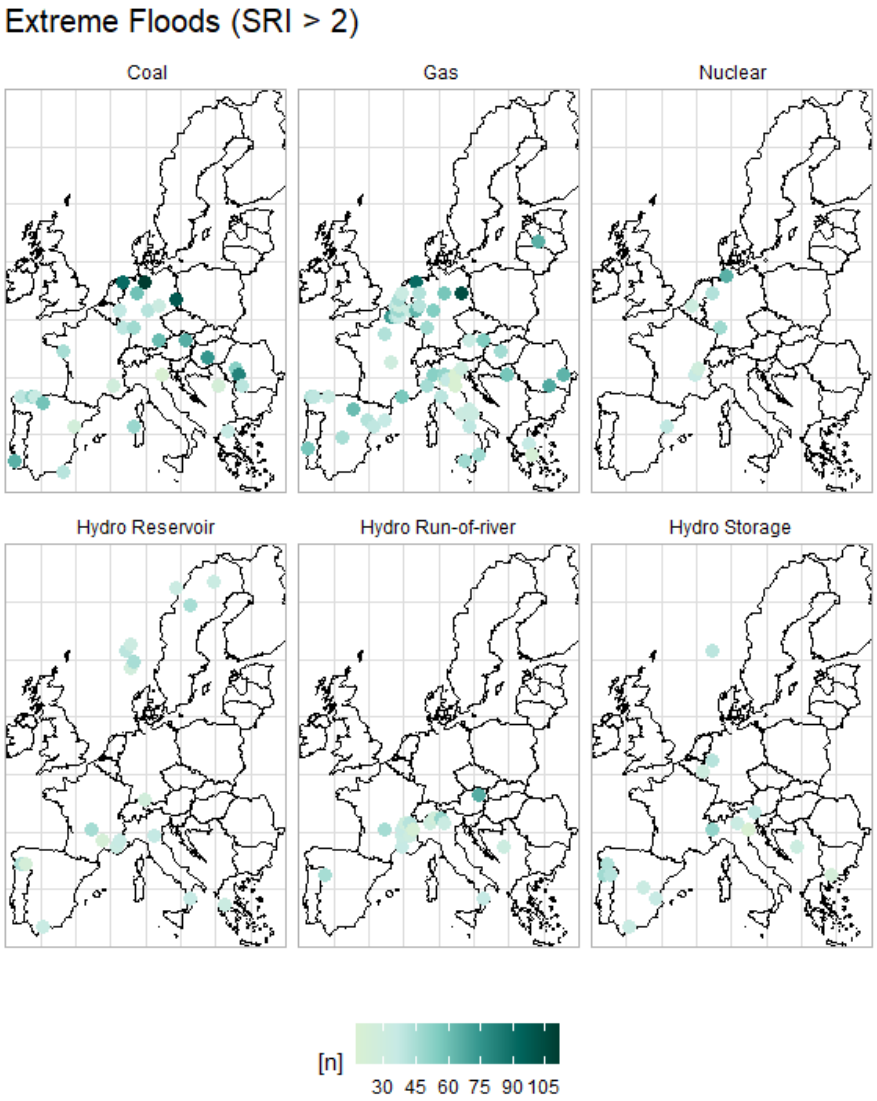

Figure 34 Location specific annual number of power plant-days with exposure to extreme floods, average of GCM output and of 2041-2050, for RCP 245.

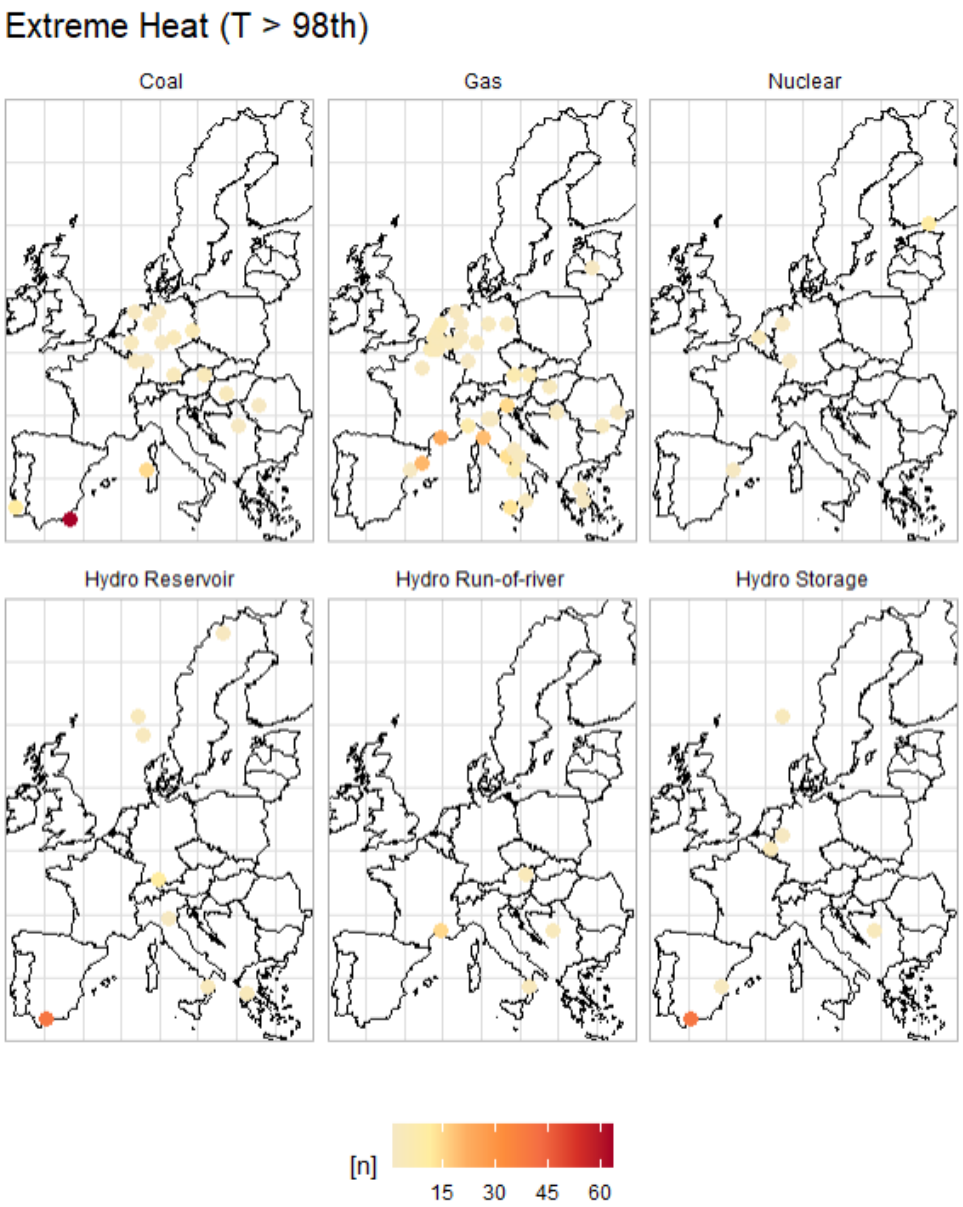

Figure 35 Location specific annual number of power plant-days with exposure to extreme heat, average of GCM output and of 2041-2050, for RCP 245.

4. Economic impacts on agriculture and forestry with and without adaptation

The results presented in this section include only a subset of the results available from the economic modeling and these results presented at the European level. The results disseminated to project partners will include NUTS2 level, member state and regional aggregation.

4.1. Expanded food security indicators

The following section presents the indicators related to the food system to capture a broader understanding of food security, including measures of availability, affordability, and price stability.

Key indicators include price trends (tracking changes in food prices over time), changes in consumer expenditures on food, and regional self-sufficiency ratios, which reflect the region's ability to produce its own food. The share of populations at risk of hunger and the changes in consumer surplus highlight the economic benefits or losses to consumers as a result of price shifts and are included as well. These indicators are presented at a European regional level in this deliverable but the modeling results are provided to project partners at a country level for European MS and large regions outside Europe.

Prices

Figure 36 shows the projected crop and livestock prices (in USD 2000 per ton) from 2020 to 2050 under three adaptation scenarios with different mitigation assumptions (RCP 2.6, RCP 4.5, and RCP 7.0). Each line is the average of the GCM ensemble of the different adaptation scenarios: high adaptation (green line), low adaptation (red line), and a reference adaptation scenario (blue line). Across all RCP scenarios, crop prices are expected to decrease over time, with higher adaptation levels consistently resulting in lower prices, indicating that adaptation measures can help mitigate price increases driven by climate change. Generally, livestock prices decline over time across all scenarios, with the highest prices under low adaptation and the lowest under high adaptation. Under RCP 2.6, livestock prices remain higher compared to RCP 4.5 and RCP 7.0, suggesting that higher levels of mitigation (which mean lower emissions from the AFOLU sectors) results in less decline in prices over time.

a)

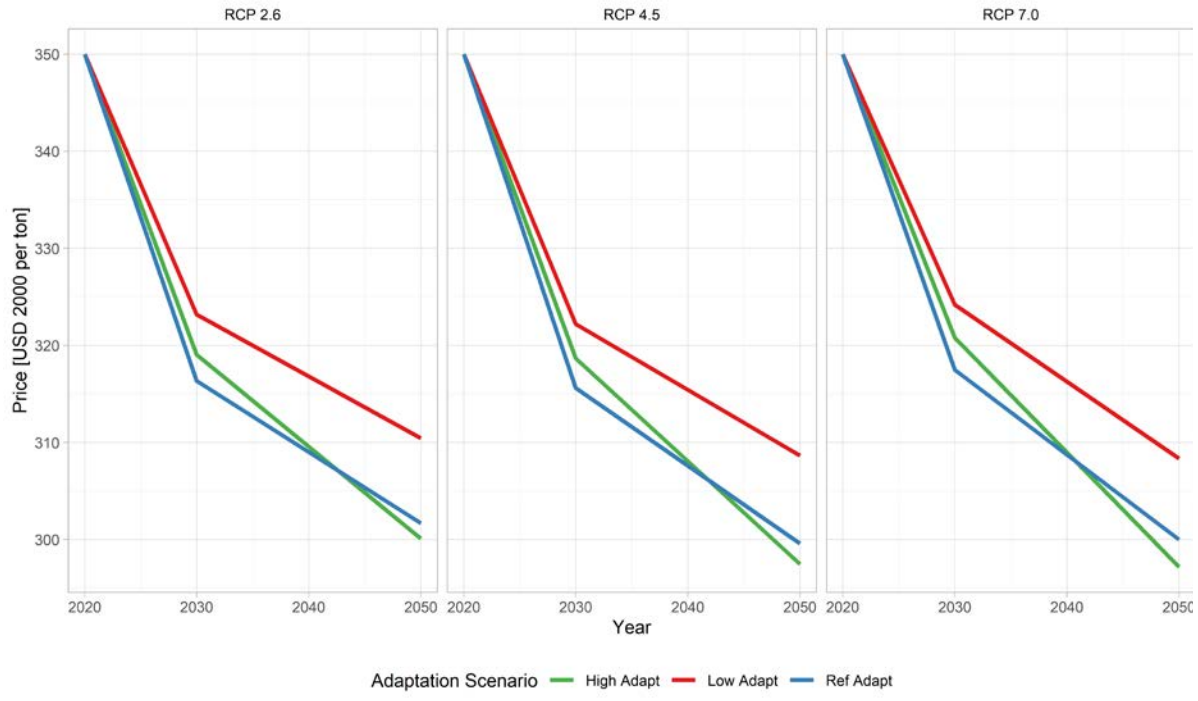

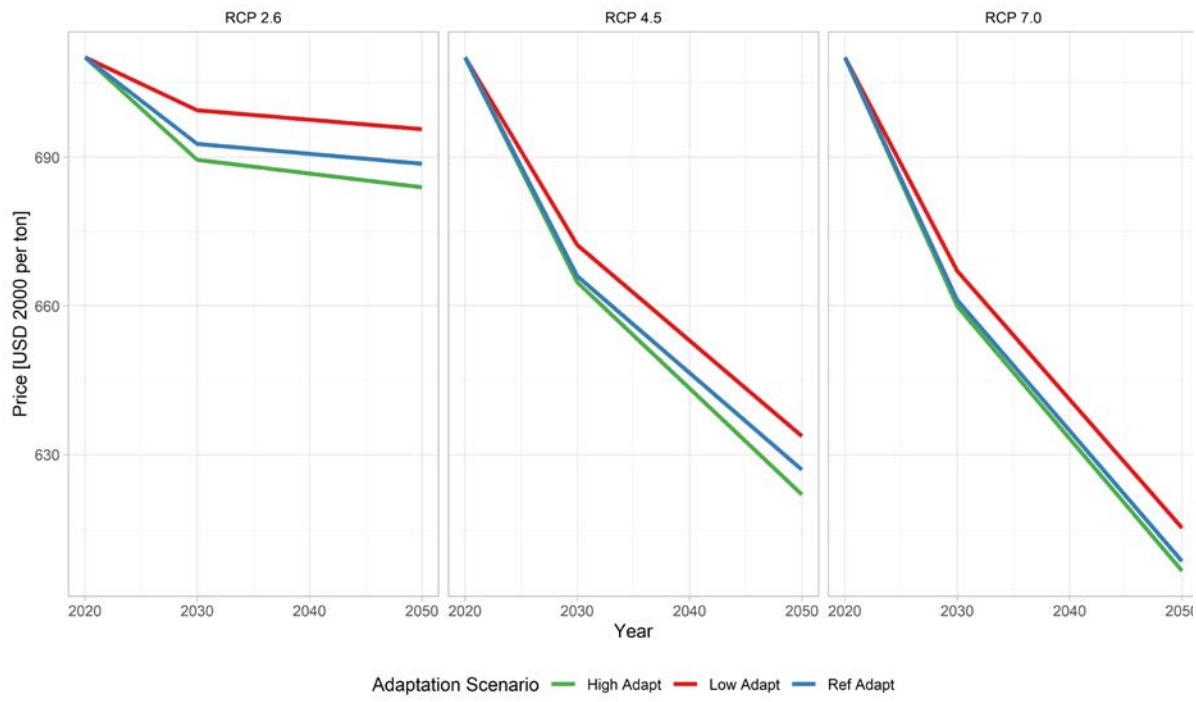

Figure 36. Price trends for selected crop, livestock and forest product aggregates for European countries by RCP. Colors represent different adaptation scenarios (Average of the GCM ensemble). Source: Palazzo, Arbelaez-Gaviria et al. in prep

Share at risk of hunger

The share at risk of hunger is calculated by simulating food demand and distribution using factors like population growth, income, and food policies (Hasegawa et al., 2019). This analysis has typically assessed how changes in food availability affect undernutrition in developing regions which do not include countries in the EU. However, as food insecurity is a global issue, with interconnected trade and environmental impacts, we examine the impacts of undernutrition from climate change as well as the adaptation scenarios on developing regions.

In 2017, about 11% of the world's population (821 million people) suffered from hunger (FAO, IFAD, UNICEF, 2018). GLOBIOM estimates to decline due to socioeconomic growth to 373 million in 2050 (Hasegawa et al., 2019). Climate change impacts are expected to exacerbate food security issues in regions that face negative impacts (Janssens et al., 2020). We find that result is robust as well in our study which included the climate impacts on more agricultural sectors. In Figure 37 we present the climate impacts on the change in population and under the different adaptation scenarios. The GCM spread is particularly high in under higher levels of warming (+30 million people under UKESM1-0-LL to -42 million people under MPI-ESM1-2-HR).

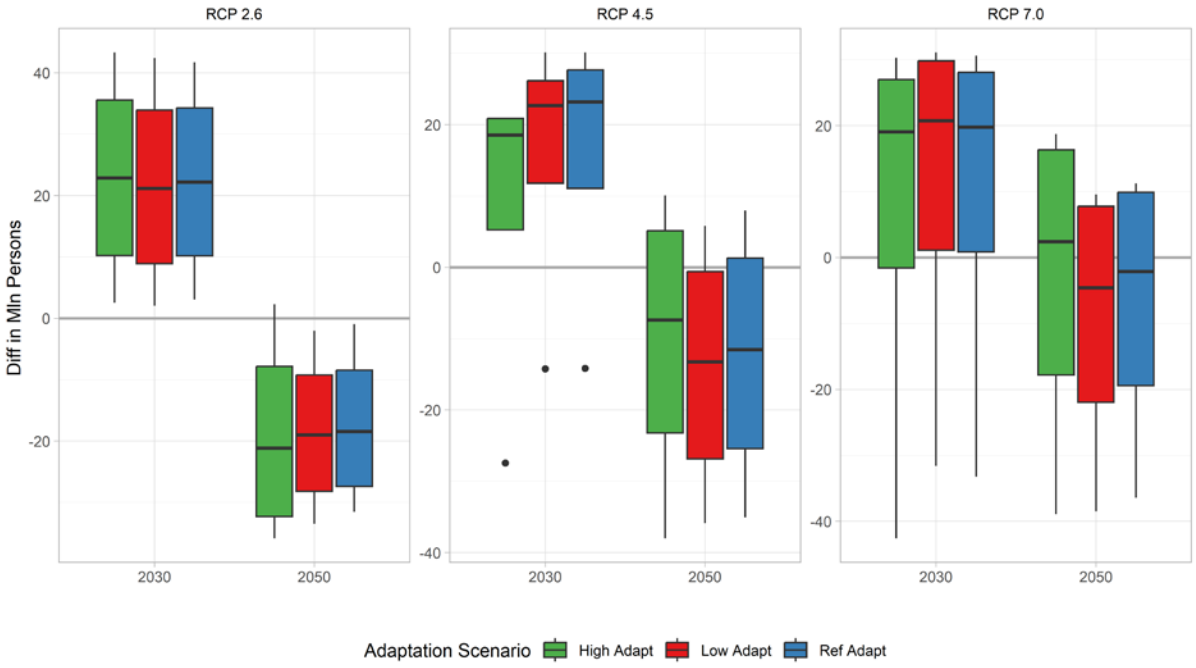

Figure 37 Change in population at risk of hunger in 2030 and 2050 under climate impacts. Relative difference to no climate change.

Consumer expenditure

In this section, we present another indicator of food security: consumer expenditure on food. We calculate the per capita consumer expenditure on food by taking the total quantity of food consumed, multiplying it by the price paid by consumers, and dividing that total expenditure by the total population. We then index these expenditures to the 2020 per capita levels to analyze how climate change impacts the cost of food for individuals and assess the impact the different adaptation scenarios have on consumer spending. This approach allows us to measure how adaptation to climate change on the producer side might affect changes in food prices.

Figure 38 shows the projected per capita consumer expenditure on all crop and livestock food (a) on only crop products (b) and for dairy (c) and for meat products (d) in 2050, indexed to 2020 levels, under different climate change scenarios (RCP 2.6, RCP 4.5, and RCP 7.0). The bars represent expenditures in a "no climate change" scenario, while the shapes indicate expenditures under various GCMs. Across all RCP scenarios, consumer expenditures generally decrease slightly in comparison to the 2020 levels, reflecting a possible reduction in per capita expenditure due to lower prices. The adaptation scenarios (high, low, and reference) show only modest differences in expenditure, suggesting that the adaptation scenarios have relatively small impact on consumer expenditures compared to the differences between GCMs or RCPs.

The per capita crop expenditure will likely decrease relative to the 2020 levels under all adaptation and RCPs and GCMs due to the decrease in the crop prices over time. In some cases, the per capita expenditures under different GCMs is lower than under no climate change. This is likely due to some regions experiencing a positive impact from climate change and resulting in more supply and thus lower prices.

The per capita dairy expenditure will likely decrease relative to 2020 levels under all adaptation and climate scenarios. However, the level of expenditure slightly varies across RCPs, with RCP 2.6 generally showing a per capita higher expenditure than RCP 7.0, this follows the same trend as the

prices for livestock products that are likely affected by the mitigation policy. In general, the impact of climate change will increase the per capita expenditures for dairy, but overall, expenditures remain lower than in 2020 across scenarios.

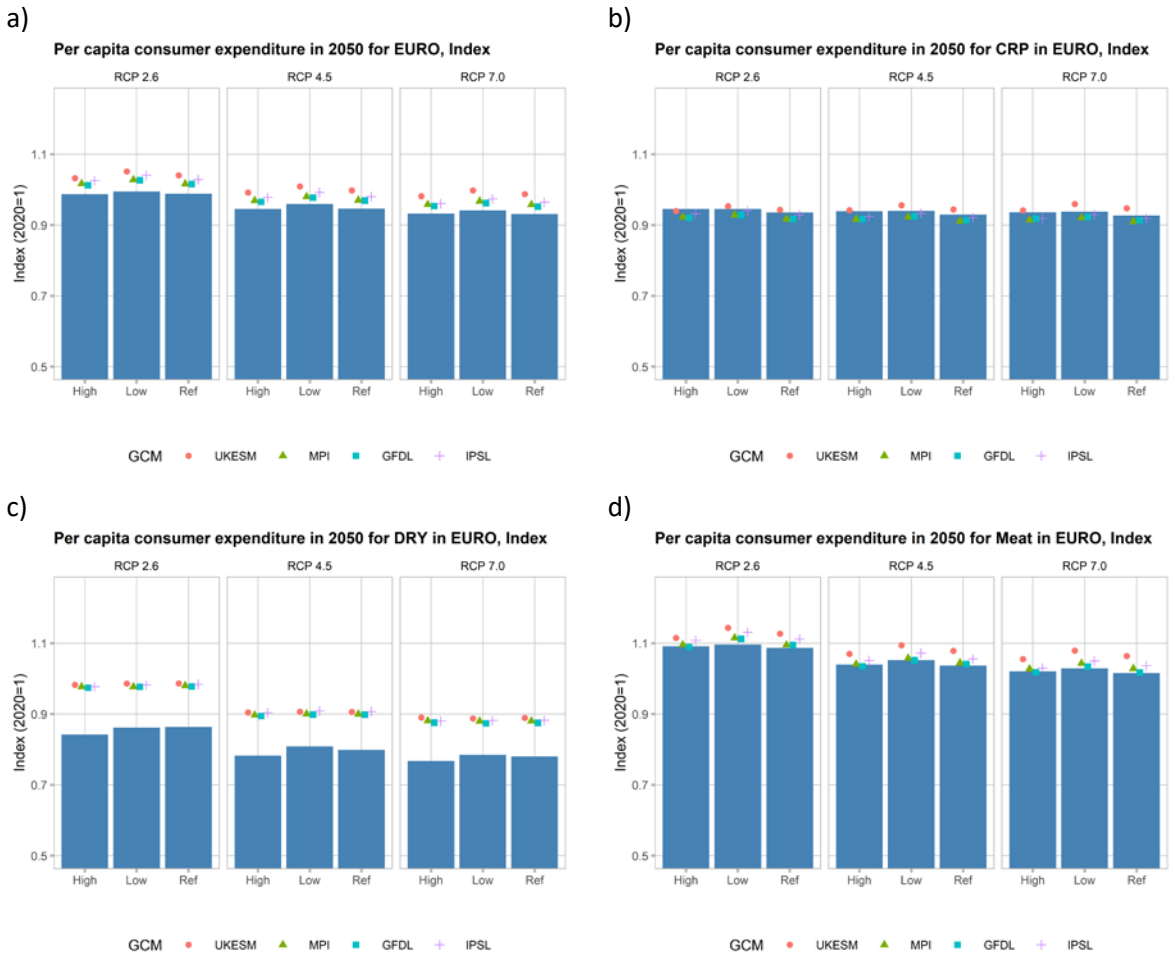

Figure 38. Per capita consumer expenditure for a) all food products, b) only crop products, c) dairy, and d) meat products in 2050 for Europe indexed to year 2020 values for the reference, high, and low adaptation scenarios under different levels of mitigation (bar indicates the no climate impact scenario, points are different GCMs) Source: Palazzo, Arbelaez-Gaviria et al. in prep

Self-sufficiency ratio

The self-sufficiency ratio (SSR) is an indicator that can be used to assess region or a country's food security because it indicates the degree to which a country can meet its food needs from its own domestic production (van Ittersum et al., 2016). We calculated this indicator as the percentage of domestic production over total domestic consumption for a particular food commodity or for the entire food supply. For ratios over one it indicates the region or country is a net exporter for a ratio under one it indicates that the region relies on imports for domestic consumption. In this case consumption includes all utilization of a product (e.g., food, feed, biofuels, and agricultural waste). Figure 39 compares the SSR in 2050 for the aggregation of all crop products in Europe under different RCPs and adaptation scenarios. The blue bars represent the adaptation scenario SSRs without climate impacts and the different shapes represent the adaptation scenario SSRs under different GCMs. The black bar shows the SSR in 2020 for reference. To allow for comparing different crops that have different utilization and weights we converted the products first to calories. Some crop products are used for bioenergy purposes however, the products are primarily used for food and feed which makes

this the most straightforward way to compare diverse crop types. We also note that SSR may look different for different major European regions and for different countries. Our results that under most GCMs, the SSR will fall below the 2020 levels in the low and reference adaptation scenario. The high adaptation scenario has the highest SSR even under climate change. We also find that the low adaptation scenario results in the lowest SSR under no climate change and under climate change.

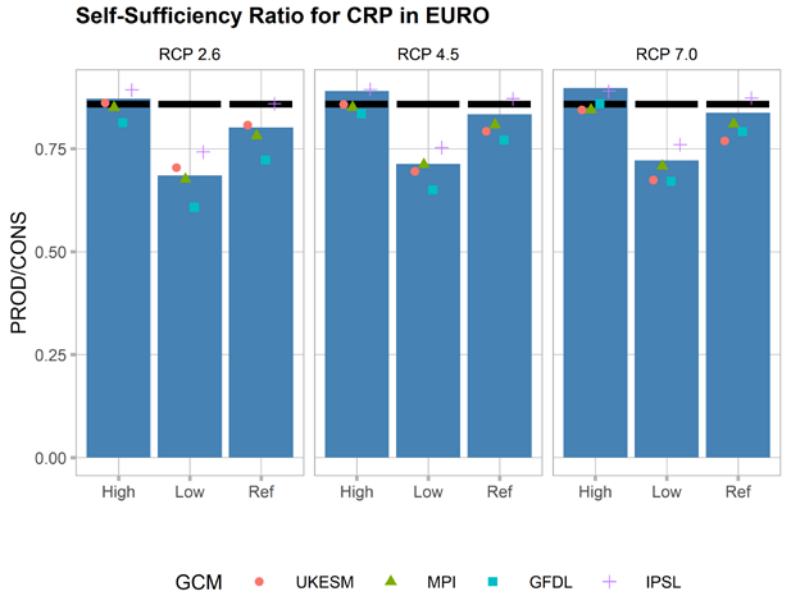

Figure 39. Comparison of the self-sufficiency ratio in 2050 (calories produced divided by calories demanded for all crop products) in Europe under the reference scenario and adaptation scenarios (shapes are the different GCMs, black bar is the SSR in 2020) Source: Palazzo, Arbelaez-Gaviria et al. in prep

4.2. Distributional effect among producers and consumers

In this section we take a focus on the adaptation scenarios and the distributional effects and impacts of the adaptation scenarios on different actors, consumers, producers of crop products and of livestock products. The indicators that we compare in this section are presented at a European regional level in this deliverable, but the indicators are based on modeling results which are provided to project partners at a country level for European MS and large regions outside Europe.

Prioritization of food supply versus value added products

Here we look at the impact of adapting to climate change through expanding irrigated area and how the expansion of irrigation impacts the self-sufficiency of the region. In GLOBIOM irrigated area will expand if it is more profitable (based on prices and productivity). **Error! Reference source not found.** compares the expansion of irrigated areas with the SSR for the European region under the GCM ensemble for the adaptation scenarios. The colors represent the adaptation scenarios and the shapes reflect the warming level (RCP). We can see the extent to which more irrigated area results in more production of products consumed in the region. Under the high adaptation scenarios the SSR and the irrigated area are the greatest, while under the low adaptation scenario the SSR is the lowest (and the irrigated area is also the lowest). When we compare the impact of the RCP on the adaptation scenario we can see that the RCP 2.6 has the lowest SSR (also shown in SSR section from Section 4.1 Expanded food security indicators). This finding may not hold in all major European regions or for each country as there is significant intraregional trade between European countries.

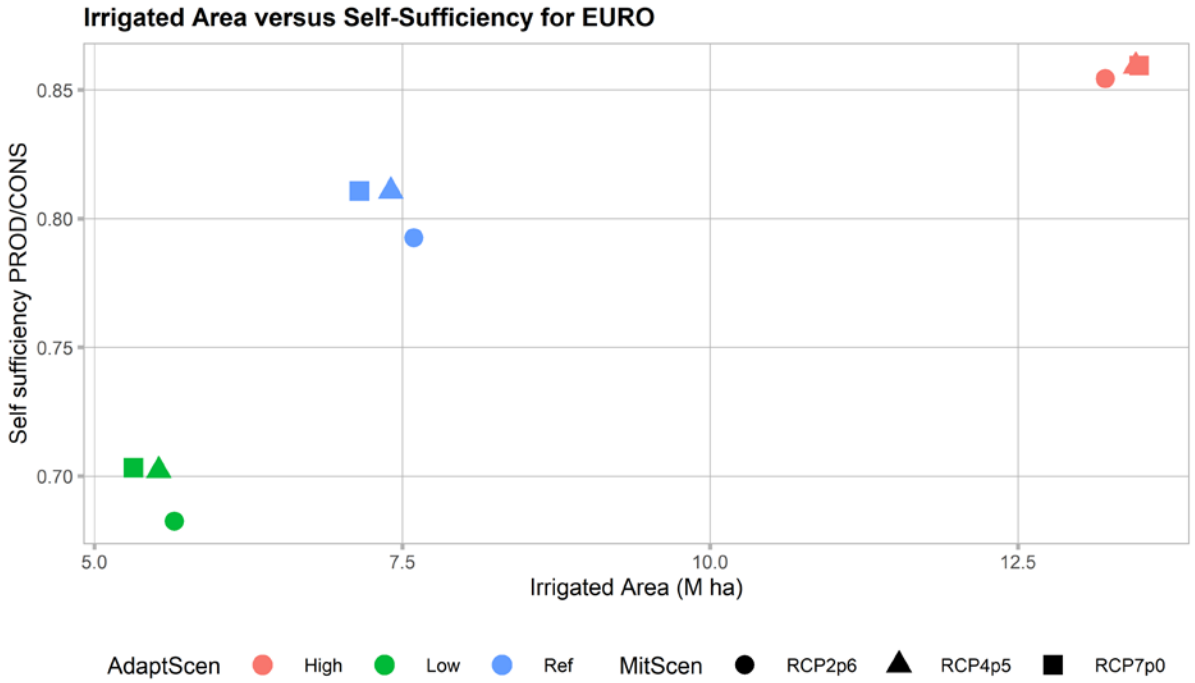

Figure 40. Scatterplot of irrigated area and self-sufficiency for all crop products for the reference scenario and adaptation scenarios in 2050 (average of the GCM ensemble) Source: Palazzo, Arbelaez-Gaviria et al. in prep

Producer and consumer benefits under adaptation

GLOBIOM solves for the market prices for primary products, such as raw agricultural goods, to represent their value at the initial stage of production. However, many products gain additional value as they are transformed into final goods for consumers. To estimate this additional value (i.e., the value added"), we use the GTAP database which captures the cumulative value added throughout the supply chain, including processing, packaging, and distribution.

For example, wheat has a market price as a primary product. But by the time it reaches consumers in the form of bread, it has accrued value through milling, baking, and transportation. This added value is essential to understand the total economic contribution of primary products for retail.

We compare this calculated value added for primary products with the consumer surplus. Consumer surplus is a measure of the benefit consumers gain when they pay less for a product than the maximum they would be willing to pay. It reflects the difference between consumers' perceived value of a good and its actual price, providing an indication of affordability and consumer satisfaction. **Error! Reference source not found.** compares the value added for producers for all agricultural products in the European region with the consumer surplus for all agricultural products consumed by consumers under the GCM ensemble for the adaptation scenarios. The colors represent the adaptation scenarios and the shapes reflect the warming level (RCP). We can see the extent to which consumers or producers benefit from the adaptation scenarios in the region. We find that high adaptation scenarios do not result in more value added for producers (likely due the price effect which an increase in supply lowers the price for producers), and conversely the high adaptation scenarios in all cases result in the highest consumer surplus (due to the same price effect). The adaptation scenarios under the higher emissions pathway (RCP7.0) generally show lower consumer surplus and value added, which could suggest that more severe climate impacts could reduce the economic benefits for consumers and producers alike.

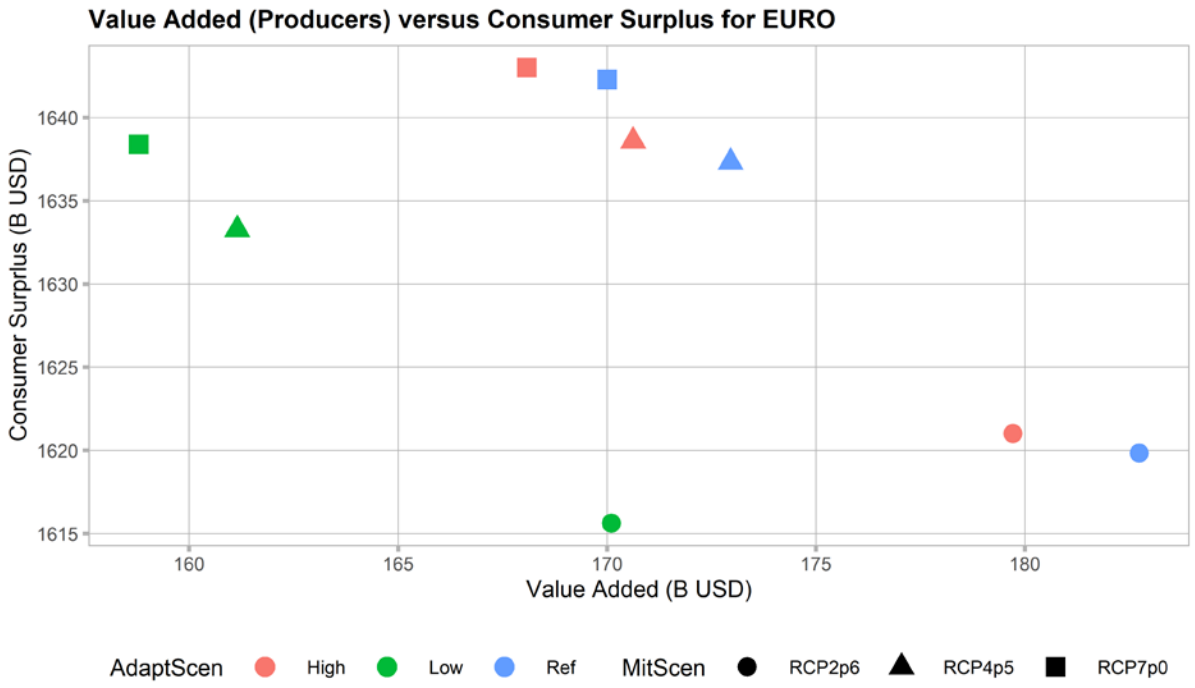

Figure 41. Scatterplot of value added (producer benefits) and consumer surplus for the reference scenario and high and low adaptation scenarios () Source: Palazzo, Arbelaez-Gaviria et al. in prep

Producer adaptations to climate impacts

The optimization modeling of GLOBIOM takes into account the behavior of farmers to adapt to changing conditions and market signals. The model assumes that farmers can make adaptations to maximize their economic benefits and meet the demands of a changing market. These adaptations are driven not only by the production conditions (and therefore the climate impacts) but also by changing consumer preferences, fluctuating market prices and climate targets. **Error! Reference source not found.** presents the change in the total production (in calories) when various shocks and adaptions are considered. The bars represent the GCM UKESM1-0-LL and the error bars represent the spread of the GCMs and RCPs. Here we consider the shock to farm productivity and profitability from the climate change impacts on yields as "CC" as well as the shock on profitability for meeting climate targets (e.g., paying carbon taxes on emissions from production and land use change). The shock bars are negative because they are compared to the adaptation scenario under no mitigation and no climate change.

In the category of autonomous adaptation, one strategy involves changes in management practices, including crop switching. Farmers are re-evaluating their crop choices based on climatic conditions and market demand. For instance, as certain crops become less productive due to heat stress or change in precipitation patterns, farmers may shift to more resilient varieties or entirely different crops that can better withstand these changes. Additionally, farmers can relocate their crop production to different areas to optimize yields. As seen in the figure, these adaptations in management practices increase the production compared to the no climate change reference. The ARRF and ARIR show the area response where transitions from different crop management systems to more productive systems (e.g., from rainfed to irrigated systems) were not considered. Finally the final bar column shows the actual impact compared to the no climate change reference, where we can see that for some GCMs the high adaptation scenario would result in higher production compared to the no climate change reference but for others it remains negative.

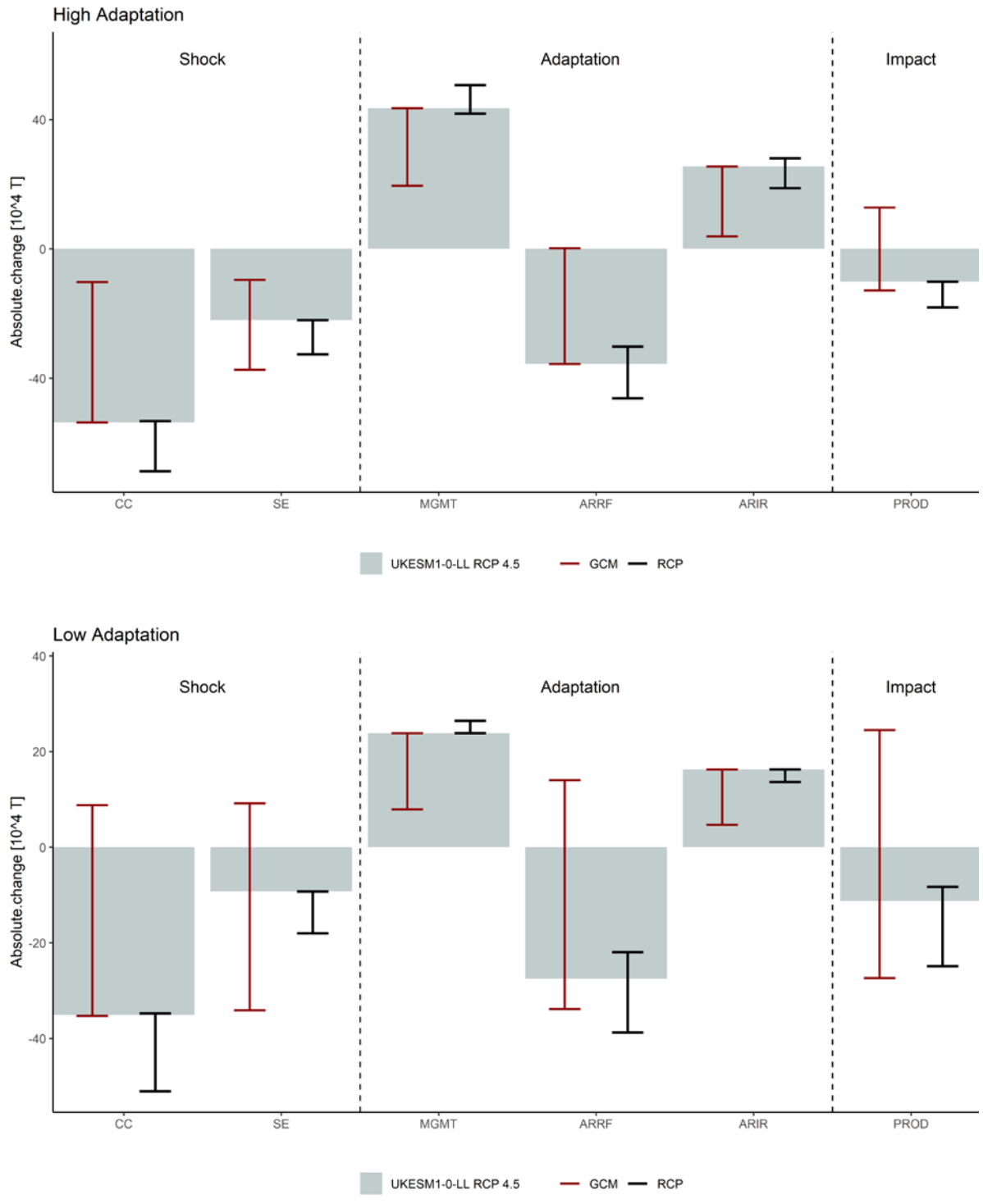

Figure 42. Absolute differences in the climate shock (from reference scenario with no climate change) differences in calories/or tons produced for all crop and livestock products for European countries (difference is reference scenario and high and low adaptation scenarios Source: Palazzo, Arbelaez-Gaviria et al. in prep

Here we examine the impact of expanding irrigated area on total crop production. Figure 43 shows a comparison of the irrigated area and calories produced on European cropland for the average of the GCM ensemble. The high adaptation scenario results in more crop production under all RCPs. However, it should be noted that the irrigated area expansion is limited to crops covered in GLOBIOM (e.g., field crops) and does not include fruits or vegetables.

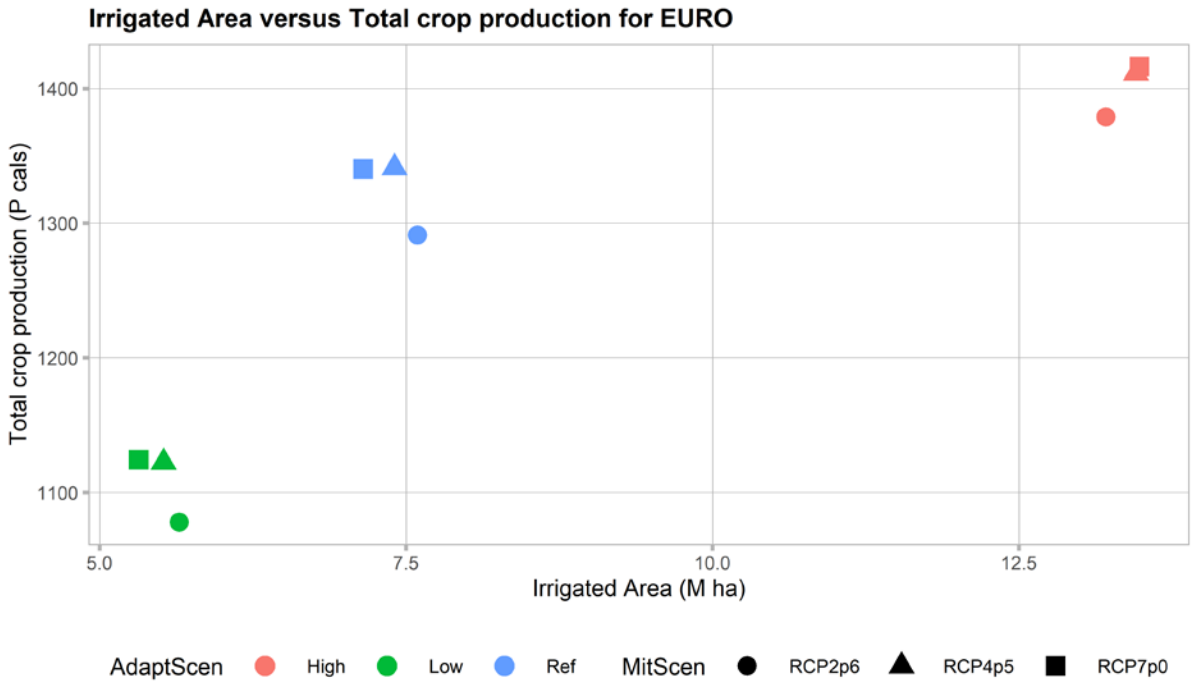

Figure 43. Scatterplot of irrigated area and production for the reference scenario and adaptation scenarios in 2050 (GCM average) Source: Palazzo, Arbelaez-Gaviria et al. in prep

Transitions in livestock systems

The livestock sector is a significant source of greenhouse gas (GHG) emissions, particularly methane (CH_4) from enteric fermentation and nitrous oxide (N_2O) from manure. In Europe, implementing mitigation policies aimed at reducing these emissions could play a critical role in achieving broader climate targets, such as those set out in the European Green Deal and the Paris Agreement. Transitioning livestock systems towards more sustainable practices, including reductions in livestock numbers or changes in feeding practices to improve efficiency, can significantly reduce these emissions.

Figure 44 shows the difference in grassland area in European countries in 2050 under the GCM ensemble compared with the ruminant calories produced. We can see that under lower warming scenarios (and increasing mitigation targets) the grassland area declines for all adaptation scenarios as extensive systems are less productive in terms of kg per unit of GHG emissions produced. Under the RCP 4.5 and RCP 2.6 mitigation scenarios, grassland area declines slightly for the high adaptation scenario compared to the reference scenario though more calories are produced due to the increase in flexibility for livestock systems to transition to more productive systems.

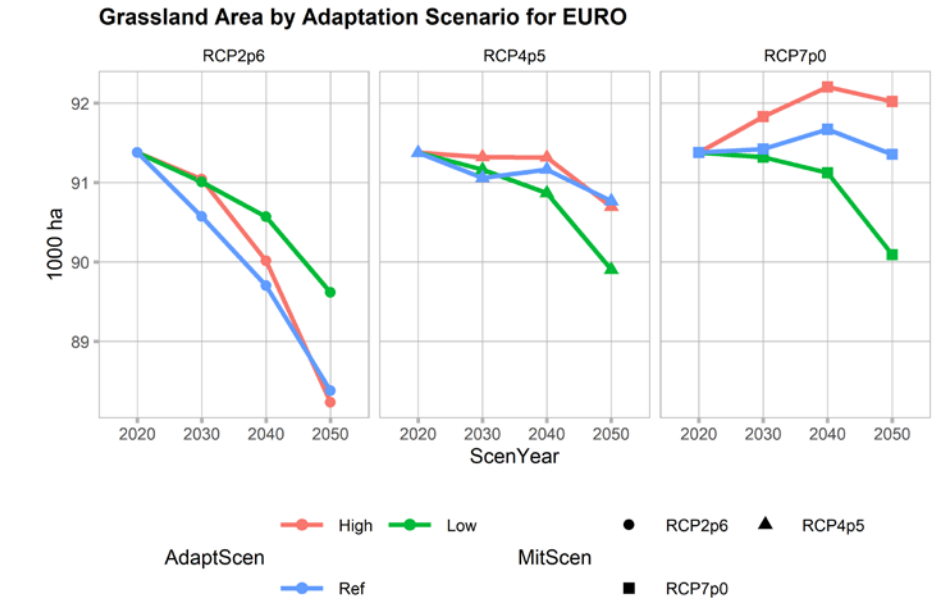

a)

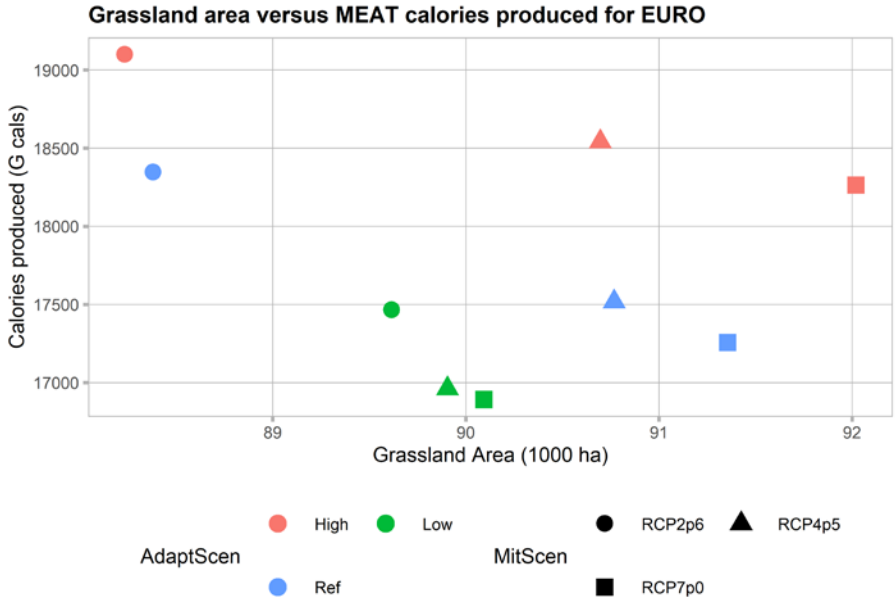

b)

Figure 44. Change in grassland area over time under different mitigation and adaptation scenarios (a) and grassland area compared to ruminant meat calories in 2050 for European countries (b) (average of the GCM ensemble) Source: Palazzo, Arbelaez-Gaviria et al. in prep

Trade

In this section we look at the distributional effects of the adaptation scenarios through intraregional trade (i.e., trade from European countries to European countries) and the per capita consumer expenditure to give insights into how different regions might manage food security under climate change. By examining the share of imports from intraregional trade, we can assess how much a region relies on neighboring trading partners. Regions that depend heavily on imports from outside their region may face higher risks of price shocks if global supply chains are impacted by climate change. A higher proportion of intraregional trade can enhance a region's resilience by reducing dependency on sources that may be affected differently by climate change or trade policies. Under the high adaptation scenario, the trade costs are lowered within Europe to simulate more liberalized trade

expansion. In the low adaptation scenario, the trade costs are increased to simulate further frictions in trade.

Figure 45 presents a comparison of the share of imports supplied through intraregional trade versus the per capita consumer expenditure for four different agricultural commodities: maize, wheat, ruminant meat, and dairy, under the adaptation and the GCM ensemble of the warming scenarios. Under the high adaptation scenarios there is a higher share of trade between European countries across all the products and warming scenarios. For maize, the increase in intraregional trade also results in lower per capita expenditure for maize. For wheat, the increase in intraregional trade for the high adapt scenario does not result in significant changes in the per capita expenditure when compared to the reference scenario. The low adapt scenario has the lowest intraregional trade and the highest per capita expenditure for both maize and wheat. For livestock products the high adapt scenario results in an increase in intraregional trade (significantly for ruminant meat, but less significantly for dairy), when compared to the reference and low adapt scenarios, however the impact on consumer expenditure is marginal. This demonstrates that the trade policies of the adaptation scenarios have little much more impact on producers of livestock products than consumers. The mitigation policies have also significantly more impact on consumer expenditures of livestock products as has been raised in the previous sections.

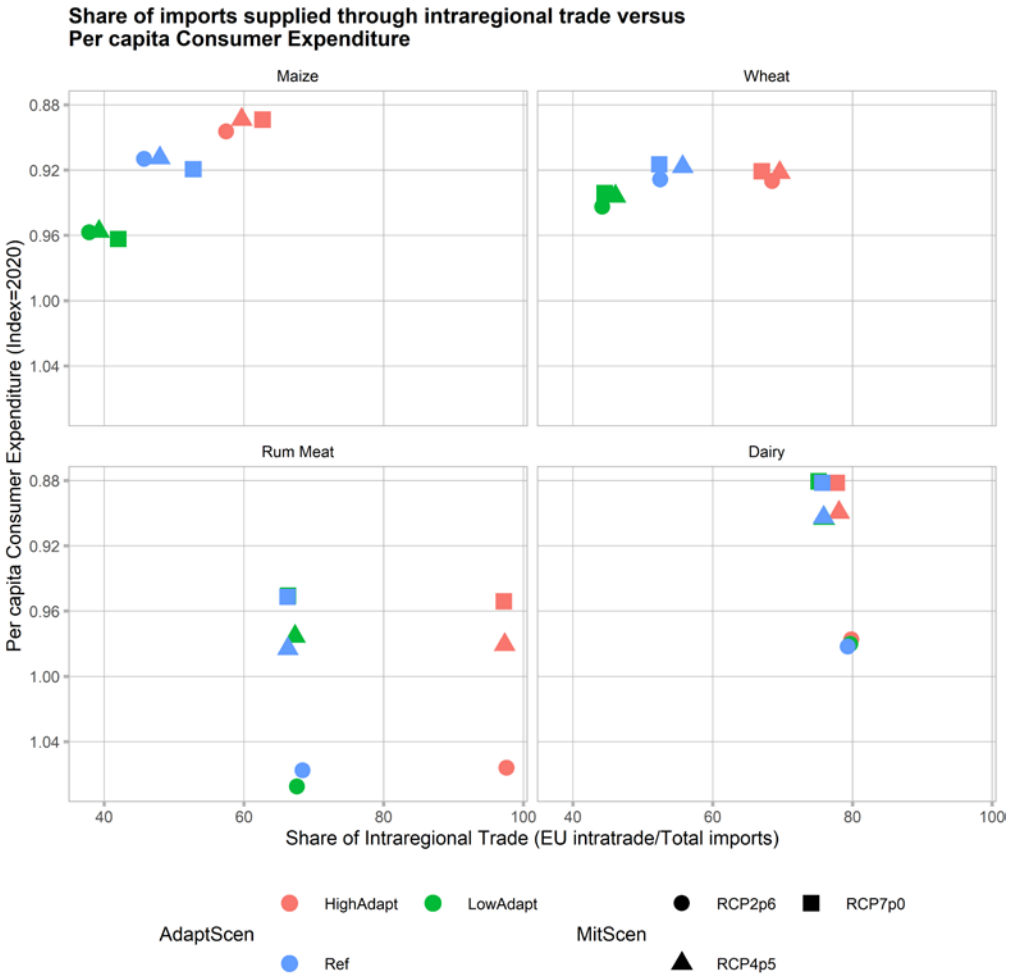

Figure 45 Scatterplot of share of intraregional trade and SSR for the reference scenario and adaptation scenarios in 2050 (average of the GCM ensemble).[6] Source: Palazzo, Arbelaez-Gaviria et al. in prep

[6] Note that the Y-axis is reversed in this figure to ease the presentation of information.

4.3. Adaptation costs

This section provides an overview into the adaptation costs associated with irrigation expansion and energy costs. Future adaptation costs in the energy sector are based on back-of-the-envelope calculations that translate the direct, physical adaptation needs shown in Section 3.3 into energy expenditure or costs.

Irrigation adaptation costs

As a part of ACCREU we have expanded the investment expanded the investment module to consider irrigation investments for EU countries. The irrigation adaptation cost calculations are based on an update from Palazzo et al. (2019).

Table 10 provides an overview of components that make up the full cost of irrigation based on Rogers et al. (1998) conceptual overview of costing water for irrigation. In all the scenarios farmers are responsible for the operations and maintenance of the systems, which have been included in the model as production costs. Additionally, farmers are responsible for paying per unit cost of water used for irrigation. The partial subsidies on the capital costs to upgrade and expand water delivery systems are publicly funded, meaning not included in the producer cost optimization. The costs associated with the adaptation costs are divided into expansion costs

Table 10 Overview of the types of irrigation costs of irrigation as defined by Rogers et al. (1998)

<table>
<tr><th>Irrigation cost of irrigation</th><th>Reference</th><th colspan="2">Responsible for costs</th></tr>
<tr><td colspan="2">1.Operation and maintenance</td><td colspan="2" rowspan="4">Producer (within GLOBIOM as production cost)</td></tr>
<tr><td>a. Energy (gasoline, diesel, electricity, animal power, or human power)</td><td>Sauer et al. (2010), FAO (2016)</td></tr>
<tr><td>b. Labor</td><td>FAO (2008), Sauer et al. (2010), FAO (2016)</td></tr>
<tr><td>c. Routine maintenance and wear-and-tear</td><td>FAO (2008)</td></tr>
<tr><td colspan="2">2. Capital costs</td><td>Large scale infrastructure</td><td>On farm</td></tr>
<tr><td>a. Engineering, engineering management</td><td>Inocencio et al. (2005), Inocencio et al. (2007), FAO (2016)</td><td rowspan="2">Public Sector (in ex-post investment cost calculation as expansion costs, upgrade costs, and efficiency costs)</td><td rowspan="4">Producer (within GLOBIOM as production cost and land conversion cost)</td></tr>
<tr><td>b. Parts and material</td><td>Inocencio et al. (2005), Inocencio et al. (2007), FAO (2008), FAO (2016), Rosegrant et al. (2017)</td></tr>
<tr><td>c. Interest and finance costs</td><td>Inocencio et al. (2005), Inocencio et al. (2007), FAO (2008)</td><td rowspan="2">Public Sector (in ex-post investment cost calculation as depreciation)</td></tr>
<tr><td>d. Training, technical assistance, institutional development, capacity strengthening</td><td>Inocencio et al. (2005), Inocencio et al. (2007), FAO (2008), Rosegrant et al. (2017)</td></tr>
<tr><td>e .Administrative costs</td><td>Inocencio et al. (2005), Inocencio et al. (2007), FAO (2008)</td><td colspan="2" rowspan="2"></td></tr>
<tr><td>f. Depreciation</td><td>Schmidhuber et al. (2009)</td></tr>
</table>

3. Resource costs		
a. Opportunity costs of alternative water uses	Toan (2016)	Producer (within GLOBIOM as the water price)
b. Taxes, licenses, and government levied resource fees	Van Koppen et al. (2005)	

Figure 46 highlights the varying investment priorities needed under different climate and adaptation scenarios. In the High adaptation scenario (which has the largest expansion of irrigated area), there are significantly large investments needed all RCPs, with expansion costs (e.g., parts and materials) being the most substantial, followed by Maintenance and Efficiency (e.g., improving the systems to reduce water conveyance losses). The Low and Reference scenarios show considerably lower investment levels due to the decline in irrigated area compared to the base year. The irrigation investment costs are provided at a national, aggregate region, and European regional level to the Work Package 4 models.

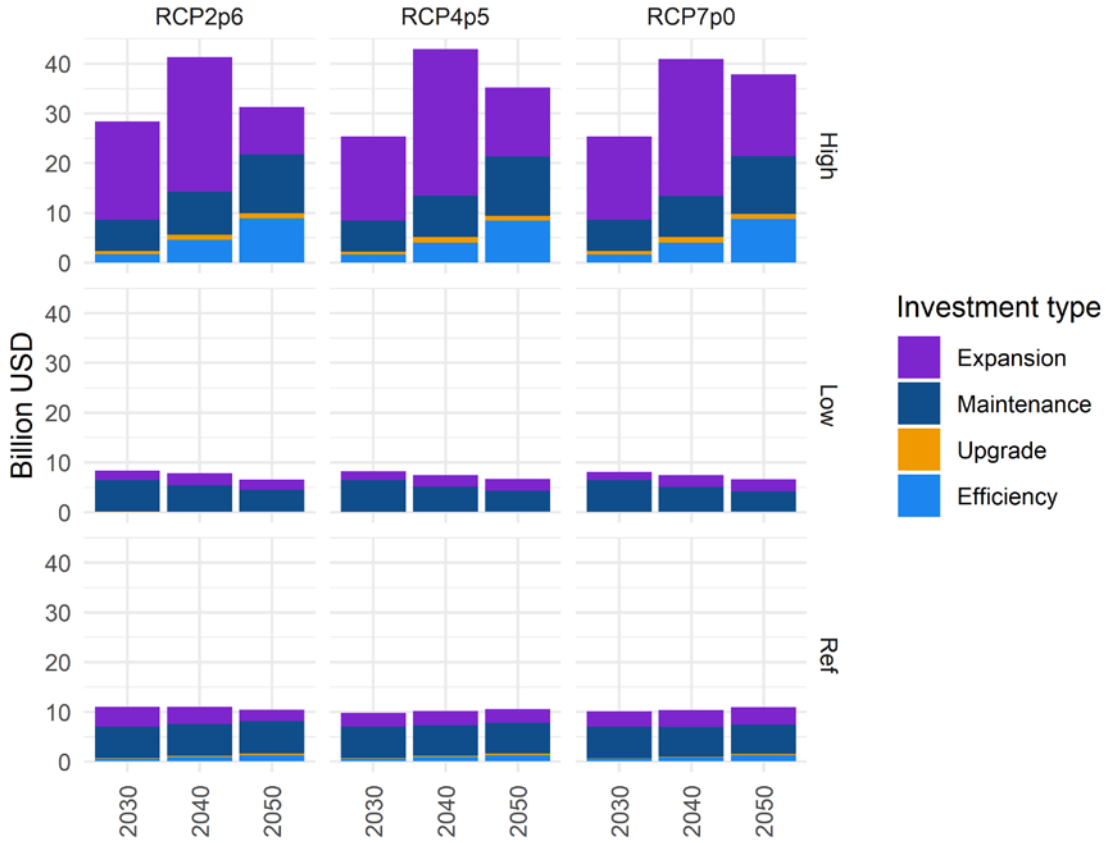

Figure 46. Irrigation investment cost for Europe compared to no climate impacts in the reference scenario and high and low adaptation. (average of the GCM ensemble) Source: Palazzo, Arbelaez-Gaviria et al. in prep

Energy costs

We adopt a simplified approach and project future adaptation costs in the energy sector assuming electricity and gas prices constant to the 2019-2023 levels and no market adjustments in demand or supply other than the ex-ante change inferred from the empirical analyses. We compute average prices of electricity and gas across household and non-household sectors exploiting EUROSTAT data,

associating to commercial, industrial and agriculture demand changes the energy prices of the non-household sector. These back-of-the-envelope calculations provide a first indication of expenditure changes across EU countries: we find that Italy and Spain are the countries with the highest increase in expenditures due to the electricity demand for adaptation, totaling across all sectors around 7-8 billion USD in 2050 and 17-19 billion in 2100 in each country (RCP 4.5). On the other hand, Germany is the country that experiences the largest reduction in costs from lower heating needs, around 10 billion USD in 2050 and 2100 (RCP 4.5) (see Figure 47, panel a). The results for the whole EU region highlight how the importance of higher adaptation costs for cooling versus for lower heating costs changes over time: in the "Reference" adaptation scenario, in 2030 adaptation costs in the energy sector are negative since fuel cost reductions are higher than electricity increases (net costs are -7 billion USD), in 2050 the two compensate with one another (net costs are –0.2 billion USD) and in 2100 cooling needs more than compensate the heating reductions, leading to an increase in costs of around 44 billion USD (see Figure 47, panel b).

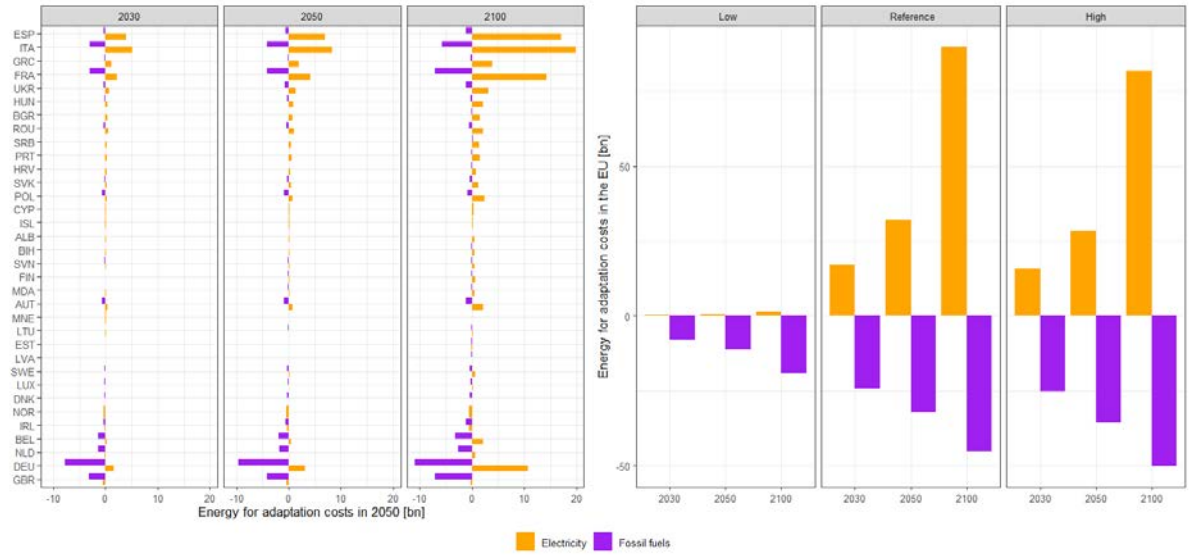

Figure 47. Projected costs for electricity (a) and fossil fuel energy demand due to adaptation (b), by period and adaptation scenario under RCP 4.5.

More comprehensive adaptation costs associated with energy demand could be computed by integrating the econometric simulations - that provide partial equilibrium projections of the potential, ex-ante changes in energy demand – into CGEs and IAMs, accounting for price-induced substitution and income effects that only macroeconomic approaches can describe. This approach enables to identify not only direct energy expenditures associated with adaptation, but also indirect costs such as the additional investments in electricity generation and transmission capacity.
Adaptation costs associated with air conditioning be computed by developing an appliance stock model of investment, operation, and retrofitting to estimate the private cost of cooling for climate change adaptation. This analysis will be based on the projections of AC ownership developed for this Deliverable, enriched with data on country-level cost and technological parameters. This data can be used to operate a dynamic stock turnover and energy use model.

Adaptation costs associated with planned power outages can be computed in terms of foregone profits. An additional source of adaptation costs results from the operational (maintenance) costs associated with the management of an outage (e.g. technical staff engaged in the remedial actions required for the plant to restart). Since these costs are typically higher when power plant operators incur in a forced outage with respect to a planned outage, adaptation though planning a scheduled interruption can result in net benefits from the situation with no adaptation (and a forced outage).

The identification of the costs associated to such maintenance operations is technology specific and can vary depending on the country, the operator and the specific power plant.

Interactions of the econometric analyses developed with OSeMOSYS will enable the modeling to identify adaptation costs across several domains, including: i) Investments in AC adoption and building upgrades to tackle increased cooling demand; ii) investments in generation and storage infrastructure to address increased loads, intermittent generation and supply disruptions; iii) increasing utilization factor of other available technologies to deal with supply disruptions; iv) potential for electricity trade to address intermittent generation or supply disruptions.

5. Impacts of dynamic land use and land cover change in hydrological modeling, Two-direction soft coupling of CWatM-GLOBIOM

The following section describes the conversion of the downscaled GLOBIOM results into CWatM. The section presents the methodology and offers an example of including projected changes in landcover on the water cycle.

A two-step information exchange facilitates the coupling between GLOBIOM and the Community Water Model (CWatM). In the first step water availability is used as input into GLOBIOM to indicate how much water is available for irrigated agriculture (see Figure 48).

GLOBIOM is run over the scenario period under various socioeconomic, climate, and economic constraints (including water availability for irrigation). The water available for irrigation (see following section) is projected from CWatM and used as in input to the GLOBIOM model (Step 1 in Figure 48). The model outputs from GLOBIOM including projected changes in landcover and land use (including for agricultural expansion and intensification), are downscaled using downscalR (Step 4 Figure 48) and fed back into CWatM (Step 0 in Figure 48) to account for the impacts of projected land cover on the water cycle.

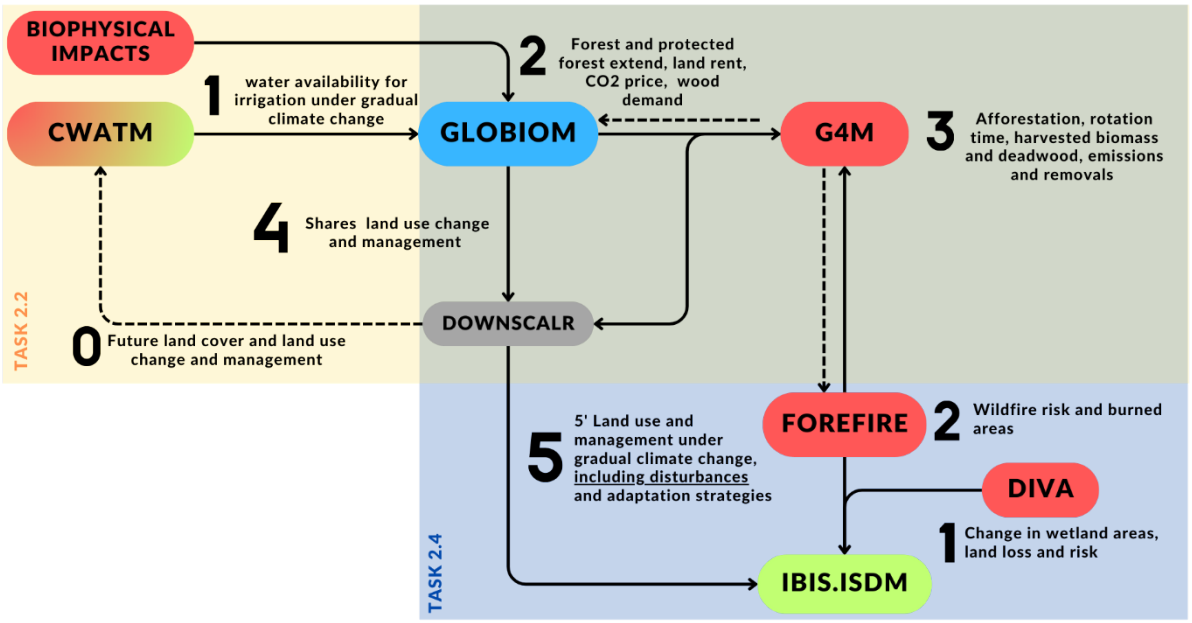

Figure 48 Schematic representation of information exchange between ACCREU models within the impact modeling chain.

5.1. Downscaling GLOBIOM landcover into consistent high spatial resolution maps

The downscalR toolbox was adapted and used for downscaling European land use projections harmonized with crop and management system projections to SimU resolution. The toolbox is a statistical downscaling method that can provide consistent high-resolution projections. At the core of downscalR is an econometric high-resolution model, which relates observed land use change data to a set of driver variables. It is open-source and available as an easy-to use R package[7]. The tool originally developed for land cover distribution but in the context of ACCREU it was extended and further developed to downscale crop and management systems to the simulation unit grid with the purpose to provide inputs to the hydrological and biodiversity modeling tasks of the project.

An overview of the downscaling framework is depicted in Figure 49. For the sake of simplicity and readability of the document crops and management systems will be hereafter only called "cropsys". Cropsys is the combination of one of the 17 GLOBIOM crops and one of the 4 management systems. The aggregate land use and cropsys projections stem from the macro-level model GLOBIOM (Aggregate projections). These are time- series of national projections and downscaled higher resolution projections should exactly add up to them, when aggregated. The main components of downscalR are represented in four colored boxes.
These are:

- **Prior module:** This module provides a consistent way of formulating priori information on the spatial distribution of land-use and cropsys change. It has two main subcomponents: the econometric models allow for prior construction when observed change patterns are available. The econometric models can be specified in a flexible manner to suit modeler's needs. They are multinomial logit type models. The module relies on a combination of static (as in not time variant) and projected high-resolution input data. The other subcomponent consists of sets of exogenous priors. These can be based on, for example, exogenous data sets (such as crop yields and prices) or expert knowledge. An additional add-on allows to mix exogenous and econometric priors in a flexible manner in case both are available for a specific transition. If no past observations are available, then the model falls back to the exogenous priors.
- **Target module:** The target module is employed to create gross cropsys changes from the level maps that are provided by the macro-level model. The modeler can specify which transitions are forced to zero in case information about impossible changes (irrigated rice to low input ground nut) is available.
- **Downscaling module:** The downscaling module takes as input the priors from the prior module (updated using projections of land use change drivers) and uses a bias correction optimization method to output high-resolution land use and cropsys change data, consistent with the macro-level model targets and the target module.
- **Mapping module:** The mapping module provides an interface for sharing the downscaled output in net CDF format.

[7] Source code available on GitHub: https://github.com/tkrisztin/downscalr

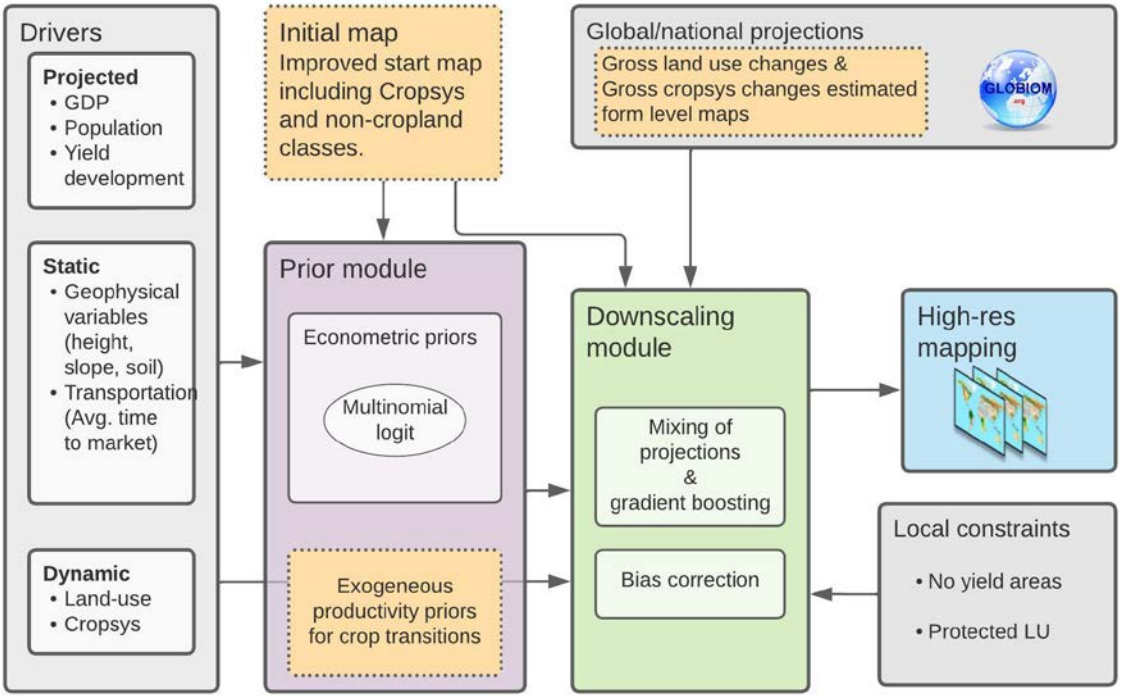

Figure 49 Conceptual outline of the downscalR model. SRP denotes short rotation plantations.

Within the downscalR model, we track six separate land use classes: grassland, other agricultural land, forest, wetland, other natural lands, artificial and other land as well as the 69 cropsys combinations that can be found in Table 1. When downscaling GLOBIOM outputs, the allowed land-use change transitions of GLOBIOM are respected: only transitions between cropland, grassland, forest, and other natural land as well as cropsys combinations excluding the subsistence management system are allowed, artificial, other agricultural areas, wetland, and subsistence cropsys combinations remain constant. Land-use prior transitions are estimated using the econometric prior module, further outline in the next section. Cropsys transitions priors are based on yield, price, and cost information at the grid.

Table 11 List of crops, management systems and land-use classes handled by the DownScale module.

Long name	CROP
Barley	Barl
Beans, dry	BeaD
Cassava	Cass
Chick peas	ChkP
Groundnuts, with shell	Gnut
Maize	Corn
Millet	Mill
Oil palm fruit	OPAL
Potatoes	Pota
Rapeseed	Rape
Rice, paddy	Rice

Long name	management system
subsistence	SS
low input	LI
high input	HI
Irrigated	IR

Long name	land use
Grassland	GrsLnd
Wetland	WetLnd
other natural land	NatLnd
Forest	Forest
other agricultural land	OagLnd

Seed cotton	Cott
Sorghum	Srgh
Soybeans	Soya
Sugar cane	SugC
Sunflower seed	Sunf
Sweet potatoes	SwPo
Wheat	Whea

urban and other land	NotRel

5.1.1. Prior module

The input variables to the prior module, as well as their sources are summarised in Table 2. The variables used to construct the prior transitions are either static or dynamic. Static variables are not updated during the projections (since no exogeneous or endogenous projections are available), while dynamic variables are updated every projection time step. The prior module relies on a set of dependent variables, based on economic theory of land use (e.g. see Nerlove, 1979), where the main factor of land use change is the relative profitability of various land uses and the cost of conversion. Hence, the main indicators for prior construction (whether based on stylized facts or more stringent modelling) are aimed at measuring the relative land use profits or conversion costs.

We utilize a ten-year land use change map from ESA-CCI covering the period of 2000 to 2010 as dependent variable to estimate the econometric models. These land cover products are available at a 300x300m resolution and they provide robust and harmonized maps for obtaining gross land use change transitions between all land-use classes.

In the econometric framework we model land use change decisions within an economic framework following Nerlove (1979). In each 5 arcminute grid cell i (with $i = 1, \dots, N$) consider the decision of a representative land user who has to economically optimize division of the cell among J land use classes. In a given time horizon between t and $t + h$ (where h denotes the horizon) the land user decides independently for each land use j (with $j = 1, \dots, J$) on what share of the land is kept in use j or converted to any one of the other $J - 1$ land use classes. The land user decides this based on the net profits associated with switching to the new land use class minus the cost of land conversion.

The utility of land-use conversion from the original land use can be expressed in the framework of the random utility model:

$$u_{ij} = \mu_{ij} + \varepsilon_{ij}, \qquad \text{(Eq. 27)}$$

where u_{ij} denotes the utility of converting from the original land use to land use j. The utility is assumed to be a linear combination of μ_{ij}, a mean process of relative net profits and costs of land use conversion, and ε_{ij}, a random error term.

Based on random choice theory, the land-owner will choose to convert land to land use class j over an alternative land use class j^* ($j^* = 1, \dots, J$) when the utility of j is higher than that of j^*. When considering land use shares, this implies that the share of land-converted – denoted by y_{ij} – directly depends on the probability:

$$y_{ij} = p(u_{ij} > u_{ij^*}, \forall j \neq j^*) \qquad \text{(Eq. 28)}$$

If we assume that ε_{ij} is logistically distributed, the random choice framework in Eq. (28) gives rise to a multinomial logit specification. The multinomial logit prior estimation model is specified as (Cameron and Trivedi, 2005):

$$y_{ij}^{t+1} = \frac{\exp\left(\mu_{ij}^{t}\right)}{\sum_j \exp\left(\mu_{ij}^{t}\right)} \quad \text{(Eq. 29)}$$

Here we have introduced the time dimension t (with $t = 1, \dots, T$), with y_{ij}^{t+1} denoting the share of land converted in the time period t to $t+1$. This is clearly a function of the log-odds μ_{ij}^{t} at time t. So far we have not specified the construction of these log-odds μ_{ij}^{t}: it is a linear combination of a set of explanatory variables and their coefficients, which are to be estimated:

$$\mu_{ij}^{t} = \alpha_j + f\left(y_i^t\right)\beta_j^1 + x_i^t\beta_j^2 + z_i\beta_j^3, \quad \text{(Eq. 30)}$$

where α_j is the land use specific intercept, $f\left(y_i^t\right)$ is a $1 \times J$ vector of land use area shares at time t, which are dynamically updated when projecting the model. x_i^t is a $1 \times k_1$ vector collecting a set of time-varying (projected) land use changes drivers associated with the 5 arcminute grid cell i. z_i is a $1 \times k_2$ vector with static land use change drivers. β_j^1, β_j^2, and β_j^3 are the corresponding coefficients, which are to be estimated within the framework. The list of land use drivers is outlined Table 12.

Estimating β_j(with $\beta_j = [\beta_j^{1\prime}, \beta_j^{2\prime}, \beta_j^{3\prime}]'$) is done using the Bayesian framework of Polson et al (2013). We assume the rather non-informative prior setting of a Gaussian with zero mean and 10^4 variance for β_j. The estimation follows the Markov-Chain Monte Carlo algorithm laid out in Polson et al (2013). Our results are based on 5,000 iterations, where the first 2,500 were discarded as burn-in.

Having estimated β_j the model in Eq. (29) can be readily projected in time by updating $f\left(y_i^t\right)$ and x_i^t. More formally the projected posterior means of the model can be expressed as:

$$\bar{y}_{ij}^{t+1} = E\left[p\left(y_{ij}^{t+1}|\mu_{i1}^{t}, \dots, \mu_{iJ}^{t}\right)\right] \quad \text{(Eq. 31)}$$

where $\bar{y}_{ij}^{t=1}$ denotes the expected value of the posterior projections. The model could be projected on its own as a high-resolution land use change model, but for downscaling the projections need to fulfil specific requirements (i.e. matching exactly the macro model values at a given aggregation level).

Table 12: Variables used in calibrating the downscalR econometric prior module.

Type	Variable	Description	Source
		Dependent variable	
	Land use change	Panel of land use change transition 2000 to 2010	ESACCI LC maps
		Explanatory variables - dynamic	
	Land use	Land use shares at initial time in pixel	ESACCI LC maps
	Cropsys	Crops and management systems at initial time in pixel	SPAM consistent with GLOBIOM harmonization
		Explanatory variables - projected	
Land rent	Average crop yield	Land use dataset; for 18 crop types and 4 management systems	Skalsky et al. (2008)
Socio-economic	GDP	Gross domestic product in pixel	Tobias et al. (2017)
	Population density	Population density in pixel	Goldewijk et al. (2018)
		Explanatory variables - static	
Transportation	Travel time to market	Gridded travel time for goods to closest market	Uchida and Nelson (2008)
Biophysical	Forest yield	Harvested wood yield	G4M
	Soil type	Dominant soil type in pixel	Skalsky et al. (2008)
	Slope	Dominant slope in degrees in pixel	

Type	Variable	Description	Source
	Altitude	Average altitude in m in pixel	

5.1.2. Target model

The target module uses two states (usually two temporally subsequent allocations of crop and management systems) described by the macro-level model as input. Together with prior information about which changes are considered implausible it generates a set of changes that ensure the transition from one to the other state. In matrix notation:

$$s_{t2} = A_{21} s_{t1}. \quad \text{(Eq. 32)}$$

It finds a transition matrix A_{21} such that state s_{t2} is the matrix product of the transition matrix and state s_{t1}. To ensure some structure on the transition matrix we try to follow as closely as possible an identity matrix, which would basically keep everything constant from state one. With this assumption magnitudes of the flows are forced to be as small as possible, while fulfilling Equation 32. Additionally, the modeler can set specific flows to zero which are assumed to not be plausible from a biophysical perspective.

5.1.3. Downscaling

For the downscaling, GLOBIOM provides aggregate targets at the regional level per projected time period t. A specific region is comprised of n distinct pixels. Let a_i denote the area of pixel i. Let Y_j^{t+1} be the region-specific gross land use, crop and management system change targets of change to land use j between time t and $t+1$, with $\sum_j Y_j^t = \sum_i a_i$. The downscaling can be expressed as:

$$\min_{\gamma_1,\dots,\gamma_J} \sum_j \left(Y_j^{t+1} - \sum_i \zeta_{ij}^{t+1} a_i\right)^2. \quad \text{(Eq. 33)}$$

subject to

$$\zeta_{ij}^{t+1} = g_{ij}^t \frac{\gamma_j \exp(\mu_{ij}^t)}{\sum_j \gamma_j \exp(\mu_{ij}^t)},\ g_{ij}^t \in [0,1]. \quad \text{(Eq. 34)}$$

The downscaling solves for the parameter γ_j to minimize the sum of squared differences to the aggregate regional totals. ζ_{ij}^{t+1} are the econometric priors, where the share of the econometric projected $\exp(\mu_{ij}^t)$ is adjusted by γ_j for the whole region. The econometric prior shares are multiplied by the pixel specific areas to obtain the per ha gross land use change.

The binary indicator g_{ij}^t can be exogenously supplied to allow for land-use change restrictions for specific pixels. This mechanism enables the downscalR to model protected areas.

5.2. Converting GLOBIOM landcover into CWatM inputs

After the downscaling has been completed, the GLOBIOM land cover classes need to be converted to land cover classes that can be taken up by CWatM. GLOBIOM uses multiple landcover classes, including general information on landcover and specific management information, e.g., high-input wheat, irrigated wheat, etc. On the contrary, on its most basic *modus-operandi*, CWatM uses six different landcover classes: Sealed (e.g., built-up) area, water, forest, grassland (including rainfed agriculture), irrigated cropland (excluding paddy), and irrigated paddy.

As GLOBIOM does not provide water landcover or sealed area landcovers, we fix these to the static landcover map used by CWatM. The remaining landcover classes are grouped and summarized, where each GLOBIOM landcover is assigned for one or more CWatM landcover classes, as shown in Table 13.

Table 13: concordance table between GLOBIOM and CWatM landcover classes.

GLOBIOM landcover	CWatM landcover
Forest_[Year]	Forest
PltFor_[Year]	Forest

[CropName]_HI_[Year]	Grassland
[CropName]_LI_[Year]	Grassland
[CropName]_SS_[Year]	Grassland
GrsLnd_[Year]	Grassland
NatLnd_[Year]	Grassland
OagLnd_[Year]	Grassland
WetLnd_[Year]	Grassland
NotRel_[Year]	Grassland
[CropName]_IR_[Year]	Irrigated Non Paddy (For all crops except rice)
Rice_IR_[Year]	Irrigated Paddy

The last step is ensuring that the sum of all landcover fractions equals one. This balancing procedure uses the following equation (35): fixing the water and sealed area landcovers to those represented by the static landcover map. Where $f_{l,j\epsilon G,t}$ is the area fraction in grid cell *l* of landcover *j* in year *t*. This procedure is only applied to the GLOBIOM land covers (i.e., *jϵG)*.

$$f_{l,j\in G,t} = f_{l,j\in G,t} - \frac{f_{l,j\in G,t}}{\sum_{j\in G} f_{l,j\in G,t}} \times \left(\sum_{j\in G} f_{l,j\in G,t} - 1\right) \quad \text{(Eq. 35)}$$

5.3. Comparing hydrological simulations using static and dynamic landcover to demonstrate projected landcover effects on the water cycle

Compared to static landcover input data, testing the model response to dynamic is pursued by setting hydrological simulations at a European scale and spatial resolution of 5'. Both simulations provide monthly average outputs for the year 2050, whereas the only difference between these two simulations is the landcover input data (see Table 14).

Table 14: General information on the landcover data used in each simulation.

Landcover type	**Static**	**Dynamic**
Spatial coverage and resolution	Europe, 5'	Europe, 5'
Landcover year	2010	2050, SSP2 (GLOBIOM)

The main differences in landcover between the static and dynamic simulation are shifts between forested area and grassland (e.g., rainfed agriculture, pasture, bare land, natural non-forested land, etc.). At the European scale, the dynamic landcover results in 3,495 km^2 of forest (-1% relative to the static landcover), 3,396 km^2 of grassland (+0.8%), 226.3 km^2 of irrigated cropland (-2%) and 6 km^2 of irrigated paddy (-2.5%). However, these changes vary across countries. For example, forest loss is observable in Albania (ALB), Portugal (PRT), Greece (GRC), Italy (ITA), and Spain (ESP; see Figure 50). Oppositely, forest area increases are shown for Austria (AUT) and Bulgaria (BGR), and both France (FRA) and Sweden (SWE) show relatively fixed landcovers.

Surface runoff (i.e., direct runoff in CWatM) is immediately affected by changes in the landcover, and is expected to increase with forest loss, due to reduced interception, evapotranspiration, and infiltration. It follows that countries with less forest area in the dynamic simulation also demonstrate

higher runoff (positive relative difference in Figure 51) , including Greece (GRC), Italy (ITA), Portugal (PRT), and Albania (ALB). Austria (AUT) and Bulgaria (BGR) show the opposite trend, and Sweden (SWE) and France (FRA) show very low differences.

Dynamic landcover also results in different irrigation withdrawals (see Section 3.2.1), lower in Albania (ALB) and Greece (GRC), which also show a reduction in irrigated cropland (Figure 50). In Bulgaria, increased irrigation withdrawal is probably associated with increased evapotranspiration and/or lower soil moisture, as irrigated cropland or paddy landcover remains largely unchanged. These differences highly impact the water stress in each country under different scenarios, as expressed by the water stress index. The monthly water stress in Eq. 36 for a given country *r* ($WS_{r,t}$) is calculated as the ratio between the average monthly water withdrawal and the average monthly water availability (represented as the average runoff), and is aggregated to an annual value as follows:

$$wsi_r = \frac{\sum_{m=1}^{12} wsi_{r,m} \times ww_{r,m}}{\sum_{m=1}^{12} ww_{r,m}} \quad \text{(Eq. 36)}$$

The water stress in many European countries (assuming the total water demand is satisfied using either surface water, or sustainable/ unsustainable groundwater abstraction) is severe, reaching extreme levels of almost 12.5 in Portugal (PRT; see Figure 52). Countries with reduced irrigated cropland also show lower water stress (e.g., Greece, GRC; Albania, ALB; and Spain; ESP), whereas Bulgaria (BGR) shows both increase irrigation withdrawal and increased water stress.
In conclusion, the Community Water Model is responsive to changing landcover, and can be used to simulate the impacts of plausible future landcover assemblies on the water cycle.

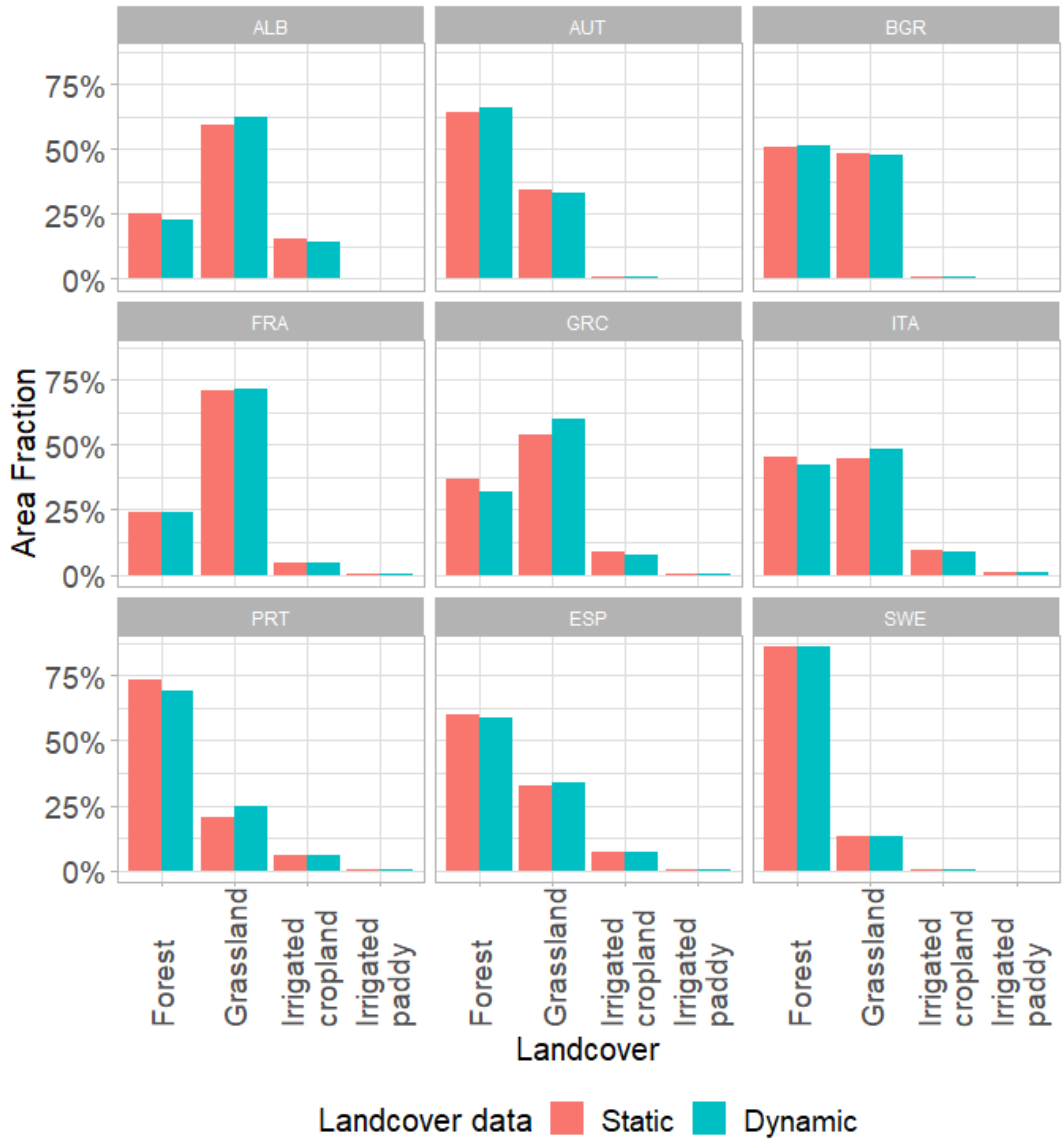

Figure 50: Differences in landcover fraction between the static and dynamic landcover input data for selected European countries.

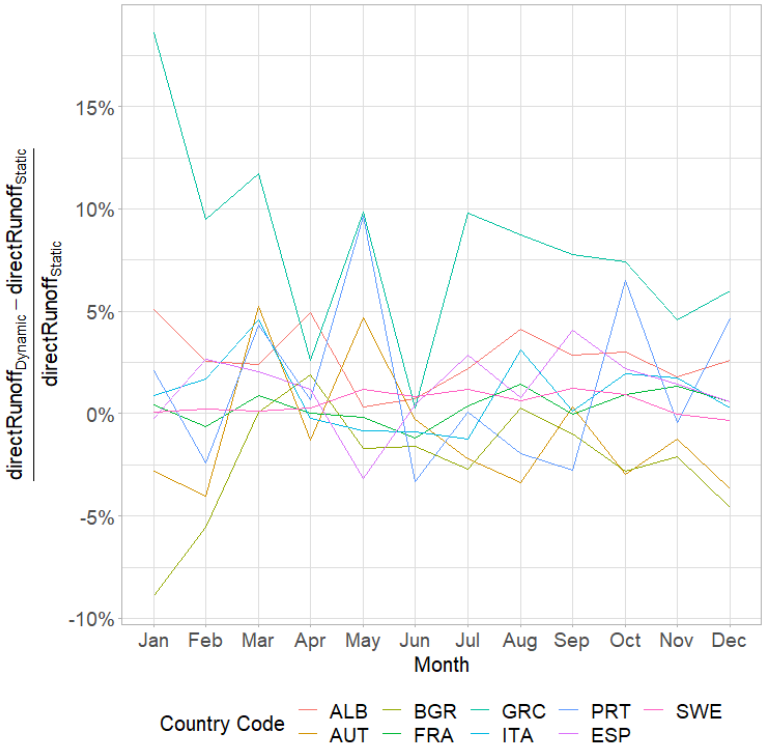

Figure 51: Relative difference of surface (direct) runoff between simulations with dynamic and static landcover data for selected European countries.

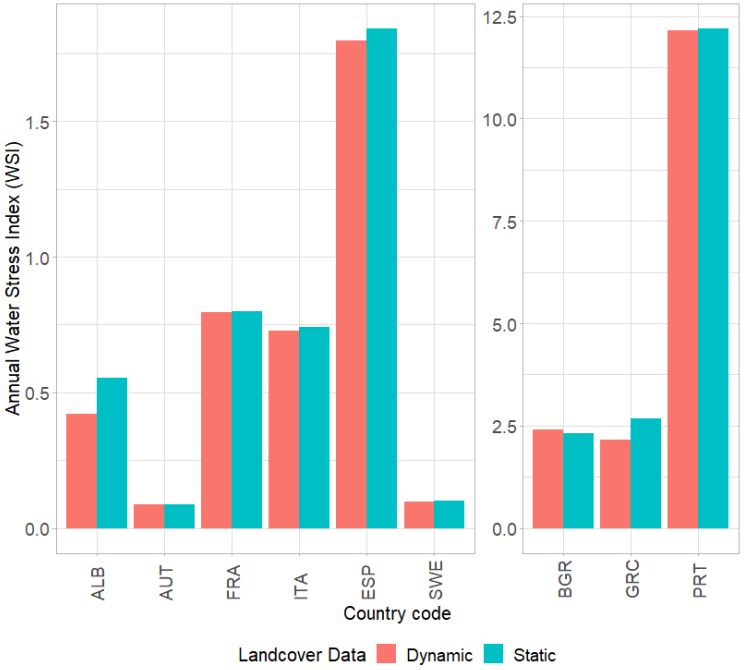

Figure 52: Relative difference of annual water stress index between simulations with dynamic and static landcover data for selected European countries. Severe water stress is associated with values equal or higher than 0.4. The simulations presented assume the total water demand is satisfied with surface water, renewable and non-renewable groundwater.

3. References

Alcamo, J., Döll, P., Henrichs, T., Kaspar, F., Lehner, B., Rösch, T., Siebert, S., 2003. Development and testing of the WaterGAP 2 global model of water use and availability. Hydrol. Sci. J. 48, 317–338. https://doi.org/10.1623/hysj.48.3.317.45290

Balkovič, J., van der Velde, M., Schmid, E., Skalský, R., Khabarov, N., Obersteiner, M., Stürmer, B., Xiong, W., 2013a. Pan-European crop modelling with EPIC: Implementation, up-scaling and regional crop yield validation. Agric. Syst. 120, 61–75. https://doi.org/10.1016/j.agsy.2013.05.008

Balkovič, J., van der Velde, M., Schmid, E., Skalský, R., Khabarov, N., Obersteiner, M., Stürmer, B., Xiong, W., 2013b. Pan-European crop modelling with EPIC: Implementation, up-scaling and regional crop yield validation. Agric. Syst. 120, 61–75. https://doi.org/10.1016/j.agsy.2013.05.008

Bergström, S., Forsman, A., 1973. Development of a conceptual deterministic rainfall-runoff model. Nord. Hydrol. 4.

Bondeau, A., Smith, P.C., Zaehle, S., Schaphoff, S., Lucht, W., Cramer, W., Gerten, D., Lotze-Campen, H., Müller, C., M.Reichstein, Smith, B., 2007. Modelling the role of agriculture for the 20th century global terrestrial carbon balance. Glob. Chang. Biol. 13, 679–706. https://doi.org/10.1111/j.1365-2486.2006.01305.x

Burek, P., Satoh, Y., Kahil, T., Tang, T., Greve, P., Smilovic, M., Guillaumot, L., Wada, Y., 2019. Development of the Community Water Model (CWatM v1.04) A high-resolution hydrological model for global and regional assessment of integrated water resources management. Geosci. Model Dev. Discuss. 1–49. https://doi.org/10.5194/gmd-2019-214

Burek, P., Satoh, Y., Kahil, T., Tang, T., Greve, P., Smilovic, M., Guillaumot, L., Zhao, F., Wada, Y., 2020. Development of the Community Water Model (CWatM v1.04) - A high-resolution hydrological model for global and regional assessment of integrated water resources management. Geosci. Model Dev. 13, 3267–3298. https://doi.org/10.5194/gmd-13-3267-2020

Burek, P., van der Knijff, J., de Roo, A., 2013. LISFLOOD, distributed water balance and flood simulation model (No. EUR 26162 EN). Ispra, Italy. https://doi.org/https://doi.org/10.2788/24719

Conley, T.G., 1999. GMM estimation with cross sectional dependence. J. Econom. 92, 1–45. https://doi.org/10.1016/S0304-4076(98)00084-0

De Roo, A.P.J., Wesseling, C.G., Van Deursen, W.P.A., 2000. Physically based river basin modelling within a GIS: the LISFLOOD model. Hydrol. Process. 14, 1981–1992. https://doi.org/10.1002/1099-1085(20000815/30)14:11/12<1981::AID-HYP49>3.0.CO;2-F

Falchetta, G., Cian, E. De, Pavanello, F., Wing, I.S., 2024. Inequalities in global residential cooling energy use to 2050. Nat. Commun. 15, 1–13. https://doi.org/10.1038/s41467-024-52028-8

FAO, IFAD, UNICEF, W.& W., 2018. The State of Food Security and Nutrition in the World 2018. Building Climate Resilience for Food Security and Nutrition, Food and Agriculture Organization of the United Nations,.

FAO AQUASTAT, 2024. AQUASTAT Dissemination System. Rome, Italy.

FAO, F. and A.O., 2024. AQUASTAT Main database [WWW Document]. URL http://www.fao.org/nr/water/aquastat/data/query/index.html?lang=en

FAO, F. and A.O., 2008. Water and the rural poor interventions for improving livelihoods in sub-Saharan Africa. FAO.

Flörke, M., Kynast, E., Bärlund, I., Eisner, S., Wimmer, F., Alcamo, J., 2013. Domestic and industrial water uses of the past 60 years as a mirror of socio-economic development: A global simulation study. Glob. Environ. Chang. 23, 144–156. https://doi.org/10.1016/j.gloenvcha.2012.10.018

Fricko, O., Havlik, P., Rogelj, J., Klimont, Z., Gusti, M., Johnson, N., Kolp, P., Strubegger, M., Valin, H., Amann, M., Ermolieva, T., Forsell, N., Herrero, M., Heyes, C., Kindermann, G., Krey, V., McCollum, D.L., Obersteiner, M., Pachauri, S., Rao, S., Schmid, E., Schoepp, W., Riahi, K., 2017.

The marker quantification of the Shared Socioeconomic Pathway 2: A middle-of-the-road scenario for the 21st century. Glob. Environ. Chang. 42, 251–267. https://doi.org/10.1016/j.gloenvcha.2016.06.004
Fridman, D., Burek, P., Palazzo, A., Wada, Y., Kahil, T., 2024. SSP-aligned projected European water withdrawal/consumption at 5 arcminutes. https://doi.org/10.5281/zenodo.13379538
Guerrero, S., Henderson, B., Valin, H., Janssens, C., Havlík, P., Palazzo, A., 2022. The impacts of agricultural trade and support policy reform on climate change adaptation and environmental performance. OECD Libr.
Hanasaki, N., Fujimori, S., Yamamoto, T., Yoshikawa, S., Masaki, Y., Hijioka, Y., Kainuma, M., Kanamori, Y., Masui, T., Takahashi, K., Kanae, S., 2013. A global water scarcity assessment under Shared Socio-economic Pathways - Part 1: Water use. Hydrol. Earth Syst. Sci. 17, 2375–2391. https://doi.org/10.5194/hess-17-2375-2013
Hanasaki, N., Inuzuka, T., Kanae, S., Oki, T., 2010. An estimation of global virtual water flow and sources of water withdrawal for major crops and livestock products using a global hydrological model. J. Hydrol. 384, 232–244. https://doi.org/10.1016/j.jhydrol.2009.09.028
Hanasaki, N., Kanae, S., Oki, T., 2006. A reservoir operation scheme for global river routing models. J. Hydrol. 327, 22–41. https://doi.org/10.1016/j.jhydrol.2005.11.011
Hanasaki, N., Kanae, S., Oki, T., Masuda, K., Motoya, K., Shirakawa, N., Shen, Y., Tanaka, K., 2008. An integrated model for the assessment of global water resources – Part 1: Model description and input meteorological forcing. Hydrol. Earth Syst. Sci. 12, 1007–1025. https://doi.org/10.5194/hess-12-1007-2008
Hasegawa, T., Havlík, P., Frank, S., Palazzo, A., Valin, H., 2019. Tackling food consumption inequality to fight hunger without pressuring the environment. Nat. Sustain. 2, 826–833. https://doi.org/10.1038/s41893-019-0371-6
Havlik, P., Leclere, D., Valin, H., Herrero, M., Schmid, E., Soussana, J., Müller, C., Obersteiner, M., 2015. Global climate change, food supply and livestock production systems: A bioeconomic analysis, in: Elbehri, A. (Ed.), Climate Change and Food Systems: Global Assessments and Implications for Food Security and Trade. Food Agriculture Organization of the United Nations (FAO), Rome.
Havlík, P., Schneider, U. a., Schmid, E., Böttcher, H., Fritz, S., Skalský, R., Aoki, K., Cara, S. De, Kindermann, G., Kraxner, F., Leduc, S., McCallum, I., Mosnier, A., Sauer, T., Obersteiner, M., 2011a. Global land-use implications of first and second generation biofuel targets. Energy Policy 39, 5690–5702. https://doi.org/10.1016/j.enpol.2010.03.030
Havlík, P., Schneider, U. a., Schmid, E., Böttcher, H., Fritz, S., Skalský, R., Aoki, K., Cara, S. De, Kindermann, G., Kraxner, F., Leduc, S., McCallum, I., Mosnier, A., Sauer, T., Obersteiner, M., 2011b. Global land-use implications of first and second generation biofuel targets. Energy Policy 39, 5690–5702. https://doi.org/10.1016/j.enpol.2010.03.030
Herrero, M., Havlik, P., McIntire, J.M., Palazzo, A., Valin, H., 2014. African Livestock Futures. Geneva, Switzerland.
Howell, T., 2005. Irrigation Efficiency. Encycl. Soil Sci. Second Ed. https://doi.org/10.1201/noe0849338304.ch191
Hsiao, T.C., Steduto, P., Fereres, E., 2007. A systematic and quantitative approach to improve water use efficiency in agriculture. Irrig. Sci. 25, 209–231. https://doi.org/10.1007/s00271-007-0063-2
Inocencio, A., Kikuchi, M., Merrey, D., Tonosaki, M., Maruyama, A., Jong, I. De, Sally, H., 2005. Lessons from Irrigation Investment Experiences: Cost-reducing and Performance-enhancing Options for sub-Saharan Africa. Final Rep. Submitt. by Int. Water Manag. Inst. 45.
Inocencio, A., Kikuchi, M., Tonosaki, M., Maruyama, A., Merrey, D., Sally, H., De Jong, I., 2007. Costs and Performance of Irrigation Projects: A Comparison of Sub-Saharan Africa and Other Developing Regions (No. 109), Research Report. Colombo, Sri Lanka.
Jägermeyr, J., Müller, C., Ruane, A.C., Elliott, J., Balkovic, J., Castillo, O., Faye, B., Foster, I., Folberth,

C., Franke, J.A., Fuchs, K., Guarin, J.R., Heinke, J., Hoogenboom, G., Iizumi, T., Jain, A.K., Kelly, D., Khabarov, N., Lange, S., Lin, T.S., Liu, W., Mialyk, O., Minoli, S., Moyer, E.J., Okada, M., Phillips, M., Porter, C., Rabin, S.S., Scheer, C., Schneider, J.M., Schyns, J.F., Skalsky, R., Smerald, A., Stella, T., Stephens, H., Webber, H., Zabel, F., Rosenzweig, C., 2021. Climate impacts on global agriculture emerge earlier in new generation of climate and crop models. Nat. Food 2, 873–885. https://doi.org/10.1038/s43016-021-00400-y

Janssens, C., Havlík, P., Boere, E., Palazzo, A., Mosnier, A., Leclère, D., Balkovič, J., Maertens, M., 2022. A sustainable future for Africa through continental free trade and agricultural development. Nat. Food 3, 608–618. https://doi.org/10.1038/s43016-022-00572-1

Janssens, C., Havlík, P., Krisztin, T., Baker, J., Frank, S., Hasegawa, T., Leclère, D., Ohrel, S., Ragnauth, S., Schmid, E., Valin, H., Van Lipzig, N., Maertens, M., 2020. Global hunger and climate change adaptation through international trade. Nat. Clim. Chang. 10, 829–835. https://doi.org/10.1038/s41558-020-0847-4

Leclère, D., Havlík, P., Fuss, S., Schmid, E., Mosnier, A., Walsh, B., Valin, H., Herrero, M., Khabarov, N., Obersteiner, M., 2014. Climate change induced transformations of agricultural systems: insights from a global model. Environ. Res. Lett. 9, 124018. https://doi.org/10.1088/1748-9326/9/12/124018

Lindström, G., 1997. A simple automatic calibration routine for the HBV model. Nord. Hydrol. 28, 153–168. https://doi.org/10.2166/nh.1997.0009

Mosnier, A., Obersteiner, M., Havlík, P., Schmid, E., Khabarov, N., Westphal, M., Valin, H., Frank, S., Albrecht, F., 2014. Global food markets, trade and the cost of climate change adaptation. Food Secur. 6, 29–44. https://doi.org/10.1007/s12571-013-0319-z

Müller, C., Robertson, R.D., 2014. Projecting future crop productivity for global economic modeling. Agric. Econ. 45, 37–50. https://doi.org/10.1111/agec.12088

O'Neill, B.C., Kriegler, E., Ebi, K.L., Kemp-Benedict, E., Riahi, K., Rothman, D.S., van Ruijven, B.J., van Vuuren, D.P., Birkmann, J., Kok, K., Levy, M., Solecki, W., 2017. The roads ahead: Narratives for shared socioeconomic pathways describing world futures in the 21st century. Glob. Environ. Chang. 42, 169–180. https://doi.org/10.1016/j.gloenvcha.2015.01.004

Palazzo, A., Batka, M., Havlik, P., Valin, H., 2019. Investment needs for irrigation infrastructure along different socio-economic pathways (No. 8744), World Bank Policy Research Working Paper. Washington D.C.

Pastor, A., Palazzo, A., Havlik, P., Obersteinner, M., Kabat, P., Ludwig, F., 2016. The future of irrigated agriculture under environmental flow requirements restrictions, in: European Geosciences Union (EGU) General Assembly. Vienna, Austria.

Rogelj, J., Popp, A., Calvin, K. V., Luderer, G., Emmerling, J., Gernaat, D., Fujimori, S., Strefler, J., Hasegawa, T., Marangoni, G., Krey, V., Kriegler, E., Riahi, K., Van Vuuren, D.P., Doelman, J., Drouet, L., Edmonds, J., Fricko, O., Harmsen, M., Havlík, P., Humpenöder, F., Stehfest, E., Tavoni, M., 2018. Scenarios towards limiting global mean temperature increase below 1.5 °c. Nat. Clim. Chang. 8, 325–332. https://doi.org/10.1038/s41558-018-0091-3

Rogers, P., Bhatia, R., Huber, A., 1998. Water as a Social and Economic Good: How to Put the Principle into Practice, in: TAC Background Paper No. 2. Global Water Partnership, p. 35.

Rosegrant, M.W.., Sulser, T.B.., Mason-D'Croz, Daniel; Cenacchi, N., Nin-Pratt, A., Dunston, S., Zhu, T., Ringler, C., Wiebe, K.D.., Robinson, Sherman; Willenbockel, D., Xie, H., Kwon, H.-Y., Johnson, T., Thomas, Timothy S.; Wimmer, F., Schaldach, R., Nelson, G.C.., Willaarts, B., 2017. Quantitative foresight modeling to inform the CGIAR research portfolio. Project Report for USAID 225.

Rost, S., Gerten, D., Bondeau, A., Lucht, W., Rohwer, J., Schaphoff, S., 2008. Agricultural green and blue water consumption and its influence on the global water system. Water Resour. Res. 44. https://doi.org/10.1029/2007WR006331

Sauer, T., Havlík, P., Schneider, U. a., Schmid, E., Kindermann, G., Obersteiner, M., 2010. Agriculture and resource availability in a changing world: The role of irrigation. Water Resour. Res. 46, 1–

12. https://doi.org/10.1029/2009WR007729
Schmidhuber, J., Bruinsma, J., Boedeker, G., 2009. Capital requirements for agriculture in developing countries to 2050, in: Expert Meeting on How to Feed the World in 2050.
Shiklomanov, I.A., 1998. World water resources. A new appraisal and assessments for the 21st century 40.
Siebert, S., Burke, J., Faures, J.M., Frenken, K., Hoogeveen, J., Döll, P., Portmann, F.T., 2010. Groundwater use for irrigation – a global inventory. Hydrol. Earth Syst. Sci. 14, 1863–1880. https://doi.org/10.5194/hess-14-1863-2010
Svoboda, M., Hayes, M., Wood, D. (Eds.), 2012. Standardized Precipitation Index User Guide. World Metrological Organization, Geneva.
Thornton, P., Nelson, G., Mayberry, D., Herrero, M., 2022. Impacts of heat stress on global cattle production during the 21st century: a modelling study. Lancet Planet. Heal. 6, e192–e201. https://doi.org/10.1016/S2542-5196(22)00002-X
Toan, T.D., 2016. Water Pricing Policy and Subsidies to Irrigation : a Review. Environ. Process. 1, 1081–1098. https://doi.org/10.1007/s40710-016-0187-6
van Beek, L.P.H., Wada, Y., Bierkens, M.F.P., 2011. Global monthly water stress: 1. Water balance and water availability. Water Resour. Res. 47. https://doi.org/10.1029/2010WR009791
van Ittersum, M.K., van Bussel, L.G.J., Wolf, J., Grassini, P., van Wart, J., Guilpart, N., Claessens, L., de Groot, H., Wiebe, K., Mason-D'Croz, D., Yang, H., Boogaard, H., van Oort, P.A.J., van Loon, M.P., Saito, K., Adimo, O., Adjei-Nsiah, S., Agali, A., Bala, A., Chikowo, R., Kaizzi, K., Kouressy, M., Makoi, J.H.J.R., Ouattara, K., Tesfaye, K., Cassman, K.G., Mason-D'Croz, D., Yang, H., Boogaard, H., van Oort, P.A.J., van Loon, M.P., Saito, K., Adimo, O., Adjei-Nsiah, S., Agali, A., Bala, A., Chikowo, R., Kaizzi, K., Kouressy, M., Makoi, J.H.J.R., Ouattara, K., Tesfaye, K., Cassman, K.G., 2016. Can sub-Saharan Africa feed itself? Proc. Natl. Acad. Sci. 113, 14964–14969. https://doi.org/10.1073/pnas.1610359113
Van Koppen, B., Namara, R., Safilios-Rothschild, C., 2005. Reducing Poverty and Gender Issues and Synthesis of Sub-Saharan Africa Case Study Reports (No. 101).
van Vuuren, D.P., Riahi, K., Calvin, K., Dellink, R., Emmerling, J., Fujimori, S., KC, S., Kriegler, E., O'Neill, B., 2017. The Shared Socio-economic Pathways: Trajectories for human development and global environmental change. Glob. Environ. Chang. 42, 148–152. https://doi.org/10.1016/j.gloenvcha.2016.10.009
Vorosmarty, C.J., Leveque, C., Revenga, C., 2005. Fresh Water, in: Rijsberman, F., Costanza, R., Jacobi, P. (Eds.), Millennium Ecosystem Assessment Vol. 1. Island Press, Washington D.C., pp. 165–207.
Wada, Y., Flörke, M., Hanasaki, N., Eisner, S., Fischer, G., Tramberend, S., Satoh, Y., Van Vliet, M.T.H., Yillia, P., Ringler, C., Burek, P., Wiberg, D., 2016. Modeling global water use for the 21st century: The Water Futures and Solutions (WFaS) initiative and its approaches. Geosci. Model Dev. 9, 175–222. https://doi.org/10.5194/gmd-9-175-2016
Wada, Y., Van Beek, L.P.H., Viviroli, D., Drr, H.H., Weingartner, R., Bierkens, M.F.P., 2011. Global monthly water stress: 2. Water demand and severity of water stress. Water Resour. Res. 47, 1–17. https://doi.org/10.1029/2010WR009792
Wada, Y., Wisser, D., Bierkens, M.F.P., 2014. Global modeling of withdrawal, allocation and consumptive use of surface water and groundwater resources. Earth Syst. Dyn. 5, 15–40. https://doi.org/10.5194/esd-5-15-2014

4. Annex

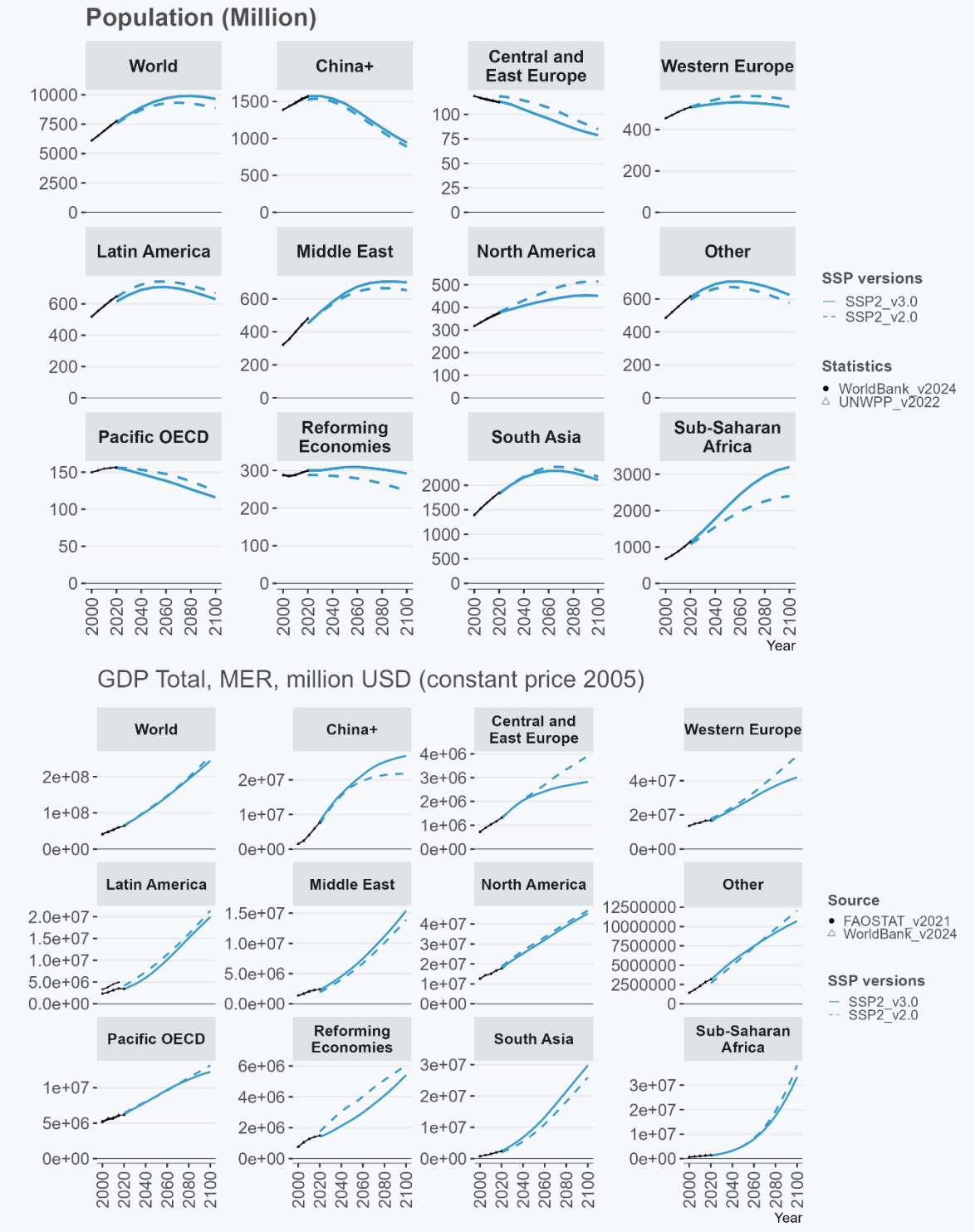

Figure A 1 Population (a) and GDP (b) growth for major global regions over the time period 2000-2100 under the 2023 SSP revision (V3.0) and the 2012 SSP revision (V2.0).

a)

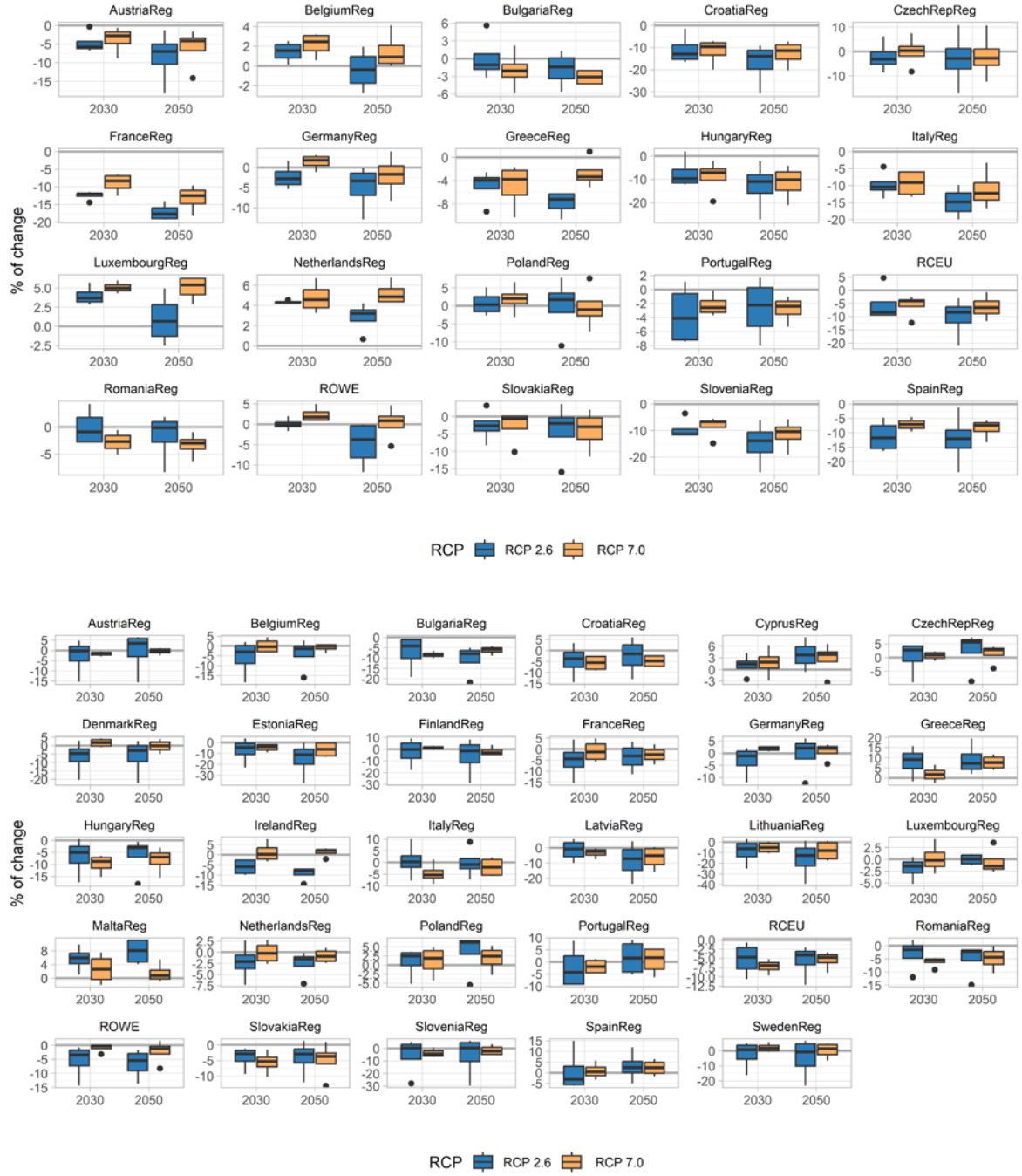

Figure A 2 Climate impacts on a) maize and b) wheat yield as modeled by EPIC-IIASA weighted by harvested area in 2000 by European country under RCP 2.6 and RCP 7.0. Percentage change with respect to yields under current climate.

Figure A 3 Change in surface water available for use by irrigation over the growing period as modeled by CWatM by European country under RCP 2.6 and RCP 7.0 and SSP2 water demand from other sectors. Percentage change with respect to surface water available under current climate and SSP2 water demand from other sectors.

Table A 1 GCM agreement in the direction of change in the surface water available for use by irrigation over the growing period as modeled by CWatM under RCP 2.6, RCP 4.5 and RCP 7.0 by European Country.

		RCP2p6	RCP4p5	RCP7p0
Northern Europe	Denmark	No Agreement	+	+
	Estonia	-	+	+
	Finland	+	+	+
	Ireland	+	+	+
	Latvia	No Agreement	+	+
	Lithuania	+	+	+
	Sweden	-	-	+
Western Europe	Belgium	+	No Agreement	+
	France	-	-	-
	Germany	+	No Agreement	+
	Luxembourg	No Agreement	No Agreement	No Agreement
	Netherlands	+	+	+
Central and Eastern Europe	Austria	-	-	-
	Czech Republic	+	No Agreement	+
	Hungary	No Agreement	-	-
	Poland	+	+	+
	Romania	No Agreement	-	No Agreement
	Slovakia	-	-	-
	Slovenia	-	-	-
Southern Europe	Bulgaria	+	No Agreement	+

	Croatia	-	-	-
	Cyprus	No Agreement	-	-
	Greece	+	No Agreement	-
	Italy	-	No Agreement	-
	Malta	+	-	+
	Portugal	No Agreement	-	-
	Spain	-	-	-
Rest of Europe	Rest of Central Europe	No Agreement	-	-
	Rest of Europe	-	-	-

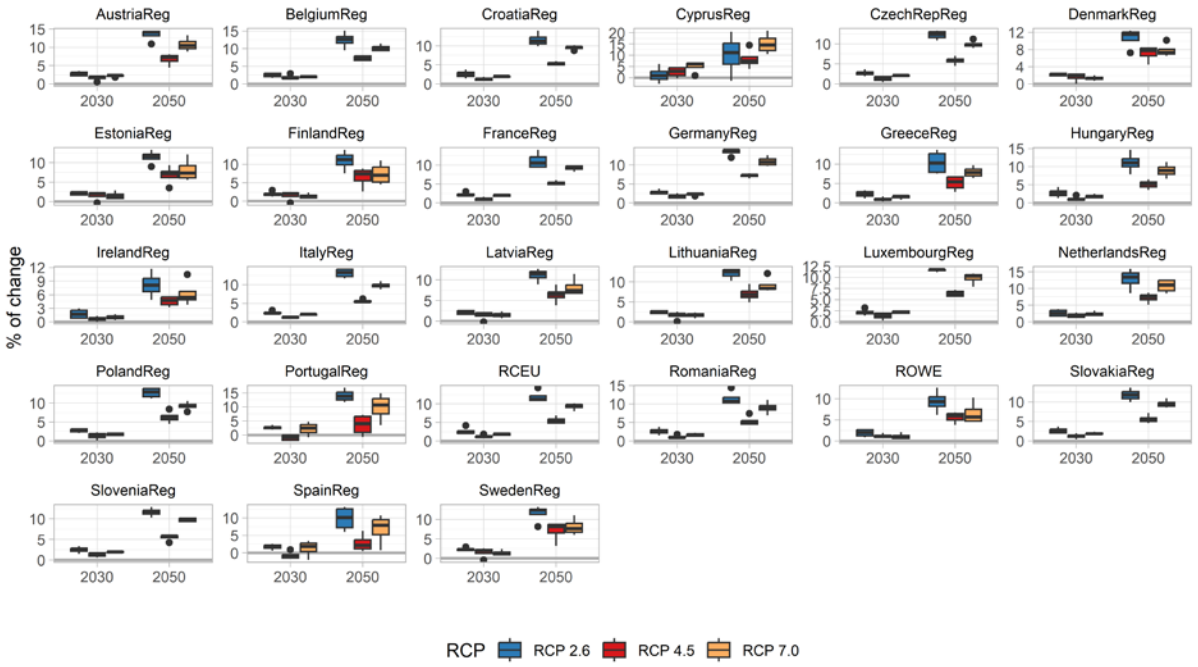

Figure A 4 Change in grassland productivity as modeled by European country under RCP 2.6, RCP 4.5, RCP 7.0. Percentage change with respect to current climate.

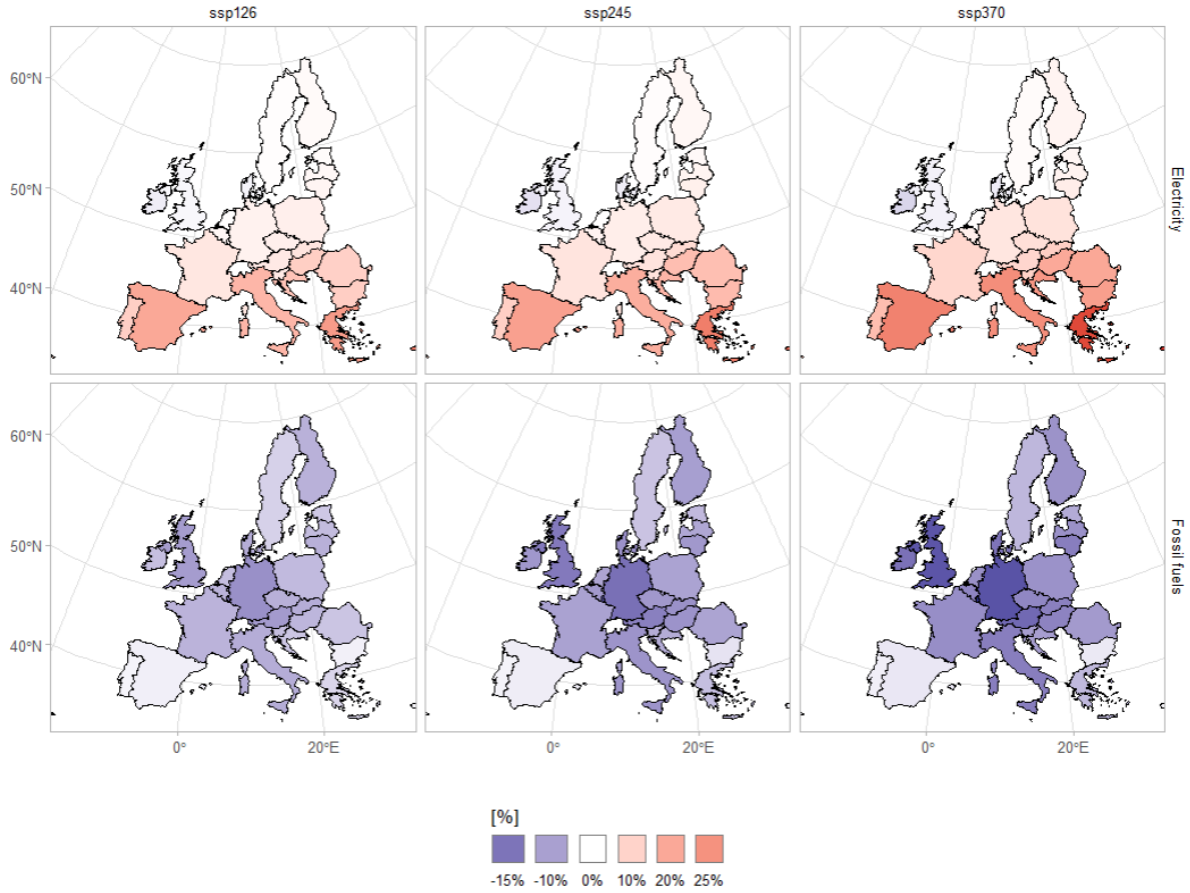

Figure A 5 Country-level final energy demand percentage change in the "Reference" adaptation scenario and RCP 4.5.

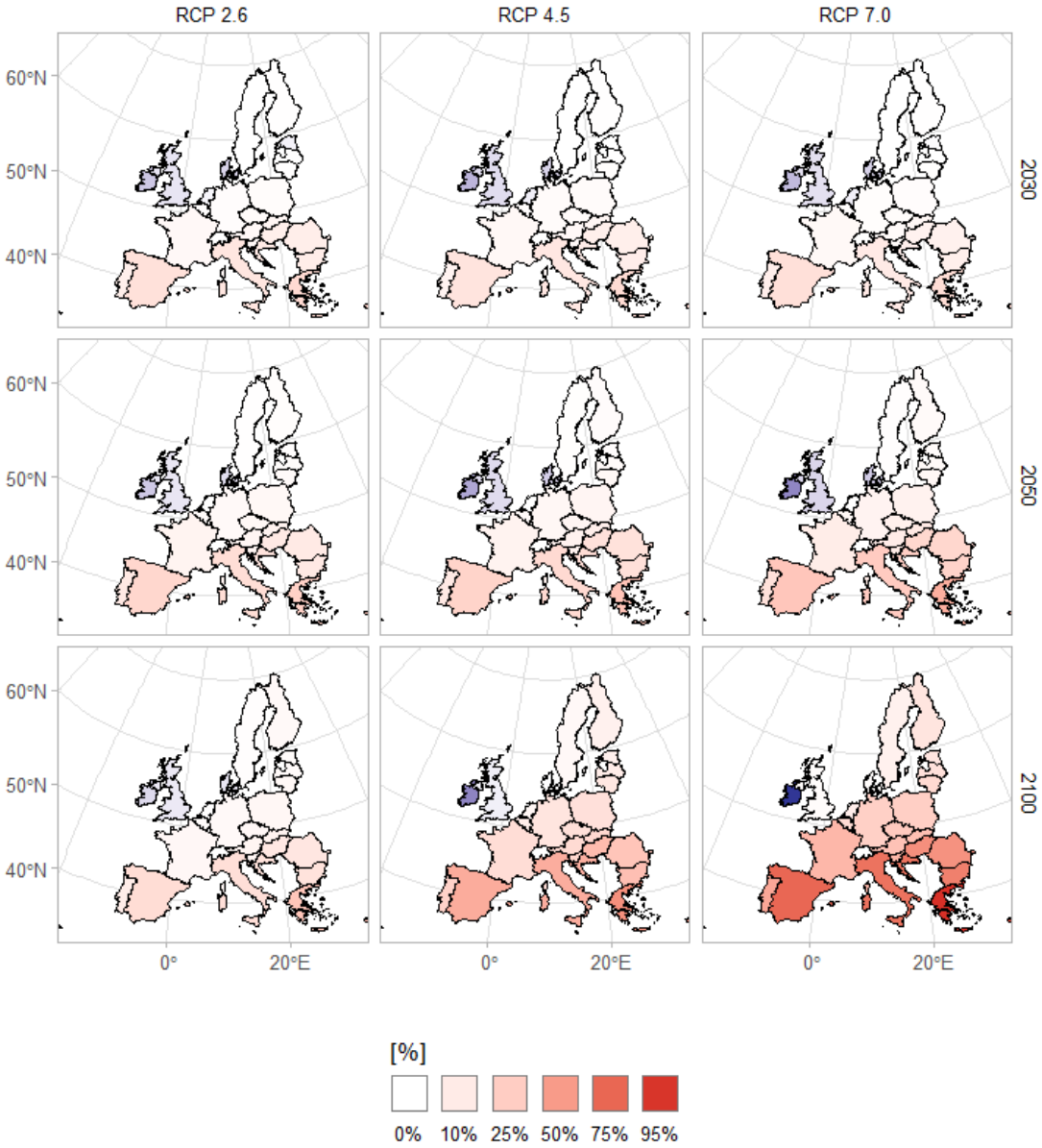

Figure A 6 Country-level final electricity demand percentage change in the "Reference" adaptation scenario across time periods and RCPs.

Figure A 7 Country-level final fossil fuel demand percentage change in the "Reference" adaptation scenario across time periods and RCPs.